

Washington University in St. Louis
Washington University Open Scholarship

All Theses and Dissertations (ETDs)

Summer 8-12-2013

Engineering poly(ethylene glycol) nanogel coatings: Developments in achieving ultralow protein adsorption and applications as substrates for stem cell culture

Casey Douglas Donahoe
Washington University in St. Louis

Follow this and additional works at: <https://openscholarship.wustl.edu/etd>

Recommended Citation

Donahoe, Casey Douglas, "Engineering poly(ethylene glycol) nanogel coatings: Developments in achieving ultralow protein adsorption and applications as substrates for stem cell culture" (2013). *All Theses and Dissertations (ETDs)*. 1130.
<https://openscholarship.wustl.edu/etd/1130>

This Dissertation is brought to you for free and open access by Washington University Open Scholarship. It has been accepted for inclusion in All Theses and Dissertations (ETDs) by an authorized administrator of Washington University Open Scholarship. For more information, please contact digital@wumail.wustl.edu.

Washington University in St. Louis
School of Engineering and Applied Science
Department of Biomedical Engineering

Dissertation Examination Committee:

Donald L. Elbert, Chair

Gregory D. Longmore

Joshua A. Maurer

Robi D. Mitra

Rohit V. Pappu

Jin-Yu Shao

Engineering Poly(ethylene glycol) Nanogel Coatings: Developments in Achieving Ultralow Protein
Adsorption and Applications as Substrates for Stem Cell Culture

by

Casey Douglas Donahoe

A dissertation presented to the Graduate School of Arts and Sciences
of Washington University in partial fulfillment of the
requirements for the degree of

Doctor of Philosophy

August 2013
Saint Louis, Missouri

Contents

List of Figures	iv
List of Abbreviations	vi
Acknowledgements	vii
Abstract	viii
1 Introduction	1
1.1 Objectives of Dissertation	1
1.2 Protein Resistant Properties of PEG	2
1.3 Strategies for PEG Surface Coatings	7
1.4 <i>In Vitro</i> and <i>In Vivo</i> Blood Compatibility of PEG Materials.....	11
1.5 Stem Cells and Biomaterials	14
2 Ultralow Protein Adsorbing Coatings from Clickable PEG Nanogel Solutions	17
2.1 Introduction.....	17
2.2 Materials and Methods	23
2.2.1 Materials.....	23
2.2.2 Nanogel Solution Syntheses	23
2.2.3 Size Exclusion Chromatography (SEC).....	23
2.2.4 Nanogel Coatings	24
2.2.5 Total Internal Reflection Fluorescence (TIRF) Microscopy	25
2.2.6 Quartz Crystal Microbalance with Dissipation (QCM-D)	25
2.1.7 Atomic Force Microscopy (AFM)	26
2.1.8 Cell Adhesion Studies.....	26
2.3 Results and Discussion.....	27
2.3.1 Synthesis and Characterization of Clickable Nanogel Solutions	27
2.3.2 Quantification of Protein Adsorption via TIRF.....	28
2.3.3 Quantification of Nanogel Coating Packing Density	38
2.3.4 Characterization of Nanogel Coating Topography	39
2.3.5 Cell Adhesion to Nanogel Coatings	43
2.4 Conclusion	50
3 Patterned Cell Adhesion with PEG Nanogel Coatings for the Direct Reprogramming of Fibroblasts to Cardiomyocytes	51
3.1 Introduction.....	51
3.2 Materials and Methods	57
3.2.1 Pattern Stamping	57
3.2.2 Direct Reprogramming.....	58
3.2.3 Surfaces for Reprogramming.....	58
3.2.4 Contracting Patch Quantification	59
3.2.5 Immunocytochemistry Analysis	59

3.2.6	Statistics	66
3.3	Results	66
3.3.1	Preliminary Optimization of Patterning Techniques	66
3.3.2	Non-patterned and Patterned Surfaces for Direct Reprogramming	75
3.3.3	Quantification of Functional Contraction in Differentiated Cardiomyocytes	77
3.3.4	Sarcomeric α -Actinin Expression in Differentiated Cardiomyocytes ..	83
3.4	Discussion	94
3.5	Conclusion	100
4	Conclusions.....	102
4.1	Summary of Dissertation	102
4.2	Future Directions	102
	References	107

List of Figures

Chapter 2

Figure 2.1: Strategies for synthesis and attachment of clickable nanogel solutions.....	21
Figure 2.2: Strategies for surface cross-linking of nanogel coatings	22
Figure 2.3: Copper-dependent gelation kinetics	29
Figure 2.4: SEC profiles of clickable nanogel solution and precursor	30
Figure 2.5: Table of molecular weight distributions for clickable nanogel solutions	31
Figure 2.6: Quantification of protein adsorption to nanogel coatings via TIRF	32
Figure 2.7: Fluorescent images of protein adsorption to nanogel coatings.....	33
Figure 2.8: Micrographs of Michael-addition nanogel coatings incubated in high salt solutions	36
Figure 2.9: TIRF measurements of protein adsorption on nanogel coatings of different size nanogels	37
Figure 2.10: QCM-D mass measurements of clickable nanogel coatings.....	40
Figure 2.11: QCM-D profiles of protein adsorption to clickable nanogel coatings	41
Figure 2.12: AFM profiles of clickable nanogel coatings.....	42
Figure 2.13: Cell adhesion to nanogel coatings after 1 seeding	46
Figure 2.14: Cell adhesion to nanogel coatings after 5 seedings.....	47
Figure 2.15: Cell adhesion to nanogel coatings after 9 seedings.....	48
Figure 2.16: Cell adhesion to clickable nanogel coatings attached via CuAAC and SPAAC	49

Chapter 3

Figure 3.1: Strategies for patterning cell adhesion with PEG nanogel coatings.....	62
Figure 3.2: Cell adhesion on nanogel coatings capped with various molecules.....	63
Figure 3.3: Cell adhesion on tris-capped nanogel coatings	64
Figure 3.4: Pattern integrity of cells adhered via patterned fibrinogen adsorption	65
Figure 3.5: Pattern integrity of cells adhered via patterned laminin adsorption.....	66
Figure 3.6: Pattern integrity of cells adhered via patterned Matrigel adsorption	67
Figure 3.7: Fluorescent imaging of a patterned nanogel coating.....	68
Figure 3.8: Patterned cell adhesion on RGD-functionalized nanogel coatings after repetitive capping	71

Figure 3.9: Pattern integrity of cells adhered via patterned RGD-functionalization of nanogel coatings	72
Figure 3.10: Cell adhesion on nanogel coatings after sham stamping.....	73
Figure 3.11: Cell adhesion to laminin-functionalized nanogel coatings.....	74
Figure 3.12: Cell adhesion to RGD-functionalized nanogel coatings	78
Figure 3.13: Cell adhesion at days 6, 9, and 12 of reprogramming	79
Figure 3.14: Cell adhesion at days 12 and 15 of reprogramming.....	80
Figure 3.15: Low objective micrographs of cell adhesion at day 15 of reprogramming	81
Figure 3.16: Quantified cardiomyocyte contraction during reprogramming	82
Figure 3.17: Size distributions of contracting cell patches.....	85
Figure 3.18: Images of small contracting patches on non-patterned laminin monolayers	86
Figure 3.19: Quantification of α -actinin expression	87
Figure 3.20: Images of α -actinin expression in cell aggregates.....	88
Figure 3.21: Images of α -actinin expression in cell monolayers	89
Figure 3.22: Images of α -actinin expression along monolayer edges.....	90
Figure 3.23: Images of α -actinin expression in elongated structures	91
Figure 3.24: Images of α -actinin expression in small cellular aggregates	92
Figure 3.25: Images of α -actinin expression within boundaries of large contracting patches	93

List of Abbreviations:

BSA: bovine serum albumin

CuAAC: copper-catalyzed azide/alkyne cycloaddition

ESC: embryonic stem cell

iPSC: induced pluripotent stem cell

MEF: mouse embryonic fibroblast

OEG: oligo(ethylene glycol)

PEG: poly(ethylene glycol)

PEO: poly(ethylene oxide)

PSC: pluripotent stem cell

SAM: self assembled monolayer

SPAAC: strain-promoted azide/alkyne cycloaddition

TCPS: tissue culture polystyrene

VS:Am: PEG-vinylsulfone cross-linked with PEG-amine (nanogel solution)

VS:BSA: PEG-vinylsulfone cross-linked with BSA (nanogel solution)

Acknowledgments

I would like to foremost thank my advisor, Don Elbert, for providing me the opportunity to work alongside him on the trailblazing pursuits he has carved for himself from a fascinating field of research. His intellectual creativity and steady support were paramount in my development as a scientist. I would additionally like to thank all my committee members for their continued time and support in helping me achieve my goals. Additional faculty and staff members of the department, including Shelly Sakiyama-Elbert, Frank Yin, Glen Reitz, Amanda Carr, Kate Ruzicka and Karen Teasdale, are thanked for their support, friendship, and reminder of the light at the end of the tunnel.

I enjoyed the best working environment imaginable within our lab group, which epitomizes collaboration and friendship. Specifically, I would like to thank Peter Nguyen, Amanda Smith, Jacob Roam, Megan Flake, and members of the Sakiyama-Elbert Lab for providing constant laughs and smiles through the many ups and downs of graduate school. Members of lab-past have also shown their continuing friendship and encouragement, including Evan Scott, Shannon Alford, and Mike Nichols. I appreciate the time they sacrificed in providing my earliest training and thank them for their well-thought advice, without which I would not have succeeded.

Finally I wish to thank my family and many unnamed friends for their unwavering love, support and patience as I withdrew deeper into the world of research. Their unquestioning belief in me has sustained me through a long and arduous endeavor, and I am truly grateful. I dedicate this work to them as a token of my appreciation.

Casey Douglas Donahoe

Washington University in St. Louis

August 2013

ABSTRACT OF THE DISSERTATION

Engineering Poly(ethylene glycol) Nanogel Coatings: Developments in Achieving Ultralow Protein Adsorption and Applications as Substrates for Stem Cell Culture

by

Casey Douglas Donahoe

Doctor of Philosophy in Biomedical Engineering

Washington University in St. Louis, 2013

Research Advisor: Professor Donald L. Elbert

The biocompatibility of biomaterials is primarily dictated by the interactions that occur at the material's interface with its biological environment. Proteins irreversibly adsorb to these interfaces within seconds to minutes of exposure, altering their structural conformation, inducing cell adhesion, and activating various cellular responses. To this end, surface modification strategies have been designed in attempts to develop "stealth" biomaterials or even biomaterials that modulate this response by inducing specific biological reactions. We sought to advance the design of biomaterial surfaces by quantitatively studying protein adsorption to ultralow protein adsorbing surfaces formed from poly(ethylene glycol) nanogel coatings of variable structural and chemical properties. We found that resistance to protein adsorption can be improved by increasing the nanogel coating's surface packing density, which is achievable using orthogonal cross-linking chemistries, such as click chemistry, under phase separation conditions. We also confirmed that PEG and albumin act synergistically within nanogel coatings to resist protein adsorption. As a demonstration of the utility for such protein resistant surfaces, we fabricated improved cell culture substrates with nanogel coatings, by spatially patterning cell adhesion and functionalizing surfaces with specific ligands. These surfaces showed superior potential for driving the direct reprogramming of fibroblasts to cardiomyocytes over the standard stem cell substratum of Matrigel and revealed insight into optimal cellular organizations for cardiomyocyte differentiation. However, we also unexpectedly found that adsorption of laminin to mercaptosilanated glass promotes a relatively high efficiency of cardiomyocyte differentiation. The findings outlined in this dissertation demonstrate that consideration of often overlooked material design parameters, in addition to the choice of material,

provides further opportunity for improving biocompatibility. We further demonstrated that the precision control of cell adhesion and substratum signaling provided by these materials has broad potential in biological applications, including stem cell culture.

Chapter 1

Introduction

1.1 Objectives of Dissertation

The overall aim of this dissertation is to further explore the protein resistant properties as well as applications of a unique polymeric coating developed by our group.⁽¹⁾ The coating is formed of nanoscale poly(ethylene glycol) (PEG) hydrogels, covalently coupled to surfaces to form thin hydrogel barriers. Chapter 1 briefly reviews the protein resistant properties of PEG, examples of strategies used to fabricate PEG coatings, blood compatibility of various PEG coatings, and how biomaterials such as PEG may be applied as substrates for stem cell culture. Chapter 1 is not meant to be conclusive and more specific introductions are provided for the research contained in Chapters 2 and 3. Chapter 2 quantitatively compares protein adsorption to various PEG nanogel coatings fabricated by means of distinct cross-linking chemistries. Specifically, Chapter 2 explores the potential for exploiting a relatively new bioconjugation chemistry, known as “click chemistry”, for creating a more sophisticated and improved nanogel coating. Indeed, we find that the orthogonality of this chemistry allows for the formation of quantifiably denser nanogel coatings of confined thickness under phase separation conditions, which translates into drastically reduced levels of protein adsorption. We also examine the effects of further cross-linking these coatings after fabrication, with inconclusive results that depend on the method used to assay for protein adsorption. Chapter 3 details the first attempt to employ these coatings as chemically defined substrates for stem cell culture. Specifically, we perform a direct reprogramming of fibroblasts to cardiomyocytes on nanogel coatings functionalized with specific adhesion ligands and compare results for various assays of cardiac differentiation against surfaces that rely on adsorption of adhesion proteins. We also use the cell resistant nanogel coatings to spatially pattern cell organization on all the substrates to determine if controlling cellular organization has potential to improve differentiation efficiency. We find that the nanogel coatings perform superiorly to the standard Matrigel coatings commonly used in stem cell culture and inadvertently discover that laminin adsorbed to mercaptosilanated glass seems to significantly increase the efficiency of cardiac

differentiation by an unknown mechanism. We do not see improvement in differentiation of patterned clusters over those on non-patterned surfaces but do see evidence suggesting that the overall reduction in cell expansion from these clusters could improve cumulative differentiation efficiency. Chapter 4 summarizes the dissertation and provides future directions for the continued progression of this research.

1.2 Protein Resistant Properties of PEG

Over the past 30 years or so, PEG, synonymous with poly(ethylene oxide) (PEO), has gained extraordinary attention for its use as a biomaterial. PEG is known to act strongly hydrophilic and cross-link into highly hydrated hydrogels, which along with other more unique phenomena contributes to the low amounts of protein adsorption observed on PEG materials. Because protein adsorption regulates, through cellular adhesion and activation, the physiological responses that foreign materials encounter, PEG quickly became an obvious choice for biomaterial design. A major drawback of PEG is that it oxidizes relatively rapidly in the presence of oxygen and transition metal ions.⁽²⁾ It was shown that *in vivo* PEG was subject to oxidation by superoxide anions and H_2O_2 liberated by polymorphonuclear leukocytes (PMNs) and macrophages during the respiratory burst.⁽³⁾ Additionally, significant losses in PEG film thickness have been measured under physiological conditions over a period of 4 weeks.⁽⁴⁾ Nonetheless, PEG remains one of the most protein resistant polymers studied to date, especially when compared to other materials using highly sensitive detection assays. Both the existence of and mechanisms by which PEG displays intrinsically superior protein resistant properties remain controversial. However, an understanding of the theories describing the unique physics of PEG are beneficial in the design of PEG based biomaterials. The simplest explanation relies on PEG's low interfacial energy with water due to its hydrophilic nature. However, PEG is more resistant than other neutral, hydrophilic polymers (dextran, agarose, polyacrylamide, etc.) which also adsorb low levels of protein.⁽⁵⁾ Not exclusive to the aforementioned ideas, "steric stabilization" is widely cited as responsible for the protein resistance of PEG. PEG is a highly flexible and mobile polymer leading to larger excluded volumes than similar polymers. The large excluded volume itself may inhibit protein adsorption, and has been cited as the primary mechanism by which soluble PEG induces protein precipitation.⁽⁶⁾ Protein adsorption to a densely coated PEG surface must compress the flexible polymer chains, at an entropic cost, as well as partially desolvate the hydrophilic chains against osmotic forces.^(5, 7)

It has been suggested that protein resistance on surfaces may be achieved by either kinetic or thermodynamic means. While kinetic resistance, or the delay of protein adsorption, may provide suitable resistance to nanoparticles, drug delivery vessels, and PEGylated proteins, all of which only require extended blood clearance times, satisfactory biocompatibility of implantable biomaterials is likely to be achieved only by thermodynamic means. Such mechanisms should establish an extremely low equilibrium level of protein adsorption on the biomaterial surface so that it resists protein adsorption for indefinitely long time periods while it remains in biological contact.⁽⁸⁾ Given the theories presented on the mechanisms of PEG protein resistance, a number of modifiable parameters clearly contribute to a polymer coating's protein resistance, including: surface coverage, molecular weight and/or chain length, chain flexibility, chain architecture, and polymer-surface attraction. It is important to recognize that in many situations, these parameters may not be able to be modulated independently of each other. Most studies are in agreement that surface coverage is by far the most important parameter, yet this is often the most difficult to control.⁽⁹⁾ Increased surface coverage is primarily achieved by increasing the polymer grafting density. However, theoretical calculations with mean field theory have shown that the surface coverage necessary to prevent any protein adsorption is not experimentally achievable.^(8, 10) An obvious aim of biomaterial design then may be to develop coating techniques that result in increased surface coverage, either through techniques that improve grafting density or by means to overcome this limitation.

Grafting density has strong implications on the molecular mechanisms by which PEG is theorized to act. Namely, steric repulsion is thought to be achieved primarily at higher grafting densities when the close packing of PEG chains forces a conformational transition of the chains from what is called a "mushroom" regime to a "brush" regime. In the brush regime chains become fully extended and do not overlap.^(9, 11-13) Grafting density and chain length are compensating factors in achieving brush conformations, as longer chains are difficult to graft at higher densities due to their larger excluded volumes but achieve brush conformation more readily for the same reason.⁽¹²⁾ However, protein adsorption has been found to increase at very high grafting densities as well, assumedly due to dehydration of the polymer chains.⁽¹⁴⁾ It is also interesting to note that Altankov et al. has found grafting density to regulate the bioactivity of adsorbed proteins, specifically fibronectin. While total protein adsorption decreased with higher grafting densities, fibroblast adhesion was optimized at an intermediate grafting density, likely due to the hydrophilic preservation

of fibronectin conformation and steric protection from biodegradation achieved by the incorporation of PEG.(15)

Surface interactions with the polymer may affect the conformation of surface bound polymer chains as well as the distribution of polymer density near the surface. It has been postulated that stronger polymer-surface interactions will increase steric repulsion at the surface level as well as compete with proteins for potential adsorption sites. This enhanced ‘thermodynamic’ barrier to protein adsorption comes at the cost of the longer range ‘kinetic’ barrier of polymer density and steric repulsion, preventing proteins from reaching the surface.(8) PEG, however, is unlikely to experience strong attractions to the surfaces it is grafted to, because it is neutral and acts strongly hydrophilic.

Molecular weight is often the first and easiest parameter investigators have experimentally manipulated. Obviously for a given polymer architecture, changes in the molecular weight will manifest in different chain lengths. Longer chains display more flexibility and thus contribute to enhanced steric repulsion by nature of their larger entropies and excluded volumes. Accordingly, molecular weight has been deemed important in kinetic barriers and not thermodynamic barriers as steric repulsion is seen as a means of the former.(8, 9) Longer chains have been shown experimentally to provide higher resistance to protein adsorption(16, 17) and these trends have been matched by cell adhesion.(17) Yet, a higher ether content has been found to decrease protein adsorption in PEG-like plasma polymer films that measured similar interaction forces, suggesting an enthalpic advantage to longer chains as well.(18) Regardless, protein adsorption has been shown sensitive to molecular weight for PEG chains only below 2 kDa.(7, 19) In general, PEG has been considered relatively more flexible than other polymers of similar chain lengths, with the flexibility being quantifiable, for instance, by ¹³C-NMR.(7) However, short chain PEGs and long chain PEGs have been speculated to contribute to protein resistance via different mechanisms (i.e. hydration layer vs. steric repulsion) and in fact, a number of studies have discovered that protein resistance can be optimized with strategies that incorporate both long chain PEGs and an “underbrush” of short chain PEGs.(20, 21) Most research involving the actual engineering of biomaterials has yet to distinguish between the kinetic or thermodynamic barriers. For this reason some have argued that long-term equilibrium based protein resistance will only depend on grafting density as PEG chains consume potential protein adsorption sites and that exploitation of PEG steric repulsion may be a futile aim for biomaterial research.(9)

The grafting of ‘star’ polymers (polymers with multiple linear chain arms connected at a single point) is the best known chain architecture modification strategy to achieve superior surface coverage. Because multiple arms are brought together, star polymers (and branched polymers in general) increase the polymer density and steric exclusion volume at surface pinning sites. However, for the same reasons, star polymers do not achieve the same grafting density as linear polymers, as they experience enhanced polymer-polymer repulsion. While the use of poor solvents has been known to increase the grafting density of linear PEG (near the cloud point), optimal grafting density for star PEG was found at higher concentrations in good solvents.(10, 22) Still, under optimal grafting conditions where star PEG achieves the same volume fraction and higher overall polymer density compared to linear PEG, Irvine found higher amounts of small protein adsorption to the star PEG grafted surface.(10) He reasoned that because intermolecular crowding near the branch points of star PEG forces extended chain conformations, regions of low polymer density lie between the star molecules and between the centers of the molecules and the grafting surface. Thus, while these regions of low PEG density may still provide a kinetic barrier to protein diffusion, protein may eventually diffuse between the intermolecular edges and into the region adjacent the surface where they have space to eventually adsorb. Densely packed chains of linear PEG, on the other hand, require virtually simultaneous protein diffusion and adsorption due to the dense steric barrier providing repulsion at the surface. Groll has devised a grafting strategy that use star polymers with highly reactive groups, isocyanates, to overcome this obstacle through intermolecular cross-linking of the star PEG into a dense polymeric coating that resists protein adsorption at least as well as grafted linear PEG.(22) Andrade developed amphiphilic block copolymer surfactants containing PEG and hydrophobic blocks of either polypropylene oxide (PPO) or polybutylene oxide (PBO) that also show dependency on the copolymer architecture (linear vs. star). Chain flexibility was believed to increase the protein resistance of block copolymers over alternating block copolymers with the same PEG content despite its reduced grafting density at the same concentration.(5) While the architecture of star polymers is contentious in terms of protein resistance, it is agreed that at least for star polymers with larger numbers of arms, the increased surface density of functionalized end groups is appealing for engineering bio-functionalized surfaces, for instance ones that can elicit stronger surface mediated specific cell adhesion.(10, 23)

A more complicated explanation relates PEG’s protein resistant properties to its unique solution properties, stemming from what is believed to be a unique molecular structure. Many of

the theories that explain PEG's seemingly unique high resistance to protein adsorption relative to similar hydrophilic polyethers cite a high degree of water organization within PEG/water complexes that extends beyond the first hydration shell.(24, 25) This coordination between the PEG chains and water molecules (comprising up to 80% volume) additionally restricts conformational entropy upon protein-induced compression of the PEG chain – a step necessary for adsorption.(26, 27) An experimental survey of self assembled monolayers (SAMs) functionalized with an array of chemical moieties revealed that in addition to neutral charge and hydrophilicity, all functional groups that performed well at resisting protein adsorption were hydrogen-bond acceptors and not hydrogen-bond donors.(2) Another study found drastic improvement in resistance to protein adsorption for microcontact printed PEG comb polymers if the dry, printed surface was first incubated in water for 2 h before being immersed in the protein solution.(28) PEG is unusually soluble in water relative to other polyethers such as considering poly(methylene glycol) and poly(propylene glycol), which are water insoluble. This is believed to be due to a preferred gauche conformation of the PEG conformer that gives it a polar characteristic.(2, 29) This polar feature is lost at high temperatures as the trans conformation becomes favored, helping to explain PEG's curious phase behavior. Trans conformers are thought to predominate in regions of grafted PEG chains closest to the surface while gauche conformers are found at the end of the brush. Many, therefore, believe that the extreme 'hydrophilicity' of PEG derives not from its chemical structure but from a special conformational shape which minimally disrupts the natural hydrogen bonding structure of the surrounding liquid water. If such a theory holds true, hydrophobic driving forces for protein adsorption would be expected to be minimized by PEG.(5) While many studies have evoked even more complicated arguments, this idea is commonly cited in studies where PEG is found responsible for the observed improvement in protein resistance but in which the PEG chains are relatively too short for more complex mechanisms to apply.(30)

Many of the models for designing protein resistant PEG surface coatings assume PEG to be a completely inert barrier layer, which simply must inhibit protein interaction with the underlying surface. Here, it is prudent to address that while PEG coatings are designed to effectively resist protein adsorption to the underlying surface, possibility does exist for PEG-protein interactions and subsequent adsorption to PEG chains. Research has shown the potential for PEG to bind proteins via weak non-specific interactions, strong ternary recognitions, and hydrogen bonding.(11, 13) In one specific instance, grafting of PEG even promoted adsorption of a particular protein, α -

lactalbumin, over the uncoated surface.⁽³¹⁾ Normally, high grafting density found near the brush regime is able to avoid these interactions due to steric repulsion between chains and the reduced entropy of the chains' configuration upon protein adsorption.^(11, 13) Still, it has been found that this kinetic barrier decreases with temperature.⁽³²⁾ By no means are these numerous mechanisms by which PEG may influence protein adsorption fully understood, but it is hoped that as a more comprehensive understanding is obtained, biomaterials, including but not limited to PEG coatings, will be more intelligently designed to overcome their limitations as inert biological interfaces.

1.3 Strategies for PEG Surface Coatings

While, PEG is still most often viewed as the choice material for biocompatible materials, bulk hydrogels formed by standard solution polymerizations are too thick and do not possess the necessary mechanical properties to meet the many applications where protein resistant interfaces are required, especially implantable biomaterials (e.g. a small-diameter vascular stent with a narrow lumen). Thus, PEG has been almost limitlessly surface coupled to an array of base materials, notably poly(ethylene terephthalate) (PET), poly(dimethyl siloxane) (PDMS) or silicone rubber, metals, and polyurethanes by various mechanisms. PEG surface coatings have been fabricated using: chemisorption, physical adsorption, covalent grafting, vacuum deposition, and other intricate means. Each preparation offers distinct advantages and disadvantages. For instance, physical adsorption and chemisorption may lead to reduced stability while chemical grafting may be laborious and lack reproducibility.⁽³³⁾ Oligo(ethylene glycol)s (OEGs) on SAM surfaces were found especially susceptible to decomposition at high temperatures due to interaction with gold surfaces and dissolved oxygen.⁽¹⁴⁾ As an alternative to surface modification, implantable blood contacting materials have also been created from hybrid materials, incorporating PEG and more mechanically suitable materials, such as polyurethane, to create materials with bulk biocompatibility and mechanical strength.⁽³⁴⁾ Virtually all PEG preparations that incorporate PEG with other, less protein resistant polymers, have shown that protein resistance is proportional to the PEG content.^(7, 33, 35) Similarly, when adsorption studies are conducted with multiple distinguishable proteins, it has been repeatedly shown that smaller proteins are more likely to penetrate PEG coatings, as would be expected.⁽³⁵⁾

Block copolymers are common choices for a simple means to incorporate PEG onto a surface and are often adsorbed by either hydrophobic anchor blocks (polystyrene, polypropylene,

etc.) or electrostatic anchor blocks (poly lysine), leaving PEG blocks tethered to the surface. Diblock copolymers are well known to microphase separate, given the flexibility of their chains, to produce distinct, tunable, and reproducible morphologies. Even triblock copolymers (PS-PEG-heparin) have been shown to phase separate into three distinct regions. Pentablock copolymers (heparin-PEG-PS-PEG-heparin) with two surface free chains adsorbed by the center polystyrene (PS) anchor show a reduced but evident ability to microphase separate.⁽³⁶⁾ Many researchers have speculated that microphase separation may actually create surface morphologies that are intrinsically biocompatible. For example, George created nano-scale cylindrical PEG domains in a polystyrene matrix on silicon substrates, the dimensions and inter-domain spacing of which could be reproducibly controlled by molecular weight and processing parameters. Interestingly, he found that while protein adsorption correlated to PEG content, fibroblast adhesion was lower than what would be expected for the amounts of adsorbed protein.⁽³³⁾ In a similar study, it was found that PEG-polyurethane diblock copolymers, could modulate protein adsorption not by explicit changes in PEG content but by modulating the length of the polyurethane “hard” segment to produce microphase domains with different dimensions and amounts of PEG surface exposure. While it was found that the microphase morphology did not affect protein adsorption, per se, protein adsorption did correlate with the surface area of the PEG domains.⁽³⁰⁾

The best example of an electrostatically adsorbed copolymer is a cationic poly-L-Lysine comb polymer with grafted PEG chains, known as PLL-*g*-PEG. Increased ratios of PEG:PLL in PLL-*g*-PEG coatings showed a reduction in protein adsorption for proteins of all sizes and interestingly a higher extent of protein denaturation as measured by time-of-flight secondary ion mass spectroscopy (ToF-SIMS).⁽³⁵⁾ This design uses a cationic anchor block to adsorb to negatively charged biological surfaces, including cell surfaces due to protein glycosylation. It was found that using high molecular weight copolymers to bridge gaps in anionic binding sites, red blood cells and fibroblasts could be sterically stabilized to prevent agglutination and adsorption to fibronectin coated surfaces, respectively.⁽³⁷⁾ PLL-*g*-PEG has also been effectively grafted to metals due to the formation of negatively charged metal oxide films on the surfaces or tissue culture polystyrene due to treatment with oxygen plasma. One such study showed PLL-*g*-PEG on metal remained stable under blood flow and it was found that most of the adsorbed mass from blood was constituted of non-protein serum components,⁽³⁸⁾ while another study showed no protein

adsorption to PLL-*g*-PEG coated titanium from 30 min incubation in plasma at physiological temperature.(39)

A unique method for physical, non-covalent incorporation of PEG into base materials was proposed by Hubbell and Desai, in which PEG is dissolved within the outer layer of a base material via a mutual solvent then physically entangled within the material upon addition of a base material non-solvent to form a surface-physical-interpenetrating-network (SPIN). Protein resistance was confirmed by adsorption assays, fibroblast adhesion studies, and whole blood perfusions. Chain length dependence was revealed with optimal PEG molecular weight of 18.5 kDa.(40)

A few biomolecules show natural resistance to protein adsorption, including albumin, heparin, dextran, and phosphatidylcholine; however, none are as resistant as PEG.(41) Still, many have attempted to create hybrid biomaterials with these biomolecules and PEG in order to instill the biomaterials with unique properties. Ji et al. attempted to combine the blood compatibility of both PEG and albumin by creating a hybrid material consisting of a polystyrene-graft-PEG copolymer, functionalized with stearyl groups at the end of the PEG chains for specific adsorption of albumin. The material demonstrated a decrease in fibrinogen adsorption via competitive and preferential adsorption of albumin in a reversible manner. The authors concluded from this data that they were able to successfully create a hydrophobic-hydrophilic-hydrophobic “sandwich” (PS-PEG-albumin) structure, with the PEG chains providing enough entropy to overcome significant PS-albumin adsorption and looped PEG chains.(42) Albumin has also been internally cross-linked into nanoscale PEG hydrogel coatings,(1) which are used in the current study and, as will be demonstrated, afford a unique synergistic advantage from the albumin component in reducing protein adsorption.

Similar strategies have been implemented with heparin, which is not only protein resistant but a powerful anticoagulant. Because heparin binds to antithrombin-III catalyzing its binding and inhibition of thrombin, heparin functionalized surfaces are popular means to attempt enhanced blood compatibility of biomaterial surfaces. It is further believed that PEG spacers in heparin-functionalized PEG materials not only serves to enhance the protein resistant background but to reduce any steric inhibition of heparin-antithrombin binding that might occur at or near the surface. As such, a 4 kDa spacer was found to optimize results. The incorporation of heparin (hep) onto the PEG surface via a CBABC (hep-PEG-PS-PEG-hep) pentablock copolymer achieved mixed results;

while the combination demonstrated improved clotting times *in vitro* and *ex vivo*, platelet adhesion was actually found to increase *in vitro* with the incorporation of heparin, signaling that it interferes with PEG's protein resistant mechanisms.(36)

Many strategies have also employed plasma glow discharge in order to functionalize surfaces, including but not limited to glass and PET, with covalent attachment sites for PEG coatings.(1, 43, 44) Plasma glow discharge may be employed more universally than other methods to a number of substrates given the high energy applied to create reactive groups. Thin hydrogel films may be additionally be cross-linked on top of substrates by this method. PEG-like plasma polymer films, for example, may be fabricated by applying a diethylene glycol dimethyl ether vapor to a surface under plasma glow discharge.(18) Similarly, small molecular weight PEG (200 Da) was heated to extremely high temperatures and plasma polymerized onto PET.(45) This technique resulted in very thin, yet, highly cross-linked PEG films that retained the hydrophilic nature and platelet resistant properties of PEG, while offering the capability to easily coat intricate and otherwise difficult surface geometries.

A number of emerging strategies rely on surface initiated polymerization of PEG monomers (or macromolecules containing PEG chains) in order to create thin cross-linked films or gels confined to the surface. Hill-West devised a unique strategy for application of a 5-100 μm thick, degradable hydrogel barrier to the blood vasculature *in situ*, by adsorption of a photoinitiator component to the vessel lumen followed by subsequent application and photopolymerization of a PEG precursor solution.(46, 47) This technique allows localized polymerizations in attempt to modulate barrier thickness and create a perfectly molded and tissue adhesive hydrogel via mechanical interlocking. The *in situ* hydrogel demonstrated decreased thrombosis and intimal thickening *in vivo*, after relatively long durations that encompassed complete hydrogel degradation. In a similar manner, surface initiated polymerization of brush polymers containing PEG side chains has been widely adopted and found to resist fibroblasts adhesion for more than 3 weeks.(17, 48, 49) Surface localized hydrogels could potentially create dense PEG layers of controllable thickness that meet the specifications of vascular biomaterials and other surfaces requiring thin but dense preparations.

Most recently, a number of dense PEG coatings have been developed by the application of dense, preformed nanoscale or microscale PEG particles to surfaces.(1, 43, 50, 51) Coating surfaces

with aggregates or particles increases the polymer density within a thin coating, because larger surface coverage can be achieved with the limited amount of surface pinning sites. Nanoscale hydrogel coatings are formed by partial polymerization of star PEG solutions and are hypothesized to achieve nanoscale particle dimensions at intermediate states of gelation due to the effects of steric repulsion delaying the onset of bulk gelation.⁽¹⁾ Larger PEG “microgels” and “microspheres”, on the other hand, have been fabricated by various mechanisms exploiting solubility induced phase separation at transition temperatures, allowing functionalized PEG to be cross-linked into microparticles. One example uses poly(N-isopropylacrylamide) (pNIPAm) cross-linked into the PEG to induce phase separation at elevated temperatures and another uses kosmotropic salts to induce phase transition at elevated temperatures while still maintaining the maximal PEG content, although the latter has not been applied as a coating as of yet.^(50, 52, 53) The use of salt induced solubility effects has been well known for the optimized grafting density of linear PEG near cloud point conditions.⁽¹²⁾ In a similar manner, a PEG hydrogel adhesive was created that uses aldehyde functionalized PEG-PLA polymeric micelles, which are chemically cross-linked with polyallylamines and chemically bind cell surface amines to provide in-situ tissue adhesion.⁽⁵¹⁾ Formation of PEG coatings from larger particles could allow introduction of unique mechanical or chemical properties into protein resistant surfaces.

1.4 *In vitro* and *In vivo* Blood Compatibility of PEG Materials

Biocompatibility, or specifically the lack of nonspecific biological responses, may be nowhere more important than in vascular biomaterials. Because these materials are constantly exposed to blood and its high concentration of serum proteins, they are not only prone to strong inflammatory responses mediated by the circulating antibodies, complement, and leuckocytes, but to blood coagulation mediated by circulating platelets and plasma coagulation factors. While relatively good biocompatibility may sustain implants in larger vessels in which fast blood flow prevents the build-up of thrombus formation, extraordinary biocompatibility must be obtained for stent coatings and vascular grafts of small diameter vessels (e.g. coronary arteries) in which any blood activation can lead to rapid clotting and occlusion of the vessel. So far no satisfactory materials have been fabricated, yet, PEG hydrogels might provide an answer. Thus, an enormous amount of research is

focused on developing thin PEG based surface coatings which can effectively eliminate nonspecific protein adsorption and platelet adhesion for use in implantable biomaterials.

Thrombosis is a biological response mediated primarily by platelets. Accordingly, the ability of biomaterials to resist platelet adhesion is a common test of blood compatibility. Early studies demonstrated that 100 kDa PEG simply adsorbed to glass could adequately prevent platelet adhesion, but this simple preparation could not prevent blood coagulation.⁽⁵⁴⁾ SEM has shown that under blood flow, 20 kDa PEG hydrogels outperformed silicone rubber and PTFE in resisting platelet adhesion.⁽⁵⁵⁾ The cross-linked star PEG coating developed by Groll and colleagues was tested *in vitro* with whole blood for blood compatibility using a number of assays. The coating showed a significant reduction in plasma levels of thrombin-antithrombin (TAT) and β -thromboglobulin, indicators of coagulation and platelet activated release, respectively, over a non-coated glass substrate. Additionally, the star PEG coating showed decreased platelet adhesion, platelet aggregation, and adsorption of platelet CD41, an activated platelet antigen. However, no reduction in the activated complement marker, SC5b-9, was observed.⁽⁵⁶⁾ An earlier study, did indicate less complement activation *in vitro* (reduced C3a levels) of a PEG and PPO based polyurethaneurea hydrogel over Cuprophan, a cellulose membrane traditionally used in dialysis, but not over polystyrene.⁽⁵⁷⁾

PS-PEG amphiphilic block copolymers showed somewhat surprising results in terms of blood compatibility when compared to cross-linked PEG and PS homopolymer controls. Interestingly, while the PS-PEG copolymer showed a level of success intermediate of the PEG and PS in *in vitro* platelet adhesion and activated release studies as would be expected, *ex vivo* shunt experiments showed the copolymer demonstrating increased clotting times over both the PS and PEG control. This led the authors to suggest that the mixture of hydrophobic and hydrophilic polymers might provide optimal blood compatibility, possibly due to microphase separation.⁽⁵⁸⁾

Another *in vivo* study modified polyurethane heart valves and vascular grafts with sulfonated PEG chains (resembling the structure of heparin modified PEG materials) and implanted them within a canine shunt model for up to 39 days. The materials were examined with SEM post explantation. The sulfonated PEG was found not only to increase blood compatibility, by virtue of significantly reduced platelet adhesion and thrombus formation, but to also significantly improve the biostability of the polyurethane, as evidence by decreased crack formation, decreased calcification,

and no detectable loss in polyurethane molecular weight.(59) This study demonstrates some of the best observed, relatively long term *in vivo* results for a PEG coated biomaterial, but the duration of the study and the relevancy of the shunt model studied by no means assure the biocompatibility required for permanent implantation of device such as a small diameter vascular graft.

The lack industrial PEG based biomaterials in clinical use today stems from discrepancies in outcomes between *in vitro* and *in vivo* results. While studies have shown exceptional promise for these materials with protein adsorption (e.g. fibrinogen) and even cellular adhesion (e.g. platelet) assays *in vitro*, the success has not been matched in *in vivo* and *ex vivo* experiments. These results could imply that *in vivo* results may be affected by more than just the PEG grafting parameters discussed earlier, including grafting density, chain length, etc. A thorough comparison of *in vivo* and *in vitro* results for PEG coatings (adsorbed copolymers and covalent grafting) on various materials showed mixed results. *In vitro* PEG modification of all surfaces showed 70-95% reduction in fibrinogen adsorption, except for ePTFE most likely due to poor grafting capability. *In vivo*, decent results were observed with PEG grafting to metallic stents (greater than 85% reduction in thrombus formation), especially nitinol, with only moderate improvements on polyethylene, silicone rubber, and glass and virtually no improvement with grafting on polyethylene terephthalate (PET). The authors hypothesized that surgically induced tissue damage leading to platelet activation and aggregation is primarily responsible for these discrepancies, as *in vitro* experiments do not test resistance to large platelet aggregates. These aggregates will experience increased surface attraction and could force post-compression adsorption of the PEG to hydrophobic surface materials. Thus, they ultimately recommend implementing this consideration in future biomaterial designs but also do not discount that experimental conditions such as flow and anticoagulants (e.g. heparin for syringe drawing of blood) may contribute minor roles to some observed differences as well.(41) It is worth noting, that it becomes much more difficult to tease out the effects of individual material components and parameters *in vivo* as various contributing mechanisms of biocompatibility may work synergistically under whole flowing blood.(36) Thus, while *in vivo* experiments may better characterize the ultimate blood compatibility of biomaterials, *in vitro* experiments are still fundamentally necessary to determine the basic scientific mechanisms behind biocompatibility in order to implement better designs.

1.5 Stem Cells and Biomaterials

Stem cells are cells characterized by their ability for self-renewal and ability to differentiate into any cell type found within a particular organism. In 2006, Yamanaka et al. was the first to successfully demonstrate that pluripotency could be induced in somatic cells by the induction of four transcription factors: *Oct4* (O), *Sox2* (S), *Klf4* (K), and c-Myc (M).⁽⁶⁰⁾ Induced pluripotent stem cells (iPSCs) resemble embryonic stem cells (ESCs) but alleviate ethical concerns of sourcing and provide an appealing alternative to somatic cell nuclear transfer and cell fusion for the reprogramming of somatic cells. Pluripotency is believed to be regulated by 10-20 transcription factors altogether, including the “Yamanaka factors” (*OSKM*) and other key factors such as *Lin28* (L), and *Nanog* (N), but as shown can be induced by upregulating combinations of only several of these factors. Reprogramming is commonly performed with viral vectors that randomly integrate genes for the transcription factors into cellular DNA, but non-integrative means including plasmids, (e.g. minicircles), synthetic mRNAs, microRNAs, proteins and synthetic molecules have been implemented for reprogramming as well.^(61, 62) As many of these factors are also related to tumor formation (esp. *c-Myc*), safety can be improved by reducing the number of factors or amount of upregulation, but at the cost of an already low efficiency (< 1%) of iPSC generation.⁽⁶³⁾ Yet, stoichiometric optimization of *OSKM* transcription was found to be more efficient than equal overexpression of all the same factors.⁽⁶⁴⁾ Subtle gene expression signatures conserved among iPSCs have been found which distinguish them from ESCs⁽⁶⁵⁾ and despite very similar transcription profiles,⁽⁶⁶⁾ relatively more heterogeneous gene expression as well as slower growth rates have been observed in iPSCs relative to ESCs.⁽⁶⁷⁾ Also, transcriptional reprogramming has shown signs of epigenetic memory via methylation patterns that bias differentiation of iPSCs back toward their original cell type,⁽⁶⁸⁾ and thus, reprogramming has been found more efficient on adult stem cells than fully differentiated somatic cells.⁽⁶³⁾ Furthermore, overexpression of certain genes may also cause potential immunogenicity, even if cells are autologously sourced.⁽⁶⁹⁾ Thus, despite the common notion that ESCs and iPSCs may now be used interchangeably in research, evidence suggests some caution in drawing these assumptions.

Stem cells are naturally found in specific physical and biochemical environments, or niches, which preserve the cells’ pluripotent nature and promote self-renewal until cells are stimulated to migrate from these niches. Thus, *in vitro* culture of stem cells relies on artificial material substrates to

replicate the non-soluble environmental signals that are necessary for either stem cell maintenance and expansion or differentiation. Adherent stem cells can be influenced in a number of manners by the properties of their biomaterial substrates, including: surface chemistry, nanotopography, mechanical properties, morphological structures (e.g. fibrils, pores, etc.), and electrical properties.⁽⁷⁰⁾ Hydrogels fabricated from synthetic polymers represent ideal choices for stem cell substrates in that both their biochemical and mechanical properties can be tailored relatively easily, through covalent functionalization of polymer chains and by polymerization with modulation of cross-linker density, respectively.^(71, 72) Cross-linker density will also impact the permeability of hydrogels, though, which can greatly impact either drug delivery or paracrine signaling of encapsulated cells. In fact, hydrogel design has been shown to influence differentiation through selectively modulating permeability of paracrine factors, with cells seeded on the surface of hydrogels more prone to differentiation than cells seeded within deep microwells.⁽⁷³⁾ Also, degradability can be incorporated into hydrogels, either by copolymerization of hydrolytically degradable polymers (e.g. poly(lactic acid); PLA), formation of hydrolytic esters during polymerization, or cross-linking of enzymatically degradable peptide sequences.^(53, 74) While hydrogels can be loaded for diffusive drug release of large proteins, smaller molecules as well may be released by covalent tethering with degradable linkers or incorporation of affinity based binding molecules, such as cyclodextrin or heparin. Many of these hydrogel features may be spatially regulated, as well, by laser-guided photopatterning for initiation of the various chemical reactions.⁽⁷⁴⁾ PEG hydrogels formed around encapsulated stem cells have been used for both preservation of stemness and defined differentiation of stem cells, showcasing the versatility of the synthetic polymer matrix in customizing environments for specifically designed cellular responses.^(71, 72, 75) For instance, Hubbell et al. used the same MMP-degradable hydrogel for differentiation of pluripotent stem cells (PSCs) into cardiomyocytes as for expansion of ESCs by modulating the elastic modulus to match that of cardiac tissue as well as altering the selection of adhesion peptides to stimulate specific target integrins for early cardiogenesis. By modulating combinations of adhesiveness, degradability, and stiffness, the authors were also able to regulate the size of cell clusters that grew from single cells, as well, which may also contribute to differentiation pathways.^(72, 75)

More often, stem cells have been cultured on 2-dimensional substrates such as tissue culture polystyrene (TCPS), rather than being encapsulated within hydrogels, and as such rely on adsorption

of specific extracellular matrix proteins or non-specific adsorption of serum proteins to maintain their surface attachment. However, surface chemistry of material interfaces has long been known to affect the conformation of adsorbed proteins, which may in turn modulate cell adhesion or even differentiation. For instance, fibronectin conformation and importantly presentation of its $\alpha 5 \beta 1$ integrin binding domain that is primarily responsible for cell adhesion were modulated on functionalized SAMs, with strong $\alpha 5 \beta 1$ binding dominating on hydrophilic surfaces (esp. OH functionalities) and weaker binding via αV integrins on more hydrophobic SAMs (esp. CH_3 functionalities).(38) Using this information, the same group modulated important integrin signaling, showing cell differentiation and mineralization with immature osteoblasts adhered to fibronectin coated SAMs presenting functional groups that greatly favored $\alpha 5 \beta 1$ integrin binding over αV integrin binding.(76) A similar example exists, wherein native collagen I matrices were discovered to induce adipogenic differentiation of bone marrow stromal cells via $\alpha 1 \beta 1$, $\alpha 2 \beta 1$ integrin signaling, yet, denatured collagen I matrices induced osteogenic differentiation via $\alpha V \beta 3$ signaling from sites normally hidden within the triple helical structure.(77) In another instance, a chemically defined aminopropylmethacrylamide (APMAAm) hydrogel surface developed for ESC culture in chemically defined medium, was found to promote ESC adhesion via adsorption of albumin,(78) which is normally found to resist cell adhesion, especially when applied to hydrophilic TCPS.(24) Evidence from this study suggested protein unfolding at the interface accounted for the cell adhesion, but clearly hydrophilicity alone cannot account for the change in conformation as both surfaces were relatively hydrophilic. For these reasons, PEG hydrogels or PEG-functionalized surfaces make attractive candidates as stem cell substrates, in that they promote very minimal protein adsorption and cannot support cell adhesion without covalent incorporation of specific ligands. Proteins tethered to PEG surfaces are assumed to maintain their native conformations and thus, it becomes much easier to design specific cell receptor responses and avoid unanticipated ones. Additionally, peptides containing binding sequences may be easily conjugated as well, which precludes any concerns over which domains are being recognized. As the many conflated mechanisms behind stem cell decision making are yet to be fully elucidated, substrates that act as blank slates upon which specific cues may be independently inserted and modulated will prove valuable in expanding the multipotent capabilities of stem cells.

Chapter 2[†]

Ultralow Protein Adsorbing Coatings from Clickable PEG Nanogel Solutions

2.1 Introduction

While materials including polyoxazolines(79) and betaines(80-82) have garnered significant attention as biocompatible coatings, PEG is still widely used for the surface modification of materials requiring “inert” or specifically defined interactions with biological environments. Strategies for incorporating PEG have evolved from covalent grafting of linear or star shaped chains(23, 83) and adsorption of block copolymers(5, 33, 38) to surface initiated polymerization of patterned brush coatings(49) or microscopically thin hydrogels,(46, 84, 85) and deposition of preformed hydrogel particles.(1, 86-88) However, advances have not kept pace with the demands of implantable biomaterials as well as *in vitro* diagnostics(86, 89) both of which remain limited by the lowest levels of protein adsorption achievable.(90-92)

PEG coatings derived from microgel or nanogel solutions allow convenient means to create dense yet thin hydrogel coatings (< 100 nm), to enhance areal coverage on surfaces with sparse covalent attachment sites, and to create modular surface assemblies. Recent focus of their synthesis has targeted drug delivery applications(93-96) more so than non-fouling surface coatings.(1, 87, 88, 97, 98) Thus, many of these microgels are fabricated with hydrophobic components, often in the form of an amphiphilic copolymer, for sequestration of hydrophobic drugs along with PEG for water solubility and prolonged circulation.(93, 95, 96) Most often microgel solutions are fabricated using free radical polymerization with PEG-diacrylates,(87, 97, 98) although examples formed from addition polymerization of macromers has been well reviewed.(99) Microgel size is typically determined by the surfactant added to produce aqueous emulsions(87, 96) or inverse emulsions,(88,

[†] Chapter 2 has been adapted with permission from the following published manuscript: C. D. Donahoe et al., Ultralow protein adsorbing coatings from clickable PEG nanogel solutions: Benefits of attachment under salt-induced phase separation conditions and comparison with PEG/albumin nanogel coatings. *Langmuir* 29, 4128 (Mar, 2013).

100) although nanogels or small microgel solutions have been fabricated without the use of surfactants or organic solvents altogether.(1, 94) Relatively fewer examples exist of microgel solutions applied as surface coatings compared to their applications as drug delivery vehicles. Libera et al. has developed several examples of such coatings including PEG-amine microgels cross-linked *in situ* in the dry state with an electron beam(101) and PEG-diacrylate/acrylic acid microgel solutions electrostatically deposited on PLL.(88) Lyon et al. also has created various microgel compositions of PEG and pNIPAm to allow thermal collapse of the microgels.(97) These microgel solutions have been attached to amino-silanated glass via EDC coupling or electrostatic interactions after centrifugation or spin coating.(50, 87) In a unique approach Norde et al. studied protein adsorption and bacterial adhesion to a coating of PEG-coated silicon nanoparticles that were electrostatically deposited and cross-linked to each other with PEG-diacrylate to provide a more mechanically robust coating.(98)

We previously demonstrated multiple rounds of resistance to *in vitro* fibrinogen-promoted cell adhesion of thin coatings produced from PEG nanogel solutions(1) and quantified lower numbers of individually adsorbed proteins when compared to other popular surface coatings, including covalently coupled monolayers of: bovine serum albumin (BSA), BSA/gelatin, dextran, linear polyacrylamide, glucose, IgG, linear PEG, and multi-arm PEG.(89, 102) Interestingly, a hybrid nanogel coating of PEG cross-linked with BSA, outperformed a 100% PEG nanogel coating, although a monolayer of eight-arm PEG was shown to be more repellent than a monolayer of BSA.(89) While the mechanism behind this phenomenon remains unknown, elimination of the albumin component remains desirable for implantable biomaterials due to possible immunogenic responses(103) and gradual degradation of the protein. Here we illustrate methods for the attachment of clickable 100% PEG nanogel solutions that significantly improve the coating's resistance to protein adsorption, as measured by single molecule counting.

Numerous chemistries have been employed to expand the versatility of PEG end group functionalities and conjugation strategies. 'Click' chemistry has become immensely popular for aqueous bio-conjugations due to the high yields that are quickly achievable under mild physiological conditions.(104) Because these reactions tend to be highly specific and exclude native biomolecules, they may be incorporated orthogonally with various other reactive groups allowing construction of more sophisticated and highly functionalized biocompatible materials.(105, 106) Despite toxicity concerns for using copper in biological applications, copper-catalyzed azide/alkyne cycloaddition

(CuAAC) remains the most popular click reaction, and PEG polymers are frequently modified with these functional groups.⁽¹⁰⁷⁾ Alternatively, a variety of cyclooctynes have been designed by Bertozzi et al. and implemented in strain-promoted azide/alkyne cycloadditions (SPAAC) in order to obviate the need for a copper catalyst.⁽¹⁰⁸⁻¹¹⁰⁾ Additionally, photo-initiated thiol-ene and thiol-yne reactions between thiols and either alkenes or alkynes have garnered substantial attention.^(111, 112)

These click chemistries have been widely explored for fabricating PEG hydrogels,⁽¹¹³⁻¹¹⁶⁾ most notably by Anseth et al. and Bowman et al.,⁽¹¹⁷⁻¹²¹⁾ as well as other hydrogel materials such as poly(vinyl alcohol) or hyaluronic acid.⁽¹²²⁻¹²⁴⁾ The step-growth mechanism of these click reactions provide for homogenous networks and favorable mechanics which are tunable by the PEG molecular weight.^(113, 114, 116, 118, 121) Hydrogels have been photopatterned using both photonic reduction of the copper catalyst to produce CuAAC hydrogels^(117, 125) and photonic initiation of thiol-ene reactions, usually for functionalization of residual end groups with cysteine-containing peptides, such as RGD.⁽¹¹⁹⁻¹²¹⁾ While click chemistry has been used to create or more commonly to functionalize materials below the macroscopic scale, including polymers, dendrimers, nanodiamonds, microbeads, and micelles,^(112, 126-133) we have found only one example where it was used in cross-linking PEG to fabricate microgel solutions, which were cross-linked within mesoporous-silica templates.⁽¹³⁴⁾ Surfaces have also been endowed with clickable moieties by grafting clickable PEGs to silicon or glass substrates or by chemically modifying PEG surfaces after deposition.⁽¹³⁵⁻¹³⁸⁾ SPAAC moieties have also been applied to cellular surfaces, without the concern of copper toxicity.⁽¹³⁹⁾ Deposition of azide-terminated alkanethiolates onto gold surfaces allows for the creation of clickable SAMs.^(140, 141) Alternatively, thin coatings including a polyelectrolyte film⁽¹⁴²⁾ and PEG hydrogel⁽¹¹⁵⁾ have been cross-linked via click reactions on top of silicon or glass surfaces. Click chemistry has been used for the covalent attachment of PEG coatings to the underlying surface by using substrates such as: alkyne or thiol functionalized silanes and resins,^(115, 143, 144) azide functionalized epoxy resins,⁽¹⁴⁵⁾ or a unique cyclooctyne functionalized epoxy silane.⁽¹⁴⁶⁾

In this study we exploited separate, sequential click reactions for the cross-linking of PEG as well as its attachment to glass surfaces to form thin hydrogel coatings. Using CuAAC we found that we could rapidly generate nanogel solutions from multi-armed PEG-azide and PEG-alkyne monomers and then easily halt the polymerization with addition of a copper-chelating agent to

prevent bulk gelation (Figure 2.1A). The ability to halt nanogel growth and solution reaction is a unique feature of this system that allows for stable long-term storage, limitless reaction times on surfaces, and monolayer coverage with the hydrogel coating. Nanogel solutions were mixed with a photoinitiator and attached to mercaptosilanated glass using the UV thiol-yne reaction (Figure 2.1B). We quantified protein adsorption to this clickable nanogel coating using TIRF microscopy, which enabled single molecule (i.e. single protein) counting, but determined that hybrid PEG/albumin nanogel coatings still greatly outperformed the 100% PEG nanogel coatings attached in PBS. However, by attaching the clickable nanogel coatings in the phase-separated state using high concentrations of a kosmotropic salt, we were able to double the packing density (Figure 2.1C) and drastically reduce protein adsorption. Attaching linear PEG under phase separation, or “cloud point”, conditions has been well known to successfully increase grafting density though similar results were not obtained with star PEG.^(10, 44, 147) We also studied the effects of cross-linking density within the nanogel coating by surface cross-linking residual end groups after attachment (Figure 2.2A), which could likewise be performed under phase separation conditions with the addition of salt (Figure 2.2B). These modifications produced a surface that was comparable the PEG/albumin coatings by TIRF. However, AFM revealed drastic changes in coating morphology when coatings were further cross-linked and long-term resistance to cell adhesion was lost. Thus, the best 100% PEG coating that we have studied to date is a clickable nanogel coating attached with salt in the phase-separated state. Other 100% PEG nanogel solutions cannot be conjugated in the phase-separated state due to bulk polymerization, indicating a potentially important orthogonality of copper-catalyzed click chemistry.

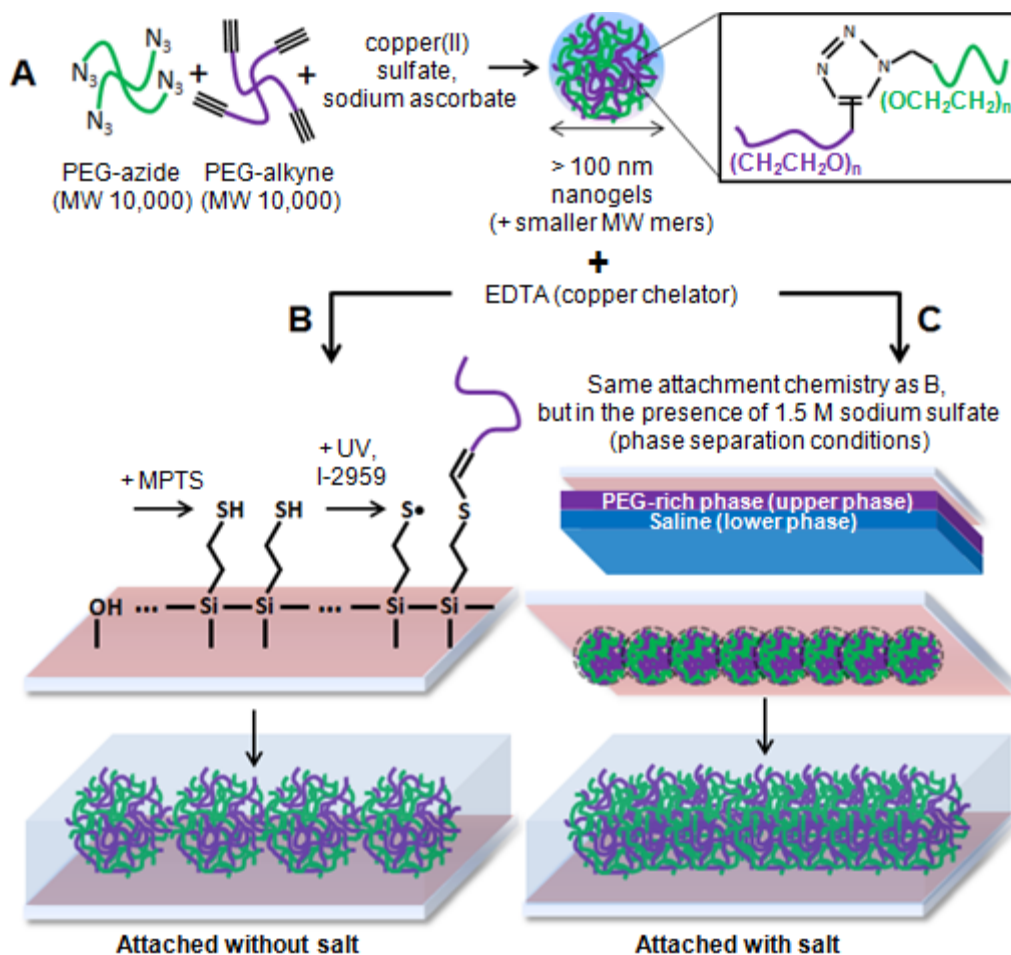


Figure 2.1: Strategies for synthesis and attachment of clickable nanogel solutions. (A) Clickable nanogel solutions were synthesized via CuAAC by mixing solutions of clickable four-arm PEG monomers with copper(II) sulfate and sodium ascorbate. The cross-linking reaction was halted by the addition of a copper chelator, EDTA. (B) Nanogel solutions were incubated on top of mercaptosilanated surfaces with a photoinitiator, Irgacure 2959, and attached under UV irradiation. (C) Alternatively, nanogel solutions could additionally be mixed with kosmotropic salts (e.g. sodium sulfate) to induce phase-separation and incubated under inverted mercaptosilanated surfaces for UV attachment as in (B), resulting in increased packing density.

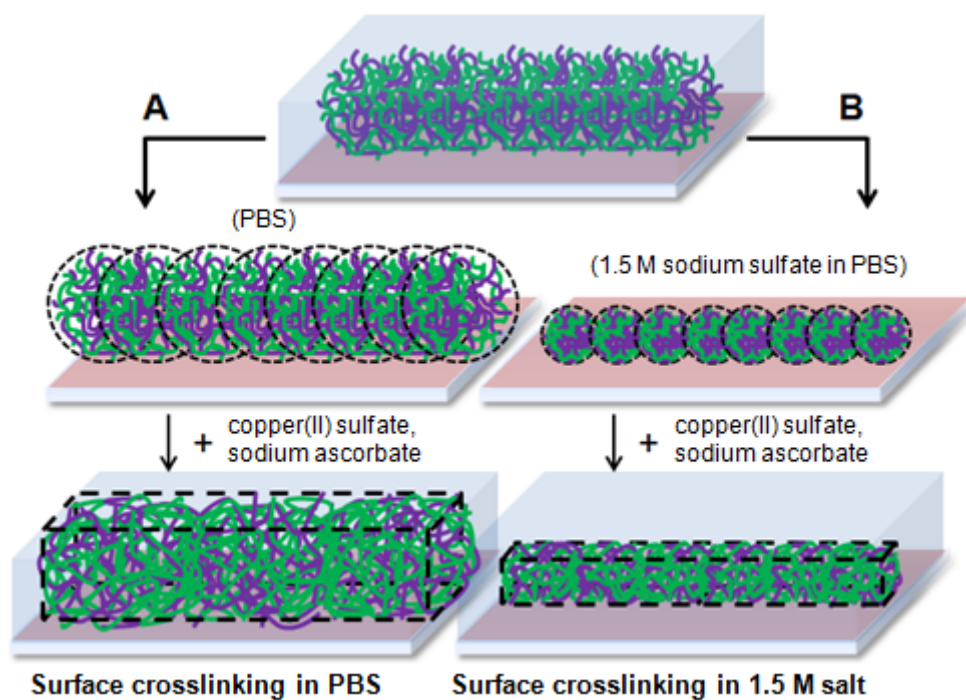


Figure 2.2: Strategies for surface cross-linking of nanogel coatings. Clickable nanogel coatings were able to undergo additional internal cross-linking after covalent attachment to surfaces. (A) This “surface cross-linking” was implemented by incubating the surface in a solution of copper(II) sulfate and sodium ascorbate. (B) Alternatively, kosmotropic salts could be included, as well, for the induction of phase-separation within the clickable nanogel coating during cross-linking, presumably resulting in a more densely cross-linked coating.

2.2 Materials and Methods

2.2.1 Materials

Unless otherwise specified, all reagents were purchased from Sigma Aldrich (Saint Louis, MO, USA). Four- and eight-arm PEG-OH MW 10,000 (Creative PEGWorks, Winston Salem, NC, USA), four-arm PEG-alkyne MW 10,000 (Creative PEGWorks), PEG-dithiol MW 3,400 (Creative PEGWorks), and dibenzocyclooctyne (DBCO-acid, Click Chemistry Tools, Scottsdale, AZ, USA) were purchased commercially. Eight-arm PEG-vinyl sulfone (PEG-VS),⁽¹⁾ eight-arm PEG-amine,⁽¹⁾ four-arm PEG-azide,⁽¹⁴⁸⁾ and four-arm PEG-cyclooctyne⁽¹⁴⁸⁾ were all synthesized from PEG-OH MW 10,000 as described previously. PLL-*g*-PEG was synthesized in a previous study from PLL MW 375,000 and monomethoxy PEG MW 5,000 at a 7:1 grafting ratio.⁽³⁷⁾

2.2.2 Nanogel Solution Syntheses

Clickable nanogel solutions were synthesized from four-arm PEG-azide and four-arm PEG-alkyne. Each was dissolved to a concentration of 200 mg/mL in a solution of phosphate buffered saline (PBS) already containing 50 mg/mL sodium L-ascorbate and filtered with 0.22 μ m syringe filters. PEG solutions were mixed at equimolar ratios of azides to alkynes, and copper(II) sulfate (10 mg/mL in water) was added at 0.004 equivalents per azide/alkyne pair (4 μ L per 1 mL of PEG) then immediately vortexed. The mixture was aliquoted into 1.5 mL microcentrifuge tubes and rotated at 40 r.p.m. at room temperature until a nanogel size of 100 nm was surpassed as measured by dynamic light scattering (DLS) in a manner described previously.⁽¹⁾ The reaction was halted by adding 10 equivalents of ethylenediaminetetraacetic acid (EDTA; 0.1 M in water) per copper (16 μ L per 1 mL of nanogel solution) and vortexed immediately. Nanogel solutions were allowed to mix for an additional hour and then frozen at -80 °C. Nanogel solutions cross-linked via Michael addition chemistry were synthesized from PEG-VS and either BSA or PEG-amine as described before and diluted to 100 mg/mL to slow the solution reaction before freezing at -80 °C.⁽¹⁾

2.2.3 Size Exclusion Chromatography (SEC)

Molecular weight distributions were approximated by SEC using a 300 x 8 mm gel filtration column packed with 5 μ m particles with 150 Å pore size (Keystone Scientific Inc., Bellefonte, PA,

USA). A chelated clickable nanogel solution (200 mg/mL), its precursor PEG-alkyne solution (100 mg/mL) including sodium ascorbate (25 mg/mL), and various solution standards of different MW linear PEGs dissolved in PBS were each injected (10 μ L) into a mobile phase of 0.5 M dibasic sodium phosphate in water flowing at 1 mL/min. The column flow through was analyzed with a UV detector at 200 nm and the peaks were integrated using *XCalibur* software between time points specified by the peak retention times of the linear PEG standards.

2.2.4 Nanogel Coatings

All nanogel coatings were attached to 12 mm round glass coverslips (Ted Pella Inc., Redding, CA, USA) or, for TIRF, 24 x 40 mm rectangular coverslips (Fisher Scientific, Waltham, MA, USA) which were mercaptosilanated as described before.⁽¹⁾ Briefly, coverslips were washed with water, ethanol, and acetone then immersed in 5% (v/v) solutions of (3-mercaptopropyl)trimethoxy silane (MPTS) in acetone for 1 h at room temperature. Coverslips were washed with acetone and cured for 25 min at 110 °C before being stored under vacuum. Volumes of clickable nanogel solutions were mixed 1:1:1 with the photoinitiator 2-hydroxy-4'-(2-hydroxyethoxy)-2-methylpropanone (Irgacure-2959 or I-2959; 0.15 mg/mL in water) and either PBS or 1.5 M sodium sulfate in PBS. Nanogel solutions without sodium sulfate were incubated on top of the glass surface and under a UV flood lamp (365 nm, 100 W) for 20 min to allow surface attachment by thiol-yne reaction. Alternatively, the coverslips were inverted on top of 100 μ L droplets of nanogel solutions which did include sodium sulfate, sandwiching the mixture with an upper PEG-rich phase between the mercaptosilane above and a hydrophobic glass dish below (treated with Sigmacote). After 5 min to allow complete phase separation, these coverslips were exposed to the same UV treatment. Michael addition nanogel solutions were incubated on top of the coverslips at 37°C for 1 h (PEG-VS/BSA) or 40 min (PEG-VS/PEG-amine) and unreacted vinyl sulfone groups capped at 37 °C with either 100 mg/mL PEG-dithiol in PBS for 30 min for TIRF or 50 mg/mL BSA or PEG-amine overnight for cell adhesion studies. All coverslips were washed thoroughly with PBS. Clickable nanogel solutions were also attached to glass without UV. Briefly, glass was silanated with (3-chloropropyl)trimethoxy silane as with MPTS above, then subjected to halide-azide exchange by incubating the coverslips with 5 mg/mL sodium azide in dimethylformamide (DMF) for 48 h at room temperature under gentle agitation.⁽¹⁴⁹⁾ The azidosilanated coverslips were then incubated with solutions of 200 mg/mL four-arm PEG-cyclooctyne in PBS for 30 min at 37 °C and washed. Clickable nanogel solutions were finally

incubated with the cyclooctyne functionalized surfaces for another 30 min at 37 °C, attaching via SPAAC. Also, non-silanated coverslips were incubated with 2 mg/mL PLL-*g*-PEG in PBS (0.22 µm filtered) for 1 h at room temperature,(37) as a standard for TIRF and cell adhesion.

2.2.5 Total Internal Reflection Fluorescence (TIRF) Microscopy

Single molecule counting of adsorbed proteins was performed with TIRF microscopy in custom flow cells which attach to the silanated coverslips to form ~50 µL channels. Nanogel coatings were fabricated *in situ* as described above, with flow cells being inverted during the UV incubation of clickable nanogel solutions attached with salt. For each experiment, a fresh solution of bovine fibrinogen was fluorescently labeled overnight at room temperature with Cy5 dye (GE Healthcare Biosciences, Pittsburgh, PA). The fibrinogen was dissolved at 2.5 mg/mL in 0.1 M sodium carbonate buffer (pH 9.3) and mixed with 171x molar excess of Cy5 (10 mg/mL in dimethyl sulfoxide; DMSO). Unreacted dye was removed by dialysis. Nanogel coated flow cells were washed with 1 mL of PBS and incubated with the Cy5-labeled fibrinogen for 1 h in the dark at room temperature. The flow cells were washed again and imaged as described before.(89) Briefly, the surfaces were excited with a 640 nm, 40 mW laser and imaged with a Nikon TE-2000 inverted microscope (Nikon, Melville, NY). Five 263.6 µm x 263.6 µm images of each surface were processed with MetaMorph and Matlab, using the average count for each surface. Protein counts were normalized against standards in each experiment to account for variations in fibrinogen concentration and labeling efficiency. Statistical significance ($p < 0.05$) was calculated in Matlab using ANOVA with a post-hoc Tukey-Kramer test.

2.2.6 Quartz Crystal Microbalance with Dissipation (QCM-D)

Mass deposition was measured on 5 MHz quartz crystal sensors with 50 nm silicon dioxide coatings (QSX-303, Q-Sense, Sweden). Sensors were cleaned prior to each experiment with 10 min treatment in a UV-ozone chamber, 30 min incubation in 2% sodium dodecyl sulfate (SDS), thorough rinsing with deionized water, drying under pure nitrogen, and 10 min more of UV-ozone treatment. Cleaned sensors were silanated and immediately placed in the chambers of a Q-Sense E4 (Q-Sense). PBS was flowed over the sensors at 0.1 mL/min for at least 1 h at 22 °C and frequency (F) and dissipation (D) baselines were recorded. The sensors were removed and functionalized as described above, incubating nanogel solutions without salt on top of the sensors and nanogel

solutions with salt beneath the inverted sensors during UV treatment. Because the sensors are not transparent, UV light was applied from below in the case of the latter. The nanogel coated sensors were returned to the Q-Sense E4 and PBS was flowed over the sensors for 2 h and baselines recorded. The baselines from before and after coating application were stitched together to measure changes in F and D. Clickable nanogel coatings attached without salt remained under PBS within the Q-Sense E4 and underwent no surface cross-linking. Alternatively, clickable nanogel coatings attached with salt were surface cross-linked by changing to a flow of 1.5 M sodium sulfate in PBS for 5 min and then 1.5 M sodium sulfate, 2 mM copper(II) sulfate, and 50 mg/mL sodium ascorbate in PBS. The temperature was raised to 37 °C for all sensors and incubated for 1 h. The clickable nanogel coating attached with salt was washed with a flow of 0.1 M EDTA in PBS for 1 h at 22 °C and then PBS for another 1 h. The temperature was raised back to 37 °C and solutions of 2.5 mg/mL fibrinogen were then flowed over sensors for both conditions and incubated for 2 h. The flow was restored with PBS, after which the temperature was lowered to 22 °C and the sensors were washed for 1 h. Changes in mass were modeled with Q-Tools software (version 3.0.16.555, Q-Sense) from F and D changes between the 22 °C PBS baselines at 0.1 mL/min flow surrounding each step. The third, fifth, seventh, ninth, and eleventh overtones were input into a single-layer Voigt (viscoelastic) model with constant fluid density (1000 kg/m³) and viscosity (1.0 x 10⁻³ kg/(m·s)) assumed.

2.2.7 Atomic Force Microscopy (AFM)

Nanogel coatings were fabricated on round glass coverslips per normal. Surfaces were kept hydrated and examined under PBS in tapping mode at 1.0 Hz scanning rates using a Veeco Nanoman Scanning Probe Microscope (Veeco Instruments, Plainview, NY) and MESP tips (Bruker AFM Probes, Camarillo, CA, USA) with nominal spring constants of 1 N/m and nominal resonant frequencies of 75 kHz.

2.2.8 Cell Adhesion Studies

Nanogel coatings were fabricated on round glass coverslips per normal and incubated with 2.5 mg/mL fibrinogen for 2 h at 37 °C then washed. 3T3 mouse fibroblasts were seeded on the surfaces at 100,000 cells/cm² in Dulbecco's Modified Eagle Medium (DMEM; Life Technologies, Grand Island, NY, USA) supplemented with 10% fetal bovine serum (FBS; Atlanta Biologicals,

Lawrenceville, GA, USA) and 1% Antibiotic-Antimycotic (ABAM; Life Technologies) and imaged the next day after gentle washing. Surfaces were reseeded every two days until cell adhesion overwhelmed the surface or until 9 seedings. Cell adhesion could alternatively be promoted by conjugating a cysteine-containing cell adhesion peptide, RGD (Seq: Ac-GCGYGRGDSPG-NH₂; GenScript, Piscataway, NJ, USA), to the nanogel coating using a UV thiol-yne reaction. Briefly, 200 nmol of RGD (MW 1066.12) in 200 μ L of PBS was incubated on the nanogel surface and subjected to UV irradiation for 20 min, allowing covalent reaction between the nanogel alkynes and cysteine thiols. Percentage of surface coverage by adhered cells was approximated for some images using *ImageJ* software.

2.3 Results and Discussion

2.3.1 Synthesis and Characterization of Clickable Nanogel Solutions

Clickable nanogel solutions were successfully created by mixing solutions of four-arm PEG-azide and four-arm PEG-alkyne dissolved in PBS with high amounts of sodium ascorbate and adding small volumes of highly concentrated copper. The rate of growth was effectively modulated with copper concentration (Figure 2.3), which allowed faster production of nanogel solutions than possible with the Michael type addition.⁽¹⁾ These kinetics resemble those achieved by Hu et al.⁽¹²³⁾ To allow sufficient time for DLS measurements, we chose a concentration of 0.004 equivalents per azide/alkyne for most syntheses resulting in reaction times of approximately 2 h to reach 100 nm. Chelation with 10x EDTA stopped the growth in nanogel size and in fact, when solutions were remeasured 1 h later showed slight decreases in hydrodynamic diameter (e.g. from 111.7 to 95.0 nm). The reduction in size might stem from eliminating the pseudo-cross-links formed by copper complexes between PEG-alkynes⁽¹⁵⁰⁾ or increased hydrophilicity of the nanogels in the presence of copper, resulting in more swelling of the nanogel before chelation. We verified the capacity of copper(II) sulfate to complex multiple alkynes by adding a high concentration of copper, 0.5 equivalents, to a 20% (w/v) solution of PEG-alkyne dissolved in PBS with 50 mg/mL sodium ascorbate to form a solid hydrogel. This gel was dissolved when incubated in 0.1 M EDTA overnight. Nanogel formation was further corroborated by the large shift in molecular weight

distribution observed when comparing SEC profiles of PEG-alkyne to that of a 120 nm nanogel solution (Figure 2.4). The shift was quantified by integrating the areas between multiple time points established by linear PEG benchmarks of various molecular weights and showed large increases in fractions larger than PEG 35,000 and PEG 100,000 and a marked decrease in the fraction smaller than PEG 8,000 (Figure 2.5). This demonstrates the presence of nanogels in these partially polymerized solutions, and in much greater proportions than expected from Flory-Stockmeyer statistics.⁽¹⁾

2.3.2 Quantification of Protein Adsorption via TIRF

The ability of the clickable nanogel coatings attached to mercaptosilanated glass to resist protein adsorption was quantified using TIRF microscopy to count individually adsorbed, fluorescently labeled proteins (Figure 2.6). The irradiation time of 20 min used to attach the coatings was selected as long enough to cross-link 100 μ L bulk hydrogels of 50 mg/mL four-arm PEG-alkyne with equimolar amounts of PEG-dithiol, but short enough to minimize evaporation induced from the lamp heat. It is interesting to note that when synthesized,⁽¹⁴⁸⁾ we observed homo-polymerization of PEG-alkyne under UV, but not when using the commercial product. However, Caruso et al. observed homo-polymerization of this same commercial PEG under different conditions.⁽¹²⁵⁾ Controls including Michael addition nanogel solutions of PEG-VS cross-linked with either BSA (VS:BSA) or PEG-amine (VS:Am) were also evaluated. Cy5-labeled fibrinogen was used as a model protein relevant to blood contacting biomaterials, but we found that 1 h incubations at physiological concentration (2.5 mg/mL) saturated even the best coatings, such that adsorbed proteins could not be individually resolved and counted. Adsorption to most nanogel coatings was quantified using a 1:100 dilution of the physiological concentration (Figure 2.6A), while adsorption to several less resistant coatings was quantified using a 1:1000 dilution (Figure 2.6B). Previously, VS:BSA nanogel coatings were shown more resistant to IgG adsorption⁽⁸⁹⁾ and cell adhesion⁽¹⁾ than VS:Am nanogel coatings. Here, we confirmed the extremely low amount of fibrinogen adsorption on the VS:BSA nanogel coatings by TIRF and compared the resistance to the commonly used non-covalent coating PLL-*g*-PEG.

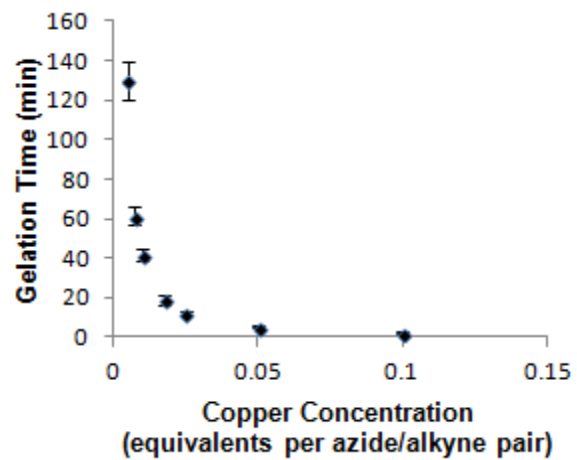


Figure 2.3: Copper-dependent gelation kinetics. Small PEG gels (25 μ L) were formed with a fixed 18% (w/v) PEG concentration and various equivalents of copper. Gelation time was measured to the nearest minute as when the solution became too viscous to pipette. Data are presented as mean \pm standard deviation ($n=3$).

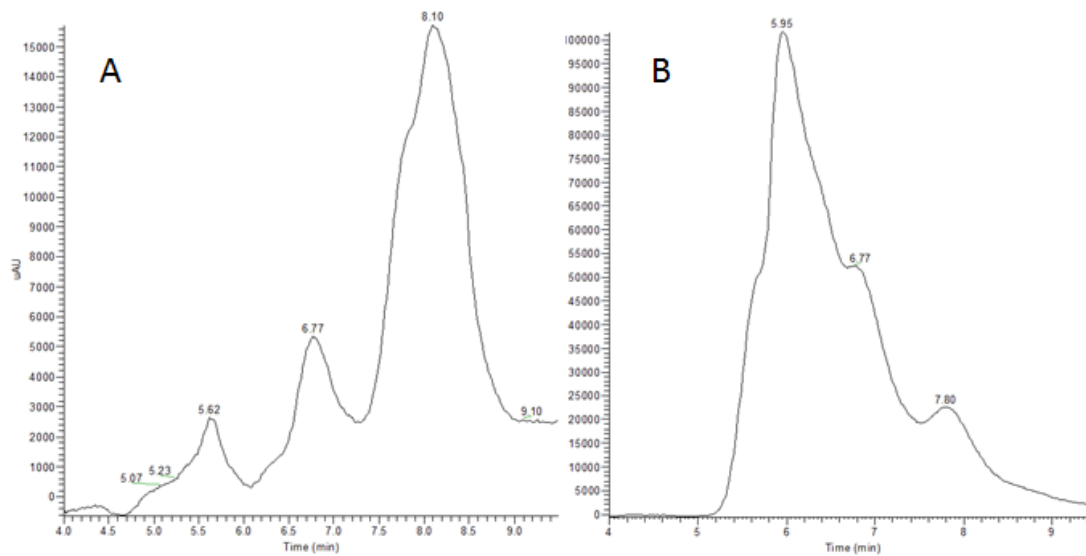


Figure 2.4: SEC profiles of clickable nanogel solution and precursor. SEC profiles monitored over a ~ 9 min period with UV detection at 200 nm of A) 10% (w/v) PEG-alkyne and B) 20% (w/v) chelated clickable nanogel (hydrodynamic radius = 120 nm) solutions show a large shift in the molecular weight distribution that results from partial cross-linking of the nanogel solution.

Linear PEG MW	PEG-alkyne (MW 10,000)	Nanogel (r = 120 nm)
> 100,000	9.22%	32.43%
35,000 - 100,000	2.07%	20.60%
8,000 - 35,000	41.55%	42.09%
< 8,000	47.17%	4.87%

Figure 2.5: Table of molecular weight distributions for clickable nanogel solutions. The molecular weight distribution as determined by SEC of a clickable nanogel solution is markedly skewed towards higher weights than that of PEG-alkyne. Percentages of UV detectable content are delineated by linear PEG benchmarks.

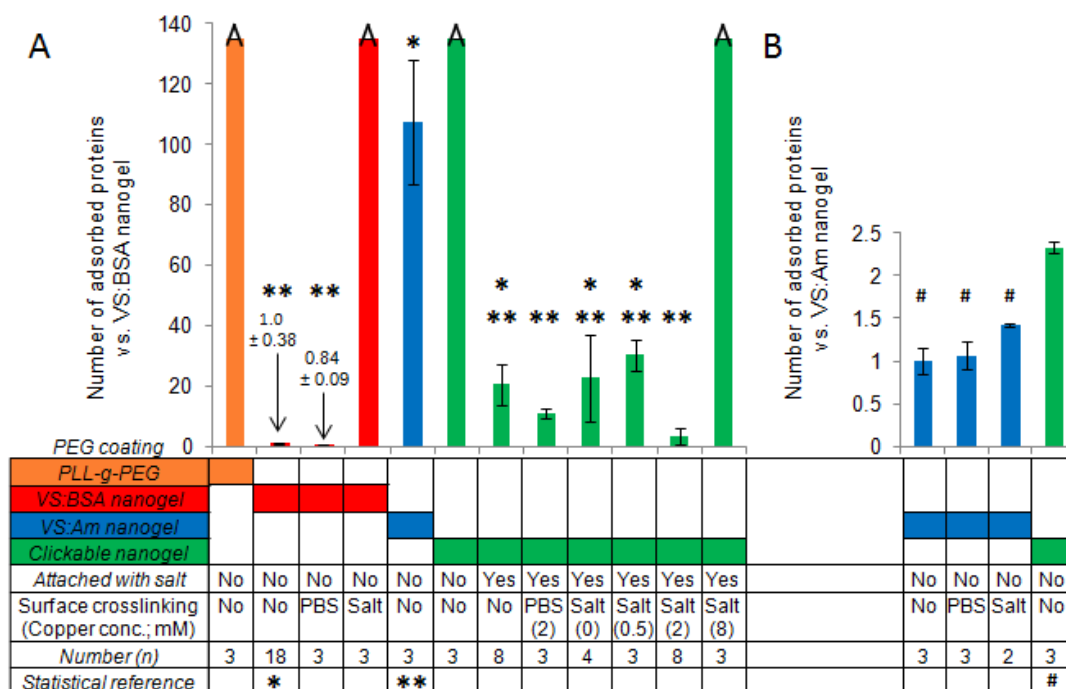


Figure 2.6: Quantification of protein adsorption to nanogel coatings via TIRF. Cy5-labeled fibrinogen molecules were counted using TIRF on PLL-g-PEG (orange) coatings as well as VS:BSA (red), VS:Am (blue), and clickable (green) nanogel coatings. Nanogel coatings were studied across a matrix of conditions including attachment with salt and surface cross-linking of the coating. Surface cross-linking was achieved in the VS:BSA and VS:Am nanogel coatings by incubating overnight in PBS or 1.5 M salt before capping the reactive groups and in the clickable nanogel coatings by incubating in PBS or 1.5 M salt spiked with sodium ascorbate and various amounts of copper for 1 h. Protein counts were normalized against standard nanogel coatings of: (A) VS:BSA or (B) VS:Am. Fibrinogen was incubated for 1 h at a (A) 1:100 dilution or (B) 1:1000 dilution of physiological concentration (2.5 mg/mL) and oversaturated counts were marked using (/). Statistical significance ($p < 0.05$) was determined for (A) and (B) separately on unsaturated counts relative to the conditions referenced in the final row with (*, **, #). Data are presented as mean \pm standard deviation.

While PLL-*g*-PEG has performed well at resisting protein adsorption as measured by relatively insensitive measurements such as Optical Waveguide Lightmode Spectroscopy (OWLS), here we found that PLL-*g*-PEG adsorbed too much fibrinogen to quantify by TIRF (Figure 2.6A). Furthermore, although the VS:Am nanogel coating adsorbed more than 100x the number of fibrinogen molecules as that of the VS:BSA nanogel coating, the VS:Am coating was still superior to PLL-*g*-PEG. Clickable nanogel coatings attached in PBS (i.e. not phase-separated) could not be quantified at the standard fibrinogen dilution of 1:100, similar to PLL-*g*-PEG. At a 1:1000 dilution of fibrinogen, clickable nanogel coatings attached in PBS adsorbed more than 2x the number of proteins as the VS:Am nanogel coatings (Figure 2.6B). The two-fold difference between the clickable and VS:Am nanogel coatings was unexpected as both are composed of 10 kDa PEG monomers cross-linked by different chemistries into similarly sized nanogel solutions. This discrepancy may be due to differences in the nanogel architecture, considering the VS:Am nanogel solutions utilize 8-arm PEGs and the clickable nanogel solutions utilize 4-arm PEGs. Differences in arm length, mesh sizes, or density of unreacted chains might account for this result, but the mechanism remains unknown. Also, potential effects of positively charged amine groups within the VS:Am nanogel coating on resisting fibrinogen adsorption cannot be discounted, although positively charged PLL has been previously found to have negligible effect on fibrinogen adsorption when coated onto negatively charged niobium oxide surfaces.⁽³⁵⁾

We then tested the resistance to fibrinogen adsorption of clickable nanogel solutions attached with salt in the phase-separated state (Figure 2.6A). When the clickable nanogel solutions were mixed with sodium sulfate to a final concentration of 500 mM, they became cloudy and rapidly phase-separated within minutes to produce a densely packed PEG-rich phase atop the solution. Glass flow cells were inverted to juxtapose the mercaptosilanated surface to the PEG-rich phase during attachment of the clickable nanogel solution, resulting in a 10-fold reduction in protein adsorption. Clickable nanogel solutions attached with salt in the phase-separated state were superior to VS:Am nanogel coatings but inferior to VS:BSA coatings (Figure 2.6A). VS:BSA and VS:Am nanogel solutions cannot be attached in the same manner without resulting in visibly thick hydrogel films. The Michael addition reaction between vinyl sulfones and amines occurs at a non-negligible rate at the higher PEG concentrations that develop after phase separation and the nanogels rapidly cross-link into microspheres and larger aggregates.⁽⁵²⁾

The other processing step studied via TIRF was the surface cross-linking of residual PEG chains left unreacted after nanogel formation and surface attachment (Figure 2.6A). Surface cross-linking was carried out by incubating the clickable nanogel coatings in PBS spiked with sodium ascorbate and copper for 1 h at 37 °C. In attempting to stitch the nanogel coatings into more densely packed hydrogel films, surfaces were also incubated in 1.5 M salt to induce phase separation along with sodium ascorbate and various concentrations of copper to promote graduated extents of cross-linking. Surface cross-linking with 2 mM copper in either PBS or 1.5 M salt provided modest improvements in resisting protein adsorption. Incubation in salt without any copper had no significant effect on overall protein adsorption but had larger variability than seen otherwise. Addition of higher amounts of copper (8 mM) eradicated any substantial resistance to protein adsorption. These saturated protein counts most likely originate from damage to the surface caused by stress introduced by the additional cross-linking. Large areas available for protein adsorption seem to be visible under TIRF microscopy when compared to fluorescent images of other nanogel coatings (Figure 2.7). Surface cross-linking was replicated in VS:BSA and VS:Am nanogel coatings by incubating the coatings in PBS or 1.5 M salt overnight at 37 °C. These incubations provided some extended opportunity for the slower Michael type cross-linking reaction, before vinyl sulfones were capped per usual. While cross-linking (i.e. incubation) in PBS provided no notable changes, cross-linking in 1.5 M salt slightly worsened the VS:Am nanogel coating and obliterated the resistance of the VS:BSA nanogel coating. The VS:BSA and VS:Am coatings were visibly damaged by the phase separation process (Figure 2.8), providing evidence for the potentially damaging effects of internally cross-linking such thin surface coatings.

To be certain that the observed differences in protein adsorption were not a product of the variability in nanogel size, we produced three stocks of different VS:BSA nanogel sizes and two stocks of different clickable nanogel sizes from the same precursor solutions of each type. Coatings produced from all sizes of the VS:BSA nanogels (53-102 nm) still outperformed coatings produced from all sizes of clickable nanogels attached with salt without surface cross-linking (84-128 nm) by similar margins (Figure 2.9). The data seem to suggest that all the nanogel sizes examined are above a threshold necessary to achieve maximal surface coverage on the silanated glass. However, nanogel formation remains critical in achieving low protein adsorption as evidenced by previous comparisons of VS:BSA nanogel solutions to monolayers of eight-arm PEG-VS.(89)

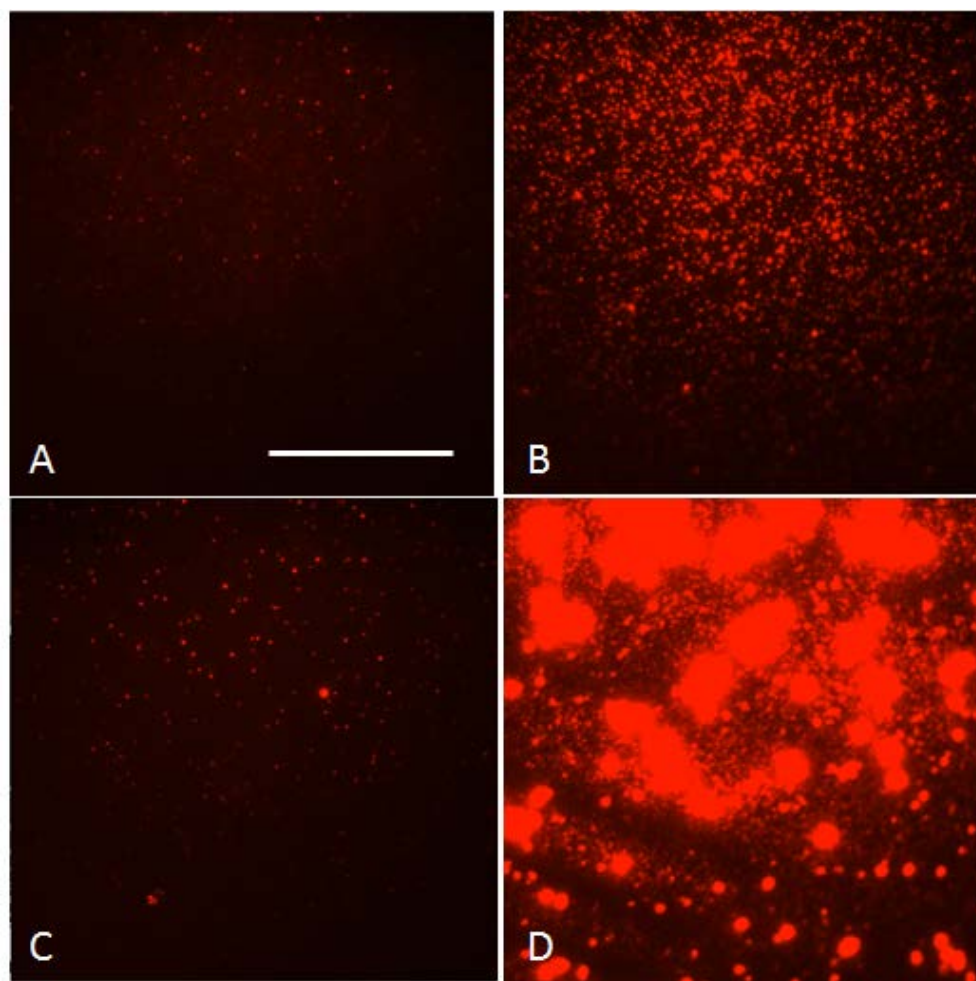


Figure 2.7: Fluorescent images of protein adsorption to nanogel coatings. Fluorescent images taken using TIRF microscopy of nanogel coatings after 1 h incubations with 0.25 mg/mL Cy5-labeled fibrinogen, including: (A) VS:BSA without surface cross-linking, (B) clickable attached with salt without surface cross-linking, (C) clickable attached with salt with surface cross-linking by 2 mM copper, and (D) clickable attached with salt with surface cross-linking by 8 mM copper. The large fluorescent spots in (D) may result from stress induced damage to the surface. The scale bar represents 100 μm .

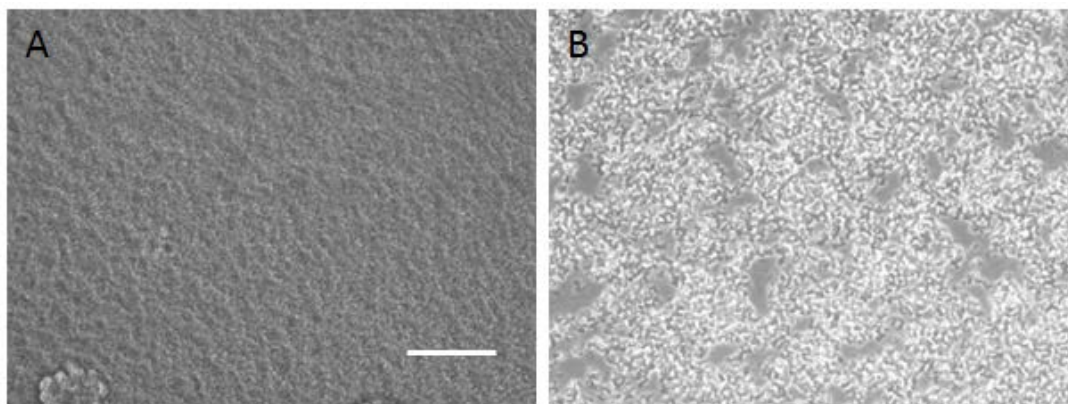


Figure 2.8: Micrographs of Michael-addition nanogel coatings incubated in high salt solutions. Micrographs of (A) VS:BSA and (B) VS:Am nanogel coatings show distinct surface morphologies after replicating surface cross-linking in 1.5 M salt by overnight incubations in 1.5 M sodium sulfate prior to capping vinyl sulfone groups. The scale bar represents 100 μm .

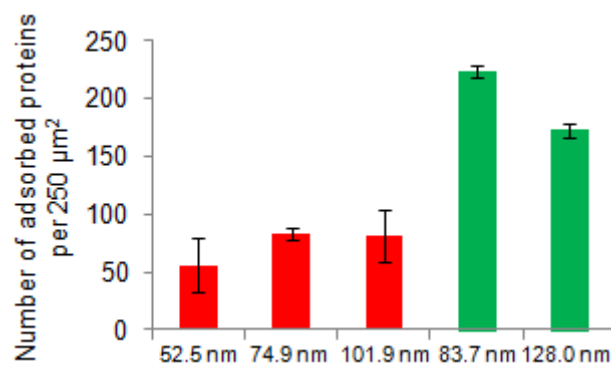


Figure 2.9: TIRF measurements of protein adsorption on nanogel coatings of different size nanogels. Counts of Cy5-labeled fibrinogen adsorbed at 0.025 mg/mL were compared across coatings produced from three different sizes of VS:BSA nanogels (red) and two different sizes of clickable nanogels attached with salt without surface cross-linking (green). The large differences in nanogel size do not account for the consistently lower levels of protein adsorption seen on VS:BSA coatings. Data are presented as mean \pm standard deviation (n=2).

2.3.3 Quantification of Nanogel Coating Packing Density

We hypothesized that the drastic improvement in protein resistance of the clickable nanogel coatings when attached with salt was due to increased PEG concentrations in the phase-separated state. We expected that collapsed nanogels would attach at higher packing densities than in the swollen state. Indeed, QCM-D found that the nanogel coatings attached with salt showed approximately twice the increase in surface density as the nanogel coatings attached without salt (Figure 2.10). The clickable nanogel coatings were attached *ex situ* under UV and QCM-D baselines measured from before and after coating the sensors were stitched together to model changes in mass. We measured the error that could be expected from removing these sensors during analysis by replicating the procedure with sensors that were left unmodified then returned to PBS flow. The magnitude of error ($244 \pm 214 \text{ ng/cm}^2$; $2.44 \pm 2.14 \text{ nm}$ of water) was found to be negligible relative to the masses of the nanogel coatings measured. The equivalent thickness of water provides a maximum estimate for the coating thickness, as we assume the nanogel coatings, comprised of unknown proportions of PEG and water, to be perhaps slightly denser than water. VS:BSA nanogel coatings were previously determined to be 1001.2 kg/m^3 using a combination of QCM-D and OWLS.⁽¹⁾ As nanogel packing density will affect the mass measurement and this calculation of average thickness, the clickable nanogel coating attached without salt (50.3 nm) appears to be packed less densely than the VS:BSA nanogel coating (75.2 nm, previously reported⁽¹⁾). However, if the clickable nanogel coating is attached with salt the average thickness increases (106.4 nm) beyond that of the VS:BSA nanogel coating. Increased packing density clearly improved the clickable nanogel coating's resistance to protein adsorption measured by TIRF, but could not alone account for the low levels found on VS:BSA nanogel coatings. Clickable nanogel coatings attached with salt seem to approach maximal packing density as the average thickness is near the approximate 100 nm diameter of the nanogels.

The clickable nanogel coating attached with salt was further used to study *in situ* the effects of surface cross-linking in 1.5 M salt with 2 mM copper. The very slight fluctuation in mass observed during this step (80 ng/cm^2) was actually less than that observed on the clickable nanogel coating attached without salt, which remained incubated in PBS but was subjected to the same temperature change to 37 °C during this step (510 ng/cm^2). This confirms that the nanogel coating was well washed after attachment and that subsequent addition of copper did not attach any residual PEG in solution but only cross-linked the existing hydrogel structure. Both coatings were next

incubated *in situ* with physiological levels of fibrinogen (2.5 mg/mL) for 2 h at 37 °C (Figure 2.11) and the additions in mass reflected the trend observed with TIRF. The unmodified clickable coating adsorbed more than 15x the amount of protein as the coating attached with salt and surface cross-linked, although this difference is not as large as the more than 50 fold difference seen with TIRF. It is possible that at the higher protein concentration used for QCM-D, the unmodified clickable coating reached a threshold of protein saturation, not achieved during TIRF.

2.3.4 Characterization of Nanogel Coating Topology

Multiple nanogel coatings were analyzed with tapping mode AFM under PBS to assess topological differences that arise from the conditions explored (Figure 2.12). Phase profiles were examined in addition to height profiles, revealing changes in material properties along the surface. Images of clickable nanogel coatings became distinctly less resolute and more difficult to obtain when attached with salt (Figure 2.12B vs. 2.12C). Although not all the nanogels of this coating are individually resolvable, AFM did not detect any deep gaps in surface coverage as evidenced by the relatively small height changes measured (less than 5 nm). It is more likely that the nanogels are packed so tightly together that the boundaries of these soft particles are actually intermeshed, impeding the ability of AFM to detect their edges. On the other hand, extended overnight surface cross-linking in 1.5 M salt with 1 mM copper strongly improved resolution of the clickable nanogel coating attached with salt (Figure 2.12D), enabling imaging on smaller spatial scales (Figure 2.12E). The phase profile clearly shows a tightly packed coating of spherical nanogels. These surfaces also exhibit curious circular patches of raised nanogels that were especially well resolved by AFM. We can assume that nanogel coatings attached with salt but without surface cross-linking are packed just as tightly since the surface attachment step is identical. Nanogels of all coatings measure reasonably close to 100 nm. Some shrinking in the final nanogel size might be expected with surface cross-linking in 1.5 M salt. However, the high packing density of these coatings may allow some reduction in nanogel size without compromising surface coverage. Otherwise, interstitial gaps may begin to appear between the nanogels as they shrink. This might explain why surface cross-linking in 1.5 M salt did not garner significant improvements in the VS:BSA or VS:Am nanogel coatings studied with TIRF. Interstitial gaps resulting from nanogel shrinkage or stress-induced surface damage may prove to be quite detrimental as they may allow adsorption of proteins that are smaller than fibrinogen within the gaps.

	Clickable nanogel coating attached without salt, no surface crosslinking		Clickable nanogel coating attached with salt, surface crosslinking in 1.5 M salt	
	Change in Mass (ng/cm ²)	Equivalent Thickness of Water (nm)	Change in Mass (ng/cm ²)	Equivalent Thickness of Water (nm)
<i>Nanogel Coating</i>	5,030	50.3	10,640	106.4
<i>Surface crosslinking step (or 37°C sham incubation)</i>	(510)	(5.1)	80	0.8
<i>Fibrinogen Adsorption</i>	1190	11.9	76	0.76

Figure 2.10. QCM-D mass measurements of clickable nanogel coatings. Changes in mass (and their equivalent thicknesses for masses of water) were measured with QCM-D for two types of clickable nanogel coatings, including one attached without salt and one attached with salt. The coating attached with salt underwent surface cross-linking in 1.5 M salt with 2 mM copper. The coating attached without salt did not undergo surface cross-linking but was incubated in PBS and raised to 37 °C as well during this step.

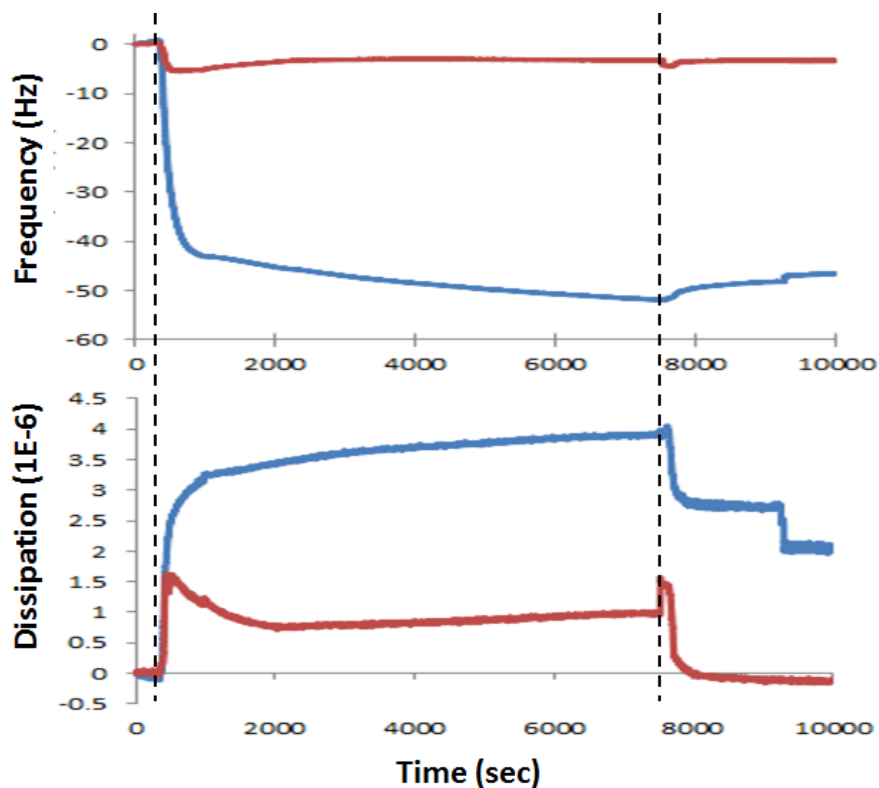


Figure 2.11. QCM-D profiles of protein adsorption to clickable nanogel coatings. Nanogel coatings were incubated with physiological concentrations of fibrinogen (2.5 mg/mL) for 2 h at 37 °C (between the dashed lines) followed by PBS at 22 °C. Frequency and dissipation profiles show large increases in mass for the clickable nanogel coating attached without salt and without surface cross-linking (blue) and a relatively smaller change for the clickable nanogel coating attached with salt followed by surface cross-linking (red).

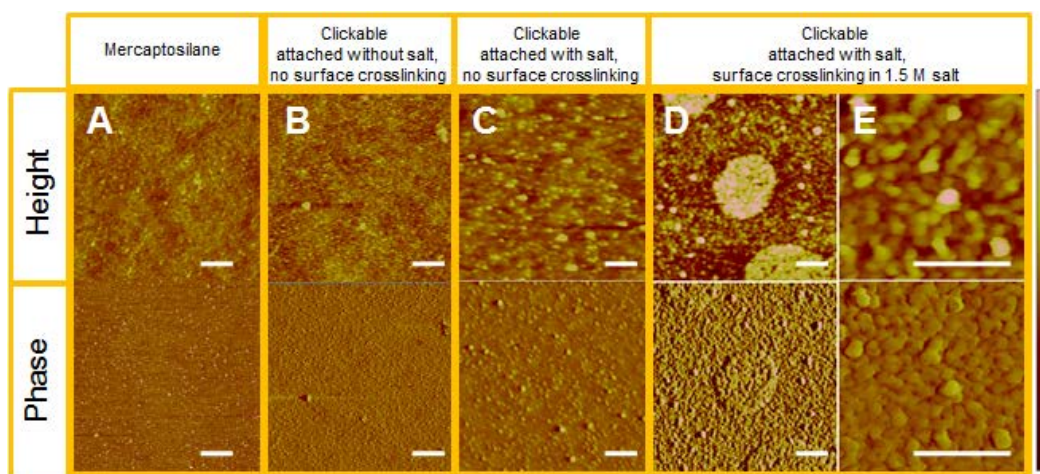


Figure 2.12. AFM profiles of clickable nanogel coatings. Images from AFM show height (top) and phase (bottom) profiles for (A) mercaptosilanated glass, (B) clickable nanogel coatings attached without salt with no surface cross-linking, (C) clickable nanogel coatings attached with salt with no surface cross-linking and (D, E) clickable nanogel coatings attached with salt with surface cross-linking overnight in 1.5 M salt with 1 mM copper. Scale bars all represent 500 nm. The images in (E) are higher spatial resolution images of the sample in (D). The color scale represents 5 nm for the height profiles of (A-C), 20 nm for the height profiles of (D, E), and 30° for all phase profiles.

2.3.5 Cell Adhesion to Nanogel Coatings

Non-specific cell adhesion was examined as a corroborative, although less sensitive method of qualifying protein adsorption, as cells attach to artificial surfaces via layers of adsorbed proteins. Surfaces were, therefore, first incubated for 2 h with 2.5 mg/mL fibrinogen to more quickly elicit any possible cell adhesion responses. We studied most of the same conditions investigated with TIRF with all surface cross-linking being performed overnight (Figure 2.13). Additionally, controls of a PLL-*g*-PEG coating, a common non-fouling surface, and an RGD-conjugated clickable nanogel coating attached with salt without surface cross-linking were seeded. Despite its inferior resistance to protein adsorption as measured by TIRF, the PLL-*g*-PEG coating completely resisted cell adhesion. Although the lack of correlation between results is surprising, other examples exist of PEG surfaces that display relatively high protein adsorption but also resist cell adhesion.⁽³³⁾ Adhesion of well-spread cells to the RGD-conjugated coating demonstrates the effectiveness of the UV thiol-yne chemistry for the attachment of cysteine-containing peptides and demonstrates a lack of toxicity from the leaching of any residual copper. Again the VS:BSA nanogel coatings performed very well with no significant cell adhesion after 1 round of seeding. However, both the VS:Am nanogel coating and the clickable nanogel coating attached with salt without surface cross-linking appeared equally cell free, despite the disparities seen with TIRF. The clickable nanogel coatings attached without salt performed noticeably worse, as expected, but displayed some degree of resistance to cell adhesion. Subtle long-term increases in cell adhesion were observed on the clickable nanogel coatings attached with salt without surface cross-linking versus the VS:BSA and VS:Am nanogel coatings without surface cross-linking, as seen after 5 rounds of cell seeding (Figure 2.14).

The surface most drastically affected by surface cross-linking was the clickable nanogel coating attached with salt. Surface cross-linking greatly increased cell adhesion on both clickable nanogel surfaces cross-linked with copper in PBS and 1.5 M salt, in contrast to the improvements observed with TIRF. The coating cross-linked with copper in PBS especially demonstrated an immediate and complete deterioration of its ability to resist cell adhesion, with a complete monolayer of well spread cells forming after 1 seeding. Surface cross-linking within these coatings may have an exaggerated effect because the higher packing density achieved by attachment with salt should allow for more cross-linking opportunities and potentially less damage to the surface. It is difficult to determine why the TIRF and cell adhesion results conflict, but is important to note that

other proteins found in the media serum that are much smaller in size than fibrinogen may contribute to cell adhesion (e.g. vitronectin). While we did not study the mechanical properties of our coatings, stiffer (more cross-linked) hydrogels do not necessarily enhance cell adhesion,⁽¹⁵¹⁾ and so increased stiffness from surface cross-linking would not necessarily account for our observations. Protein adsorption has been found to correlate with protein size on PEG grafted surfaces.⁽³⁵⁾ A potential source of discrepancy between these tests could stem from any proteins that are able to diffuse through the nanogel coating and adsorb to the underlying glass during the 1 h fibrinogen incubation. TIRF cannot discriminate between these proteins and those adsorbed to the actual nanogel coating itself, while cells would reasonably be expected to adhere only to the latter, given the proven surface coverage of the nanogel coatings. If the majority of the TIRF protein counts arise from adsorption to glass, then any steps which impede diffusion, such as denser cross-linking, would explain the TIRF observations. However, this breakdown cannot be ascertained. Importantly, the cell adhesion results agreed with TIRF on the superiority of clickable nanogel coatings attached with salt versus those attached without salt if the surface cross-linking step was omitted.

Surface cross-linking of the VS:BSA nanogel coating in 1.5 M salt led to adhesion of large cell aggregates, consistent with the increase in protein adsorption measured by TIRF. The VS:Am nanogel coating with surface cross-linking in 1.5 M salt, on the other hand, initially maintained its resistance for several rounds of cell seeding but then rapidly deteriorated after 5 rounds of seeding (Figure 2.14). The VS:BSA and VS:Am nanogel coatings with surface cross-linking in PBS maintained similar resistance to cell adhesion as their counterparts with no surface cross-linking until about 9 rounds of seeding, when subtle declines were observed (Figure 2.15). However, the extent of surface cross-linking that actually occurred overnight without salt-induced phase separation may be mild. The VS:BSA nanogel coating has been shown previously to resist fibroblast adhesion for up to 3 weeks.⁽¹⁾

Few other studies on biocompatible surface coatings have attempted to examine long-term cell adhesion. Most often, surface coatings are evaluated for long-term stability by patterning cells onto selectively adhesive regions of the surface and monitoring the long-term pattern integrity, which is deteriorated as cells migrate onto and firmly adhere to the protein resistant regions. Study-to-study comparisons are difficult as cell type, cell seeding density, media content, substrate material, and the various strategies for attaching the chemically similar polymers may affect results. The

dimensions, shapes, and ligands used to promote adhesion in patterned cell studies add additional sources of variability, making studies that compare multiple types of coatings valuable. Still several of the best examples of PEG coatings demonstrate superb resistance to fibroblast adhesion for multiple weeks similar to our results, but not necessarily for multiple months. Patterned oligo(ethylene glycol) terminated SAMs began to collapse after 1 week,⁽¹⁵²⁾ PLL-*g*-PEG grafted at high temperatures maintained pattern integrity for at least 36 days,⁽¹⁴⁷⁾ and PEG-functionalized polymer brush coatings resisted twice-a-week cell seedings for 3 weeks after which gradual increases in adhesion were observed.⁽¹⁷⁾

Finally, we also demonstrated that clickable nanogel solutions could be attached in a UV-free process to cyclooctyne functionalized azidosilanated glass, exhibiting comparable resistance to cell adhesion after 1 seeding (Figure 2.16). However, for unknown reasons, these clickable nanogel coatings produced saturated counts on TIRF (data not shown).

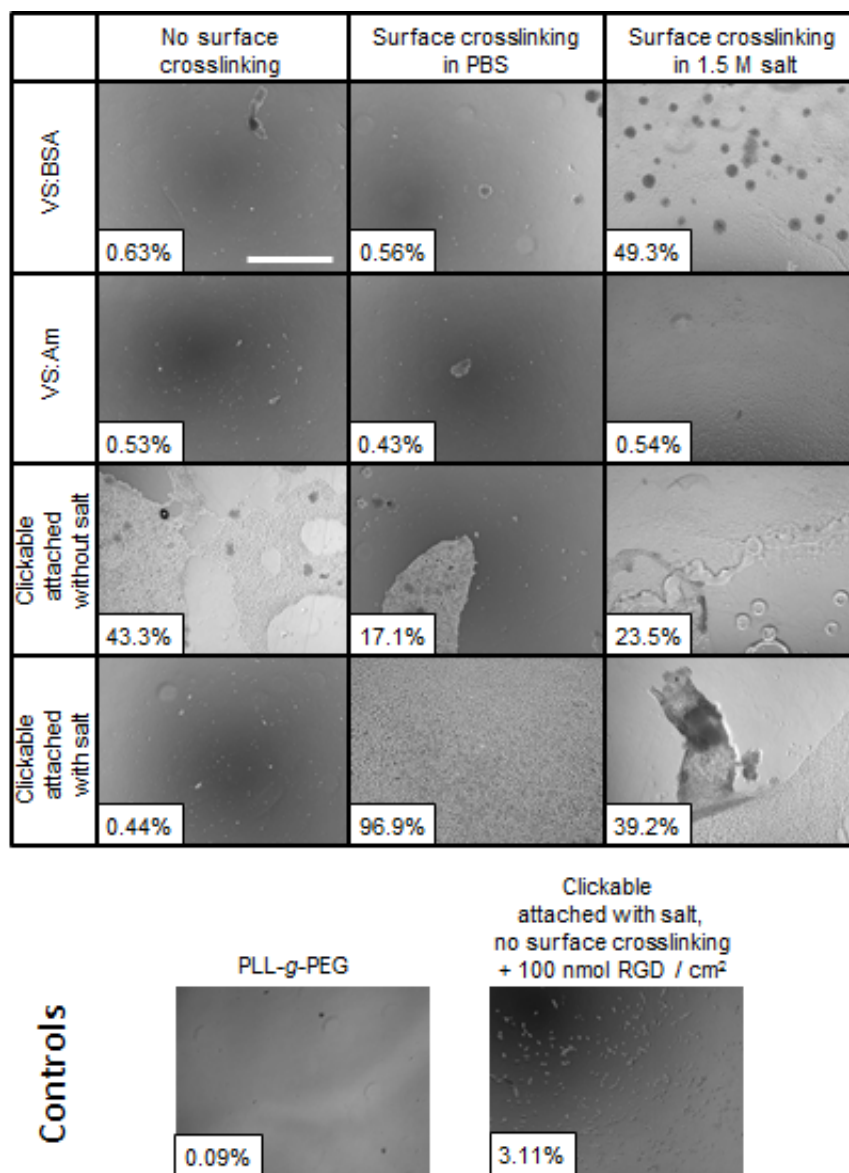


Figure 2.13: Cell adhesion to nanogel coatings after 1 seeding. Cell adhesion of 3T3 fibroblasts was examined 1 day after the first seeding at 100,000 cells/cm² on several surfaces that were incubated with 2.5 mg/mL fibrinogen for 2 h at 37°C. Surface cross-linking was allowed overnight on some VS:BSA and VS:Am nanogel coatings before capping and implemented with 2 mM copper overnight on some clickable nanogel coatings both at 37 °C. Additionally, control surfaces of PLL-g-PEG adsorbed to glass, and clickable nanogel solutions attached with salt with no surface cross-linking and conjugated to RGD via a UV thiol-yne reaction were examined. Approximate percentage of surface coverage by adhered cells is indicated in the insets. The scale bar represents 1 mm.

	No surface crosslinking	Surface crosslinking in PBS	Surface crosslinking in 1.5 M salt
VS:BSA	 0.60%	 2.12%	 23.0%
VS:Am	 4.32%	 1.17%	
Clickable attached without salt	 41.1%	 28.1%	 54.8%
Clickable attached with salt	 16.1%		 80.4%

Figure 2.14: Cell adhesion to nanogel coatings after 5 seedings. Cell adhesion of 3T3 fibroblasts was examined 1 day after the fifth seeding at 100,000 cells/cm² on several surfaces that were initially incubated with 2.5 mg/mL fibrinogen for 2 h at 37 °C. Surface cross-linking had been allowed overnight on some VS:BSA and VS:Am nanogel coatings before capping and implemented with 2 mM copper overnight on some clickable nanogel coatings both at 37 °C. Approximate percentage of surface coverage by adhered cells is indicated in the insets. The scale bar represents 1 mm.

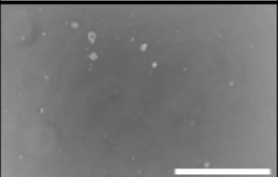
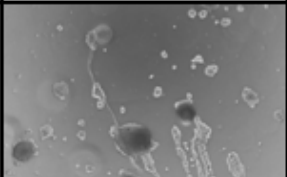
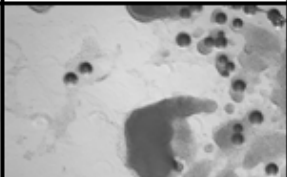
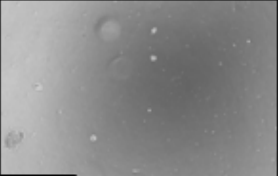
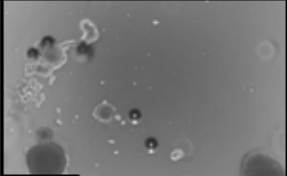

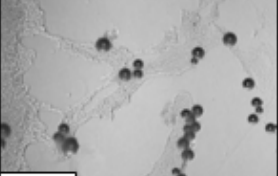
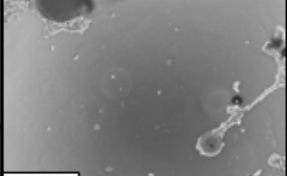

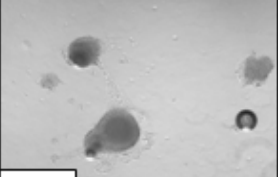


	No surface crosslinking	Surface crosslinking in PBS	Surface crosslinking in 1.5 M salt
VS:BSA	 1.05%	 7.41%	 49.7%
VS:Am	 0.94%	 4.99%	
Clickable attached without salt	 31.73%	 6.17%	
Clickable attached with salt	 7.29%		

Figure 2.15: Cell adhesion to nanogel coatings after 9 seedings. Cell adhesion of 3T3 fibroblasts was examined 1 day after the ninth seeding at 100,000 cells/cm² on several surfaces that were initially incubated with 2.5 mg/mL fibrinogen for 2 h at 37°C. Surface cross-linking had been allowed overnight on some VS:BSA and VS:Am nanogel coatings before capping and implemented with 2 mM copper overnight on some clickable nanogel coatings both at 37 °C. Approximate percentage of surface coverage by adhered cells is indicated in the insets. The scale bar represents 1 mm.

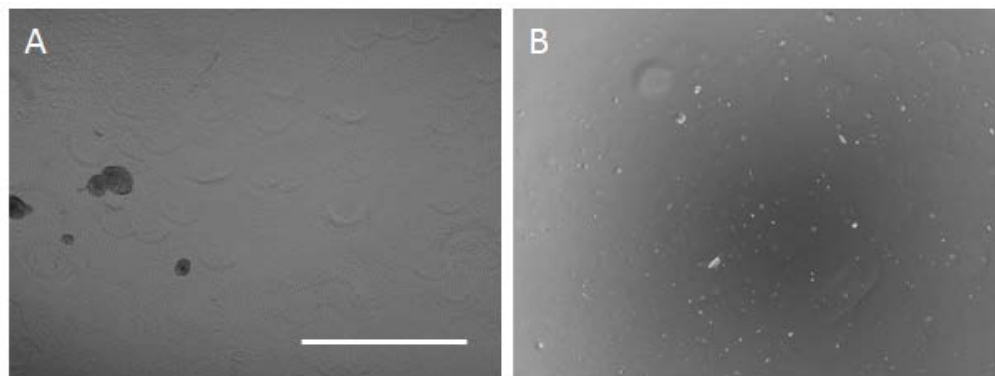


Figure 2.16: Cell adhesion to clickable nanogel coatings attached via CuAAC and SPAAC. Cell adhesion of 3T3 fibroblasts was examined 1 day after the initial seeding at 100,000 cells/cm² after incubation with 2.5 mg/mL fibrinogen for 2 h at 37 °C. Surfaces include clickable nanogel coatings attached with salt via: (A) SPAAC to a PEG-cyclooctyne interface on azidosilane, or (B) UV thiol-yne to mercaptosilane, both without surface cross-linking. The attachment chemistries appear to perform comparably in terms of cell adhesion. The scale bar represents 1 mm.

2.4 Conclusion

We have shown click chemistry to be a useful tool in the facile synthesis and attachment of 100% PEG nanogel coatings. Particularly, fabrication of nanogel solutions by CuAAC enabled attachment to surfaces in the phase-separated state without risk of bulk gelation. The increased nanogel surface density resulted in greatly improved resistance to protein adsorption by TIRF. The additional step of surface cross-linking was also easily performed with CuAAC and showed that higher cross-linking densities provide modest improvements in resistance to fibrinogen adsorption, but negatively impacted resistance to cell adhesion. These clickable nanogel coatings represent the best coatings of 100% PEG that we have examined for short-term protein resistance by TIRF and provide new insights into structural properties of coatings that affect the adsorption of proteins. The use of clickable functionalities further eliminates any non-specific conjugations to biomolecules that might occur through either reaction with insufficiently capped vinyl sulfone groups or electrostatic interactions with amine groups. However, the results further establish that PEG/albumin nanogel solutions are superior for producing protein resistant coatings, suggesting synergy between the PEG and albumin in resisting protein adsorption and cell adhesion. Lack of long-term resistance to cell adhesion currently precludes these particular PEG nanogel coatings and similar surface coatings from *in vivo* applications, including biosensors and medical implants. However, as we have demonstrated significantly lower levels of protein adsorption compared to PEG-*g*-PLL and other previously studied coatings, the nanogel coatings seem to comprise superior surfaces for *in vitro* biological diagnostics or other applications requiring strong short-term resistance to protein adsorption.

Chapter 3

Patterned Cell Adhesion with PEG Nanogel Coatings for the Direct Reprogramming of Fibroblasts to Cardiomyocytes

3.1 Introduction

Clinical stem cell treatment of myocardial infarction has been practiced with embryonic stem cells (ESCs), mesenchymal stem cells (MSCs), and within the past decade newly discovered cardiac stem cells (CSCs) with promising results.⁽¹⁵³⁾ Because of their proliferative potential, however, most basic research on cardiomyocyte differentiation has utilized either ESCs or induced pluripotent stem cells (iPSCs), resulting in remarkably similar transcription profiles⁽⁶⁶⁾ and similar efficiencies of cardiomyocyte induction.⁽¹⁵⁴⁻¹⁵⁷⁾ Reprogramming somatic cells into iPSCs provides obvious advantages in cell sourcing over use of ESCs, but now cutting-edge research is finding ways to short-cut this pathway altogether and directly reprogram somatic cells to the desired cell type.⁽¹⁵⁸⁾ Ieda et al. found that expression of three transcription factors – *Gata4*, *Mef2c*, and *Tbx5* – was able to reprogram cardiac and dermal fibroblasts into functional cardiomyocytes *in vivo*, beginning at 3 days and progressing for several weeks.⁽¹⁵⁵⁾ More recently, Efe et al. has directly reprogrammed fibroblasts to cardiomyocytes by inducing transient expression of Yamanaka factors (*Oct4*, *Sox2*, *Klf4*, and *c-Myc*) along with simultaneous treatment of a JAK-STAT inhibitor to prevent iPSC formation, and followed by treatment with cardioinductive media that includes BMP4.⁽¹⁵⁶⁾ BMP as well as TGF- β are paracrine factors secreted by cardiomyocytes that have been found to induce cardiogenic differentiation of ESCs.⁽¹⁵⁹⁾ This protocol produces unstable intermediates that are prohibited from developing into fully pluripotent cells but rather relax into defined cardiac progenitors and requires substantially shortened differentiation time compared to using iPSCs.⁽¹⁵⁶⁾ It is believed that the earliest steps in any of these reprogramming protocols involves chromatin remodeling/unwinding, which precedes transcriptional activation.⁽¹⁶⁰⁾

Differentiation is not only controlled by soluble factor signaling, but by signaling through adhesion sites to the extracellular matrix. In general, stem cells do not readily attach to any substrate but must be promoted by functionalization with specific adhesion ligands.⁽¹⁶¹⁾ Adhesion molecules not only regulate differentiation through direct signaling via cell receptors, but may indirectly influence differentiation through effects on cell stiffness, cell shape, cell proliferation, and cell migration as well. Basement membrane components form the earliest extracellular matrix of a developing embryo, with laminin expressed at the two-cell stage. Matrigel, a reconstituted basement membrane isolated from mouse sarcoma, has become the most commonly used stem cell substrate for both for maintenance of pluripotent stem cells (PSCs) and defined differentiations thereof. It is composed roughly of ~60% laminin, ~30% collagen IV, ~8% entactin, and ~2% other proteins (according to product literature) and induces cell-cell contacts and cell polarization unseen on other substrates for a variety of cell types.⁽¹⁶²⁾ While Matrigel is an improvement upon the standard of mouse embryonic fibroblast (MEF) feeder layers in terms of xenogenic contamination, the mouse derived protein matrix is still considered too unsafe for human applications. Additionally, an incomplete and inconsistent profile of Matrigel content, makes precise control and interpretation of experiments troublesome. For these reasons, many researchers have begun to explore chemically defined substrates as viable alternatives to Matrigel.

As the major component of Matrigel, laminin is considered an obvious choice to replace Matrigel. It is a heterotrimeric protein with 15 physiologically relevant combinations of its subunit isoform chains that are developmentally regulated. While laminin is known to specifically support the differentiation of neural and pancreatic cells,⁽¹⁶³⁾ its role in cardiogenesis is less understood, with some evidence showing it may also be necessary to support cardiomyocyte differentiation⁽¹⁶⁴⁾ and proper cardiac function,⁽¹⁶³⁾ especially during later stages of maturation.⁽¹⁶⁵⁾ Still others have used laminin coatings for the maintenance of pluripotent ESCs.⁽¹⁶⁶⁾ Studies of recombinant laminin isoforms revealed diverse isoform-specific effects on ESCs, from maintenance of ESC self-renewal and pluripotency (laminin-511) to rapid differentiation (laminin-111, used in this study).⁽¹⁶⁷⁾ Studies of various types of stem cells showed that iPSCs prefer Matrigel over laminin for initial attachment, but cell colonies expand better on laminin.⁽¹⁶¹⁾ Expression of pluripotency markers in this study also indicates that stemness may increase as cells form colonies from single cells. Other major extracellular matrix components include collagen and fibronectin. Collagen I has been shown necessary for cardiomyocyte differentiation,⁽¹⁶³⁾ whereas collagen IV (also found at

high concentrations in Matrigel) has been shown necessary for the maintenance and expansion of cardiac progenitor cells.(168) Fibronectin has been indicated for differentiation into mesodermal and ectodermal lineages,(163) while a growing amount of evidence suggests that vitronectin, which shares many of the same integrin receptors as fibronectin,(169) maintains pluripotency and is an equally viable alternative to Matrigel for the culture and maintenance of PSCs.(170-172)

Integrin receptors are the primary means of stem cell and cardiac cell attachment to the extracellular matrix but also initiate signaling pathways. Human ESCs have been found to produce all major components of the extracellular matrix (fibronectin, laminin, collagen I, and collagen IV) and express the corresponding integrins,(173) with strong expression of integrin subunits for laminin ($\alpha 6\beta 1$), fibronectin ($\alpha 5\beta 1$), and vitronectin ($\alpha V\beta 5$) detected in both ESCs and iPSCs.(75, 172) ESCs adhere well to fibronectin, vitronectin, and Matrigel but poorly to laminin + entactin and collagen IV, with only vitronectin and Matrigel able to support self-renewal and maintain pluripotency.(173) The developing heart shows temporal regulation of the extracellular matrix content and cellular expression of specific integrins.(174) Studies have shown that while neonatal cardiomyocytes adhere to a variety of extracellular matrix substrates, including laminin, fibronectin, and collagens I-IV, adult cardiomyocytes only adhere to laminin and collagen IV,(175) augmenting the potential importance of these latter two (or of Matrigel) for promoting cardiomyocyte maturation.

Langer et al. found that treatment of standard polystyrene or polypropylene with specific durations of UV/ozone could provide chemically defined surfaces that were optimized for adsorption of vitronectin or FBS and able to support routine stem cell culture.(170) In relatively few circumstances, defined synthetic substrates that lack xenogeneic components or recombinant proteins altogether have been successfully used for stem cell culture, including poly[2-(methacryloxy)ethyl dimethyl-(3-sulfopropyl)ammonium hydroxide] (PMEDSAH), which was used in combination with chemically defined serum-free medium.(176) Cell adhesion peptides isolated from both vitronectin and bone sialoprotein were covalently tethered to an acrylate surface cross-linked with PEG and each was capable of promoting either ESC maintenance or cardiomyocyte differentiation when cardiogenic media was applied.(177) RGD is a conserved tripeptide adhesion sequence commonly used in tissue engineering that is found in fibronectin, vitronectin, fibrinogen, and other extracellular matrix components. It is recognized by a number of integrins including all 5 αV integrins as well as $\alpha 5\beta 1$, $\alpha 8\beta 1$, and $\alpha IIb\beta 3$ integrins,(169) with especially strong affinity for $\beta 3$

integrins.(169, 178) Some research has shown binding of stem cells to RGD induces specific lineages of differentiation. RGD promoted early stages of chondrogenic differentiation of mesenchymal stem cells within PEG hydrogels(179) as well as endothelialization over cardiogenesis in PEG hydrogels seeded with ESC embryoid bodies.(180) The latter was speculated to result from reduced embryoid body aggregation rather than a direct response to integrin signaling. Given the expansive number of RGD-binding integrins, each with different affinities for RGD, and the dynamic expression of integrins in developing cardiac tissue, it is difficult to precisely predict the effects of RGD, if any, on cardiomyocyte differentiation. The abundant evidence supporting vitronectin as a substrate for stem cell maintenance, suggests RGD (its sole integrin binding sequence) should not promote differentiation. Hubbell et al. quantified integrin expression in mouse ESCs and recapitulated the extracellular matrix with an artificial PEG matrix presenting four ligands specific to highly upregulated integrins, including $\alpha 5\beta 1$, $\alpha V\beta 5$, $\alpha 6\beta 1$, and $\alpha 9\beta 1$.(75) Using RGD as the ligand specific to the first two integrins, it was found that simultaneous signaling through all of the integrins together, but none individually, promoted maintenance of ESC stemness. Interestingly, another group found that both $\alpha 5\beta 1$ and $\alpha 6\beta 1$ integrins were found necessary, along with BMP4, for mesodermal differentiation of ESCs.(181) It is important to note, that as laminin is capable of binding the $\alpha 6\beta 1$ integrin,(169) the PEG surfaces used in the current study have the potential of activating 3 of the 4 integrins isolated for stemness and both integrins necessary for mesodermal differentiation, according to these studies. Thus, overlap clearly exists among integrin signaling pathways and it is the cumulative integrated signal that is important to consider.

Finally, cellular organization can affect differentiation. For instance, spatial distribution within cellular aggregates can affect distributions of cell-cell or cell-extracellular matrix interactions as well as gradients of temperature, pH, oxygen, and soluble factors, explaining why modulation of embryoid body size has been implicated as an important variable in stem cell maintenance and differentiation.(182) Within a developing embryoid body it is expected to find a heterogeneous cellular population including cell types belonging to all three germ layers (endoderm, mesoderm, and ectoderm). Appropriate interactions between these cell types are thought to be important in inducing various types of cellular differentiation. Particularly, cardiogenic tissue relies on inductive cues from early endodermic tissue, which forms on the surface of differentiating cellular aggregates.(183) Thus, the surface area to volume ratio of embryoid bodies becomes an obvious parameter in stem cell differentiation. Endodermal tissue is believed to induce cardiac

differentiation via TGF- β and FGF protein signaling. Notably, Matrigel is believed to derive from parietal endoderm.(162) The size of embryoid bodies can be uniformly well controlled by using centrifugation of stem cells into spatially defined microwells.(184) Also, Zandstra et al. used patterned 2-dimensional colonies to create uniformly sized embryoid bodies after removal of the cell colonies from the surface.(185) This work found that the diameter of the stem cell colonies biased gene expression profiles toward certain lineages before any differentiation protocol had been established, with 400 μm embryoid bodies (vs. 200 and 800 μm) most suited for cardiac induction. Similarly, frequency of contraction has been found by some to be maximized in aggregates between 250-300 μm (186), although the proportion of cardiomyocytes in these aggregates is generally found to increase with decreasing diameter size.(187) Additionally, this study found that all size controlled embryoid bodies outperformed spontaneously formed embryoid bodies in terms of percentage of cardiomyocytes and percentage of contracting embryoid bodies.(187)

An array of traditional micropatterning techniques has been applied to the patterning of surfaces for cell adhesion, including: microcontact printing, liquid phase printing, microfluidic patterning, photolithography coupled with molecular assembly or plasma polymerization, photoimmobilization or photochemistry patterning, stencil assisted patterning, ink jet patterning, and laser guided writing.(188) Surface patterning of selectively adhesive regions on cell resistant coatings has been well practiced, usually with microcontact printing or photonic patterning. PLL-*g*-PEG is a common choice(189, 190) for a non-fouling background and was shown to maintain pattern integrity of fibroblasts for up to 13 days, with pattern degradation believed to be a result of polymer desorption or exchange with serum proteins and not of cellular processes.(191) SAMs patterned with mannitol groups surprisingly outperformed SAMs patterned with tri(ethylene glycols) in terms of long-term resistance to fibroblast adhesion, by maintaining pattern integrity for 25 days.(152) Stem cells have been seeded via adhesion molecules patterned directly onto tissue culture polystyrene, with the interstitial space passivated through incubation with pluronics, however long-term culture and/or differentiation of these cells has not been tested.(185, 192) Human PSCs have also been seeded onto photo-chemically patterned polystyrene, which showed superior scale-up capabilities over MEF feeder systems due to cellular organization.(170) More commonly, cells are patterned within microwells of a thin 3-dimensional hydrogel yielding uniformly sized embryoid bodies for differentiation rather than in monolayer clusters.(182) We have found few examples for the study of stem cell differentiation from 3-dimensional embryoid bodies formed on 2-

dimensionally patterned surfaces. Nakazawa et al. patterned 200 μm spots of gelatin onto platinum coated glass chips and passivated the interspatial area with adsorption of PEG-thiol. They found that embryoid bodies gradually formed from mouse ESCs grown on these patterns and displayed significantly higher proliferation rates and higher expression of endoderm and mesoderm markers with lower expression of pluripotency markers after 7 days of culture, compared to cells seeded in microwells.⁽¹⁹³⁾ Additionally, RGD has been patterned onto PEG hydrogels for the differentiation of mesenchymal stem cells by polymerizing the PEG around islands of gold patterned onto glass via photolithography, then peeling off the hydrogel/gold and attaching RGD via a gold-thiol bond.^(194, 195) It is reasonable to assume that many of the commonplace surface passivating strategies used in these patterning schemes are sufficient for maintaining short-term pattern integrity during routine stem cell maintenance but may not hold up for the long term culture necessary for cellular differentiation, especially if target cell types display more robust adhesion and migration.

Direct reprogramming offers distinct advantages over differentiation of PSCs, including shorter paths to differentiation and less risk of teratoma formation.⁽¹⁵³⁾ However, as this process begins with the monolayer culturing of fibroblasts on 2-dimensional substrates rather than with the formation of 3-dimensional embryoid bodies from stem cells, cellular organization has not been investigated with these protocols. It is uncertain whether the lessons learned with regards to embryoid body size apply to the spontaneously formed aggregates that arise during direct reprogramming to cardiomyocytes. Because we have measured superior protein resistance of our PEG VS:BSA nanogel coatings vs. other preparations, we hypothesized that they possess superior potential for maintaining pattern integrity over the commonplace strategies explored thus far in stem cell patterning. By implementing a simple stencil assisted patterning approach with a rubber stamp (referred to herein as stamping), we were able to either selectively pattern the nanogel coating itself onto glass substrates or selectively pattern adhesion molecules onto our nanogel coatings. This allowed us to pattern fibroblasts into discrete colonies that would hopefully force formation of size-defined cell aggregates during reprogramming. We performed direct reprogramming of MEFs to cardiomyocytes on both patterned and non-patterned substrates, including Matrigel, laminin, and PEG functionalized with laminin and RGD (PEG-laminin/RGD), all of which were attached to mercaptosilanated glass. Pattern integrity was either not maintained well enough for the 18 day experiment to draw strong conclusions on the value of patterning or was largely negated by drastic loss of cell aggregates that did remain confined but eventually detached from surfaces after over-

proliferation. However, the surviving patterned aggregates showed no indication of superior differentiation over the many spontaneously formed aggregates. Significant differences were noticed, though, between the 3 substrates, with laminin demonstrating superior performance in the number of contracting patches and staining for sarcomeric α -actinin, followed by PEG-laminin/RGD, and then Matrigel.

3.2 Materials and Methods

3.2.1 Pattern Stamping

All reagents were purchased from Sigma Aldrich (St. Louis, MO, USA) unless otherwise noted. All surfaces were fabricated on 12 mm round glass coverslips (Ted Pella Inc., Redding, CA, USA) that were mercaptosilanated as described previously.⁽¹⁾ Patterned surfaces were created via different stamping schemes (discussed in Results) all of which utilized PEG VS:BSA nanogel solutions for passivation of selected surface regions. Nanogel solutions were fabricated, stored, and covalently coupled to mercaptosilanated glass as described before,⁽¹⁾ which entails incubating the nanogel solutions (100 mg/mL) for 1 h at 37 °C on top of the mercaptosilanated glass. Stamping was implemented with 12 mm round rubber stamps (rubberstamps.net, Bettendorf, IA, USA) with protruding cylindrical posts of 500 μ m diameters. Stamps were cleaned with ethanol and water between each application, then coated with 2 mg/mL PEG-*g*-PLL for 1 h at room temperature to make the rubber surface hydrophilic. After rinsing in PBS, the stamps were inverted on top of the glass coverslips and the pair was sandwiched between two glass slides that were securely clamped together with two standard office-supply binder clips. Various solutions were applied to the interstitial space between the coverslip and rubber stamp for patterning by careful pipetting and incubated for appropriate times at 37 °C. These solutions were removed by pipetting 1 mL of PBS through the interstitial space before removal of the binder clips and stamp from the coverslip surface. Coverslips were placed in 24-well plates and washed again with PBS. Surfaces were further functionalized according to normal protocols by incubating solutions over the entire coverslip surface. The ability of various stamping protocols to pattern selectively adhesive regions was evaluated by seeding the surfaces with 40,000 3T3 fibroblasts/cm² and imaging the cell laden surfaces with phase contrast microscopy the following day after gentle washing. Cells were cultured

according to standard protocols in Dulbecco's Modified Eagle Medium (DMEM; Life Technologies, Grand Island, NY, USA) supplemented with 10% fetal bovine serum (FBS; Atlanta Biological, Lawrenceville, GA, USA) and 1% Antibiotic-Antimycotic (ABAM; Life Technologies) and pattern integrity was monitored over time by microscopy.

3.2.2 Direct Reprogramming

Mouse embryonic fibroblasts (MEFs) were reprogrammed to cardiomyocytes according to a protocol modified from Efe et al.⁽¹⁵⁶⁾ MEFs were isolated in a previous study from day 13.5 embryos of mice homozygous for doxycycline-inducible *OSKM* factors.⁽¹⁹⁶⁾ Cells were seeded at 3,600 MEFs/cm² (normalized to adhesion area) in DMEM + 10% FBS + 1% ABAM within 24-well plates containing functionalized surfaces prepared on 12 mm glass coverslips (Day -1). Reprogramming began at day 0 and was executed via timed stages of media treatments.⁽¹⁹⁶⁾ Each well was provided 1 mL of media that was changed daily throughout the protocol. All media components were purchased from Invitrogen (Life Technologies) unless otherwise noted. From days 0-5, cells were reprogrammed toward incomplete pluripotency by induction of Yamanaka factors with doxycycline and inhibition of iPSC generation via JAK-STAT inhibition. Media consisted of knockout DMEM (KO DMEM) + 2 µg/mL doxycycline (Sigma) + 0.5 µM JAK inhibitor I (JI1, EMD) + 15% embryonic stem cell qualified FBS (ES-FBS) + 5% knockout serum replacement (KSR) + 0.1 mM β-mercaptoethanol, + 1% Glutamax + 1% non-essential amino acids + 1% embryonic stem cell qualified nucleosides (Millipore). From days 6-8, doxycycline was removed, ES-FBS concentration was reduced to 1%, and KSR concentration was increased to 14% (all other components remained the same). From days 9-14, cardiogenesis was initiated with chemically defined media (CDM) that included BMP4. Media consisted of RMPI-1640 + 20 ng/mL BMP4 (Stemgent) + 0.5x N2 + 1x B27 w/o vitamin A + 0.05% BSA fraction V + 0.1 mM β-mercaptoethanol. From days 15-18, CDM was applied without BMP4.

3.2.3 Surfaces for Reprogramming

Reprogramming was conducted on patterned and non-patterned surfaces that included substrates of: laminin adsorbed to mercaptosilane, Matrigel adsorbed to mercaptosilane, and PEG VS:BSA nanogels (on mercaptosilane) functionalized with laminin and RGD. Matrigel (BD Biosciences) was applied at 11.4 µg/cm² by diluting in DMEM and applying 200 µL to each well for

1 h at room temperature according to product specifications. Laminin-111 (Sigma) was applied to both glass and nanogel coatings at a surface density of 57 $\mu\text{g}/\text{cm}^2$ by diluting in PBS and applying 200 μL to each coverslip, allowing overnight incubation at 37 °C for either adsorption or covalent conjugation via protein amines with vinyl sulfones. After laminin conjugation, RGD (Seq: Ac-GCYRGDSPG-NH₂; Genscript) was conjugated at 44 nmol/cm² to nanogel coatings via cysteine thiols to vinyl sulfones, by diluting in PBS and applying 200 μL to each coverslip for 1 h at 37 °C. Patterned laminin and Matrigel surfaces were capped with 500 μL of 200 mg/mL four-arm PEG-amine in PBS for 3 h at 37 °C before incubation with laminin or Matrigel. Functionalized PEG nanogel surfaces were capped overnight with the same, except after laminin and RGD conjugation.

3.2.4 Contracting Patch Quantification

Samples were examined under 4x and 10x objective at days 14, 16, and 18 of reprogramming to find and count patches of cells that were synchronously contracting. Approximate boundaries of the contracting patches were outlined on image files and analyzed by *ImageJ* to determine the areas of the contracting patches.

3.2.5 Immunocytochemistry Analysis

On day 18 of reprogramming, cells were fixed with 500 μL /well of 4% paraformaldehyde for 15 min and washed 3x 5 min with PBS. Cells were then permeabilized for 30 min at room temperature using 300 μL /well of a 1:1000 dilution of Triton-X 100 in blocking solution (10% goat serum + 1% BSA in PBS). Primary antibody for sarcomeric α -actinin (mouse IgG; Sigma) was diluted at 1:1600 in blocking solution and applied at 300 μL /well overnight at 4 °C. After washing 3x 5 min with PBS, secondary antibody (Alexa Fluor 594 goat anti-mouse; Invitrogen) was next diluted at 1:1000 in blocking solution and applied at 300 μL /well for 1 h at room temperature. Cells were washed again 3x 5 min with PBS and finally cell nuclei were stained with DAPI (100 ng/mL in PBS) at 300 μL /well for 30 min at room temperature. Samples were stored under PBS at 4° C in the dark. Fluorescent images taken at 4x and 10x objective were contrast enhanced and converted to binary images in *MATLAB* before calculating the surface area staining positive for each α -actinin and DAPI. Positive staining areas were tallied separately for each stain on each coverslip and the cumulative ratio of α -actinin/DAPI was calculated.

3.2.6 Statistics

All statistical significance ($p < 0.05$) was calculated in *MATLAB* using ANOVA with a post-hoc Tukey-Kramer test. All data are presented as mean \pm standard deviation, with 3 samples for each condition examined during reprogramming.

3.3 Results

3.3.1 Preliminary Optimization of Patterning Techniques

We examined two general schemes for the fabrication of patterned cell substrates using our PEG nanogel coatings as passivating backgrounds (Figure 3.1). In Scheme I, we conjugated the nanogel solution to mercaptosilanated glass coverslips under stamping. This protocol left regions of silanated glass protected from PEG conjugation beneath the stamp posts. After removal of the stamp, the vinyl sulfone groups were capped and the surface was incubated in solutions of adhesion proteins, with the patterned nanogels preventing adsorption across the surface except for exposed spots of mercaptosilanated glass created by the stamp. In Scheme II, we instead conjugated the nanogel solution across the entire mercaptosilanated glass surface prior to stamping. The reactive vinyl sulfone groups were selectively capped to create a patterned surface by incubating the capping solutions under stamping on the nanogel coated surface. After stamping, selective adhesive spots were created by incubating the surface in a solution of adhesive proteins or peptides to covalently conjugate to the vinyl sulfones protected from capping under the stamp posts.

Several molecules were considered to serve as vinyl sulfone capping reagents for the creation of patterned adhesion areas. We tested the resistance of capped surfaces to resisting RGD conjugation (Figure 3.2), as RGD will be incubated over entire surfaces of some samples (Scheme II), including the passivated background. However, several of our standard choices including BSA and cysteine showed non-specific cell adhesion over the entire surface, suggesting that RGD was inadvertently conjugated to the capped passivating background. Both BSA and cysteine (if conjugated via its amine group via the slower, less probable reaction) possess free thiols which most likely formed disulfide bonds with the cysteine-containing RGD peptide. However, PEG-amine showed no significant fibroblast adhesion and was comparable to nanogel coatings incubated with

fibrinogen rather than RGD. Given this result we also evaluated the amino molecule tris as a potential capping agent, given its high water solubility (Figure 3.3). However, even without adsorption of fibrinogen to the surface, a solution of 500 mg/mL tris was unable to achieve adequate capping and resistance to fibroblast adhesion within as short of a time frame as PEG-amine.

Scheme I was tested under several conditions, including adsorption of several different adhesion proteins. We found the best result when capping the nanogel background with 50 mg/mL cysteine for 2 h at 37 °C and then incubating the surface in a 500 μ L solution of 2.5 mg/mL fibrinogen for 2 h at 37 °C. This particular patterned surface was seeded with fibroblasts and maintained pattern integrity for up to around 53 days when cell migration was observed from the originally stamped areas (Figure 3.4). Two other samples were stamped with this same strategy, but capped with four-arm PEG-amine for 1 h at 37 °C, and then incubated with either 15 μ g laminin overnight at 37 °C (Figure 3.5) or ~24 μ g Matrigel for 1 h at 37 °C (Figure 3.6). Although both these samples showed comparable and promising patterning after initial cell seeding, the long-term pattern integrity did not hold up as well as the previous sample with significant cell migration and pattern collapse emerging between 6 and 10 days. It is presently uncertain, whether the differences between the performance of the fibrinogen sample and the laminin or Matrigel samples stems from the difference in capping reagent or from the reactivity or adsorption of the adhesion protein solution with the passivated nanogel background. Additionally, differences in the volume of media and frequency of media changes may have contributed to the aggressiveness of the cells in terms of their proliferation and migration. We were able to visualize the nanogel coating formed via Scheme I, by fluorescently labeling the surface with an amino-reactive dye, DyLight 488, after the stamping step and prior to any capping or protein incubation (Figure 3.7). These images revealed a well formed pattern (Figure 3.7 A) with minor damage in the form of scrapes appearing consistently below many of the patterned spots (Figure 3.7A and 3.7D). Most spots in the center region of the coverslip formed crisp edges with the nanogel coating (Figure 3.7B) while many spots near the border of the coverslip seem to show spots with rough edges surrounded by damaged nanogel coating (Figure 3.7C).

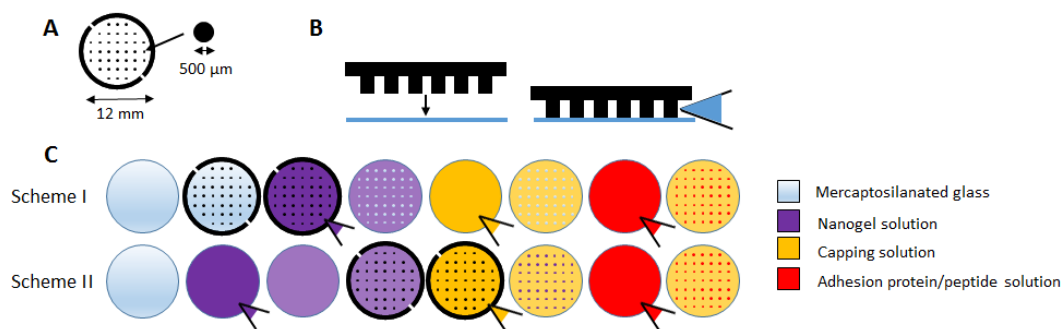


Figure 3.1: Strategies for patterning cell adhesion with PEG nanogel coatings. Surfaces were patterned for cell adhesion using (A) a 12 mm diameter rubber stamp that possessed 500 μm posts by (B) clamping the stamp to 12 mm glass coverslips and applying solutions to the interstitial space between the two with a pipet. (C) Patterns of adhesive molecules were fabricated with stamping via one of two schemes. In Scheme I, nanogel solutions (purple) were conjugated to mercaptosilanated glass under stamping, followed by whole surface incubations with capping solutions (yellow) to quench vinyl sulfones and then whole surface incubations with protein solutions (red) to create adhesive spots by adsorption to the unprotected mercaptosilanated glass. In Scheme II, the entire mercaptosilanated glass was first coated with nanogel solution (purple) before vinyl sulfones were selectively quenched with application of capping solutions (yellow) under stamping. The entire surface was then incubated with protein/peptide solutions (red) to allow covalent functionalization of the nanogel coating in spots with uncapped vinyl sulfones.

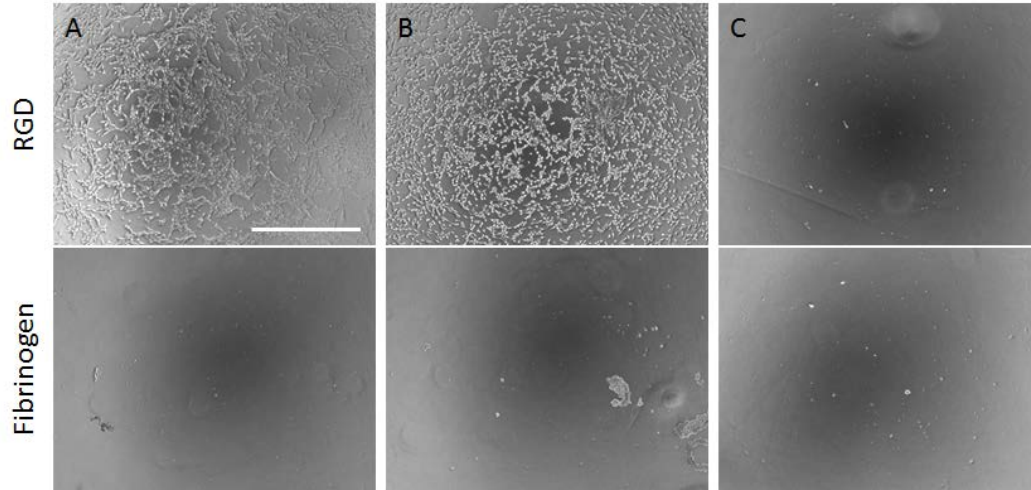


Figure 3.2: Cell adhesion on nanogel coatings capped with various molecules. Cell adhesion of 3T3 fibroblasts was examined on VS:BSA nanogel coatings capped at 37 °C with (A) 200 mg/mL BSA overnight, (B) 50 mg/mL cysteine for 1 h, or (C) 200 mg/mL four-arm PEG-amine for 1 h, all of which were then incubated with either 100 nmol RGD for 1 h (top) or 1.25 mg fibrinogen for 2 h (bottom) at 37 °C. Scale bar represents 1 mm.

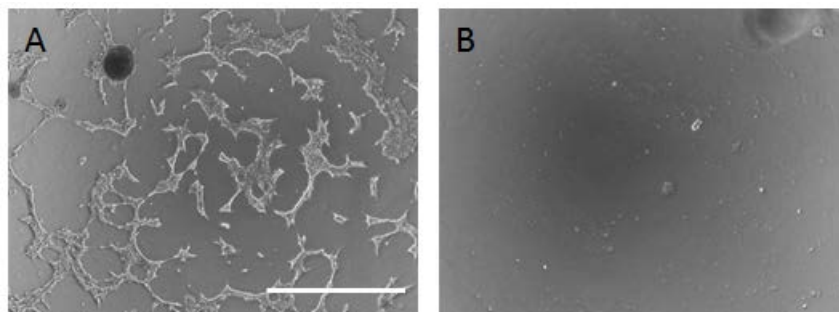


Figure 3.3. Cell adhesion on tris-capped nanogel coatings. Cell adhesion of 3T3 fibroblasts was examined on VS:BSA nanogel coatings capped at 37 °C with 500 μ L of 500 mg/mL tris for (A) 3 h or (B) overnight. Scale bar represents 1 mm.

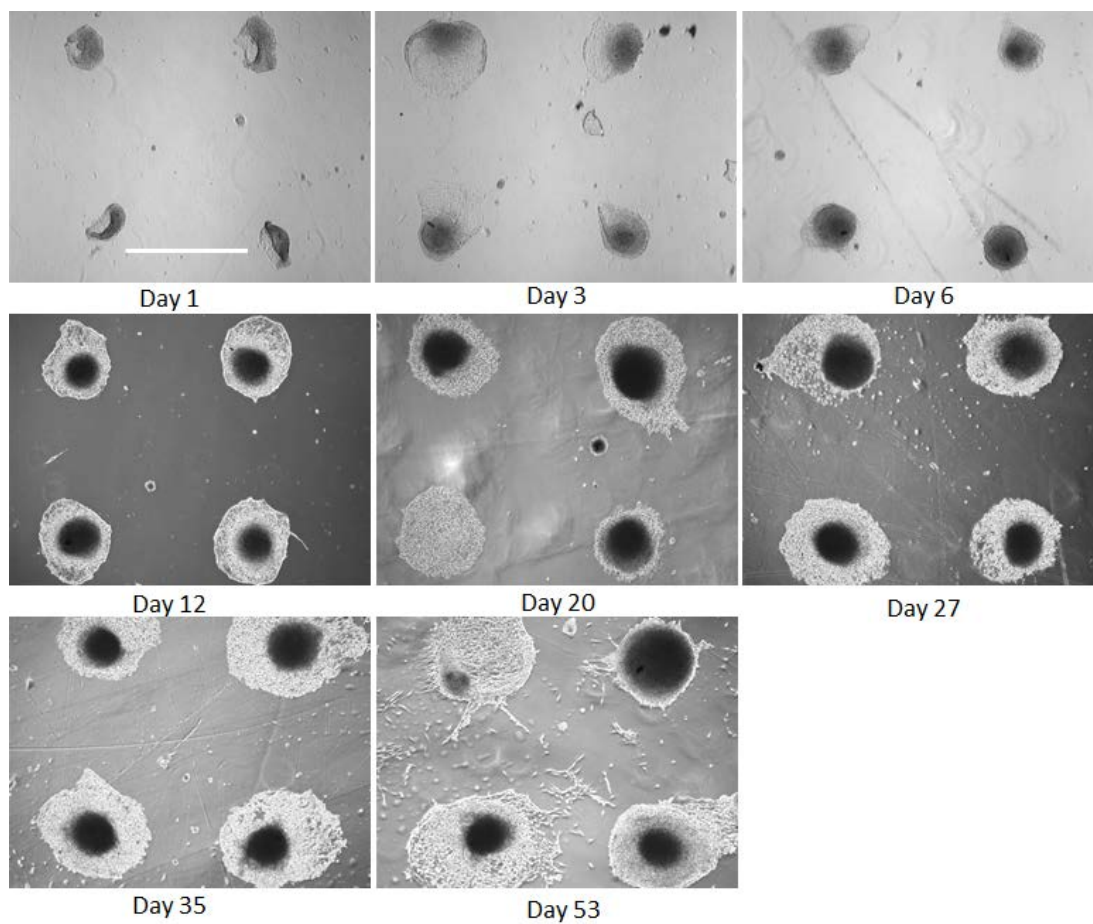


Figure 3.4: Pattern integrity of cells adhered via patterned fibrinogen adsorption. Pattern integrity of 3T3 fibroblasts was examined for up to 53 days on a surface patterned via Scheme I, in which the mercaptosilanated coverslip was incubated with VS:BSA nanogel solution under stamping and then capped with 50 mg/mL cysteine for 2 h at 37 °C and incubated with 2.5 mg/mL fibrinogen for 2 h at 37 °C. Scale bar represents 1 mm.

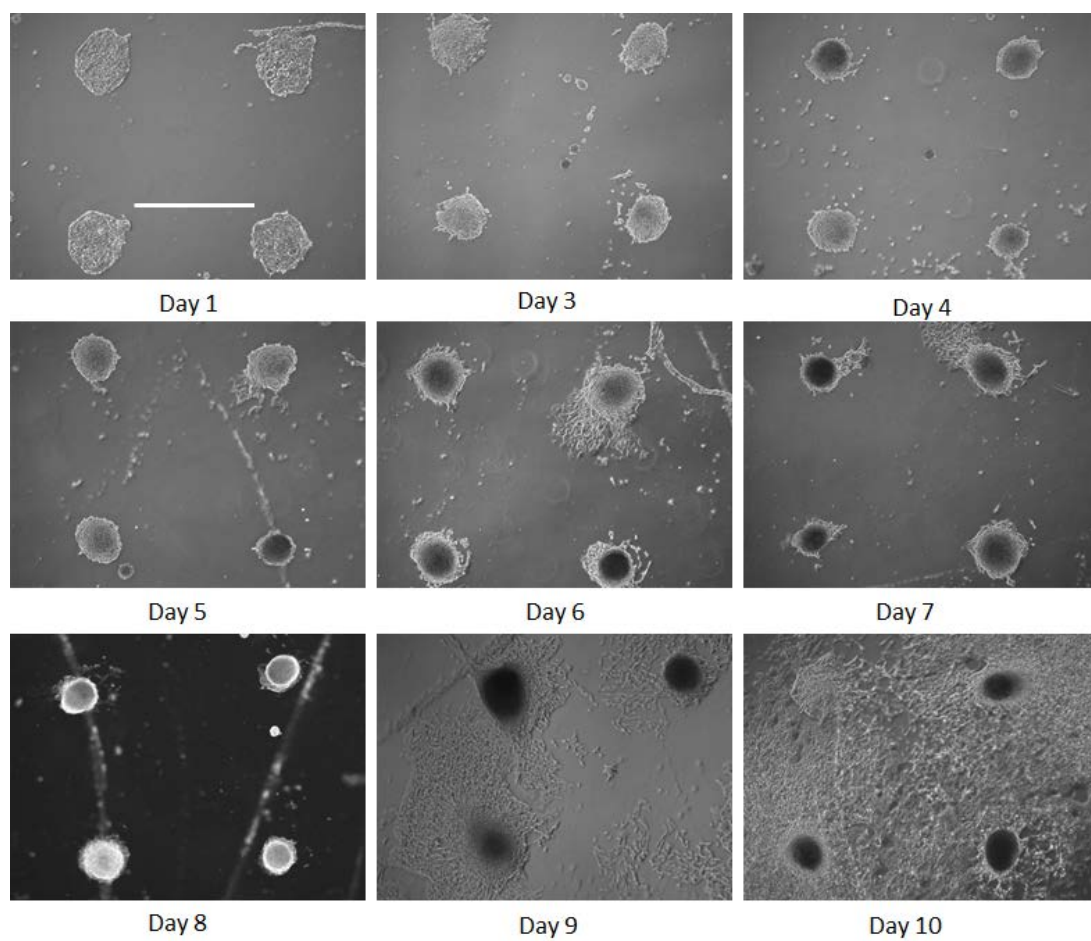


Figure 3.5: Pattern integrity of cells adhered via patterned laminin adsorption. Pattern integrity of 3T3 fibroblasts was examined for up to 10 days on a surface patterned via Scheme I, in which the mercaptosilanated coverslip was incubated with VS:BSA nanogel solution under stamping and then capped with 200 mg/mL PEG-amine for 1 h at 37 °C and incubated with 15 μ g laminin overnight at 37 °C. Scale bar represents 1 mm.

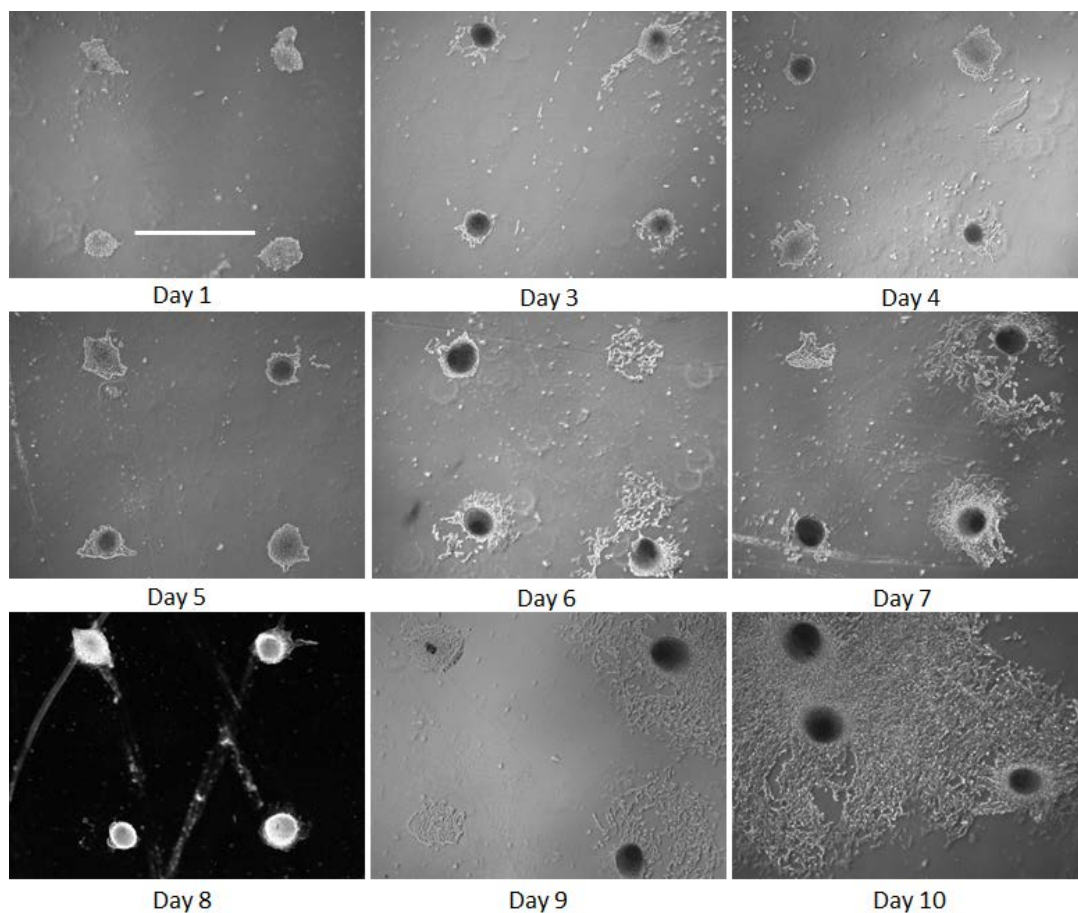


Figure 3.6: Pattern integrity of cells adhered via patterned Matrigel adsorption. Pattern integrity of 3T3 fibroblasts was examined for up to 10 days on a surface patterned via Scheme I, in which the mercaptosilanated coverslip was incubated with VS:BSA nanogel solution under stamping and then capped with 200 mg/mL PEG-amine for 1 h at 37 °C and incubated with ~24 μ g Matrigel for 1 h at room temperature. Scale bar represents 1 mm.

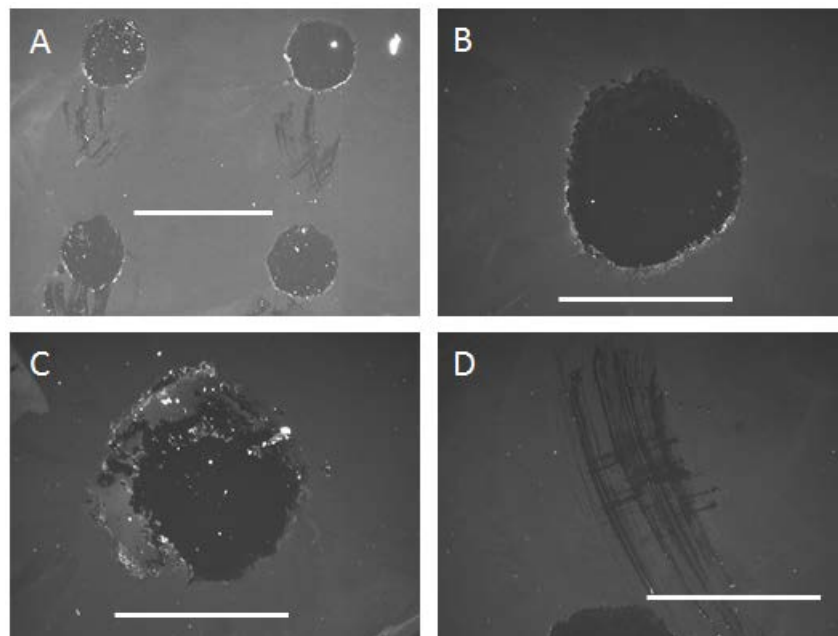


Figure 3.7: Fluorescent imaging of a patterned nanogel coating. Fluorescent labeling with amino-reactive DyLight 488 of a VS:BSA nanogel coating fabricated via Scheme I without capping or subsequent protein incubation shows uncoated mercaptosilane spots under (A) 4x objective or (B, C, D) 10x objective. Spots found near the center of the coverslip (B) seem to possess more defined edges than some found near the border of the coverslip (C). Scrape-like marks may also be consistently found beneath many of the patterned spots (A, D). Scale bars represent 1 mm (A) or 500 μm (B-D).

The volume of liquid contained on one 12 mm coverslip beneath the rubber stamp was approximated to be 55 μL , which is notably less than the 150 μL incubated on top of the surfaces for standard nanogel coating procedure or the 500 μL incubated with the nanogel coated coverslip to cap residual vinyl sulfone groups (typically performed within a 24 well plate). The reduced volume seems to have a pronounced effect on the efficacy of the capping solution when using Scheme II, compared to non-patterned nanogel coatings capped with the full 500 μL for the same durations of time. We tested this hypothesis by replacing the 200 mg/mL PEG-amine capping solution within the stamped coating every 5 min during a 1 h incubation at 37 °C and noticed some improvement in pattern integrity, with less cell adhesion observed in the interstitial space after incubation with 50 nmol RGD (Figure 3.8). Interestingly, the pattern generated using Scheme II with repetitive capping showed pattern collapse at around the same time frame as the laminin and Matrigel patterns generated with Scheme I, between 6 and 9 days (Figure 3.9).

When applying stamping to nanogel coatings as in Scheme II, the effect of the high mechanical pressure on the thin nanogel coating must be considered. To study these effects we performed sham stampings in which nanogel coatings were clamped together with the stamps and filled with PBS to preserve hydration. The stamps and binder clips were removed at several time points and the entire surface was then capped overnight per normal with 500 μL of 200 mg/mL PEG-amine, such that the entire surface should resist cell adhesion. However, after seeding 3T3 fibroblasts on the surfaces it was revealed that the areas beneath the rubber stamp showed significant cell adhesion if applied overnight and some cell adhesion at lesser time points (Figure 3.10). Interestingly, the nanogel coating subjected to 1 h stamping showed more severe cell adhesion than that subjected to 3 h stamping, suggesting that not only the duration of stamping but the amount of pressure applied by the binder clips could influence the results. The pressure is not necessarily normalized as the binder clips are all manually adjusted to fit the coverslip and stamp set up. All binder clips were afterwards adjusted to attempt to provide the minimal pressure necessary to secure the stamps to the nanogel coated coverslips. These results also indicate the value in optimizing stamping times such that application of capping solutions is reduced to the minimal time required to adequately quench vinyl sulfones. Rubber stamps became noticeably stuck to the glass coverslips after overnight applications, requiring significant prying force to remove them from the surface. Such a phenomenon was rarely observed on 1 h applications, suggesting that indeed the application duration and not just the amount of pressure impacts the surface. The exact affect the

stamping has on the surface is unclear but could include adsorption of the PEG to the stamp and subsequent removal/breakage from the coverslip surface or dehydration of the hydrogel network beneath the stamp. The detrimental effect of dehydration was demonstrated on a nanogel surface which was allowed to dry overnight at 37 °C and was then rehydrated, capped, and seeded with fibroblasts (Figure 3.10D). The extensive fibroblast adhesion implies that the dehydration has an irreversible damaging effect to the PEG network that diminishes its innate protein resistive properties. These findings also indicate that the potential to implement a microcontact printing protocol on the nanogel surfaces might prove difficult, considering these protocols are normally performed by stamping dried proteins onto relatively dry surfaces, although PEG hydrogels have been used as substrates.⁽¹⁹⁷⁾

As laminin has been shown important for cardiomyocyte differentiation, we explored the potential of using it as the primary adhesion molecule on our nanogel coatings by covalently coupling it to the vinyl sulfones. We used a slightly higher amount of laminin (25 µg/sample), compared to what is found in Matrigel coatings (15 µg/sample) of the same area and similar studies that have adsorbed laminin to TCPS.⁽¹⁹⁶⁾ We found that laminin was not able to promote fibroblast adhesion on VS:BSA nanogel coatings (Figure 3.11A-D) and only promoted moderate fibroblast adhesion on VS:Am nanogel coatings (Figure 3.11E-H) if residual vinyl sulfone groups were left uncapped after laminin conjugation. The latter suggests a synergy between the covalently attached laminin and serum proteins conjugated to the residual vinyl sulfones, neither of which promoted cell adhesion alone.

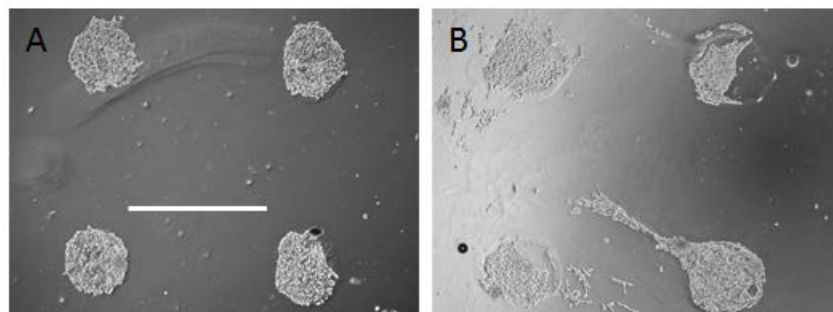


Figure 3.8: Patterned cell adhesion on RGD-functionalized nanogel coatings after repetitive capping. Pattern integrity of 3T3 fibroblasts was examined on VS:BSA nanogel coatings patterned via Scheme II, by capping with 200 mg/mL PEG-amine for 1 h at 37 °C under stamping and then incubating with 50 nmol RGD overnight at 37 °C. The capping solution was replaced every 5 min (12 times) in (A) but not in (B). Scale bar represents 1 mm.

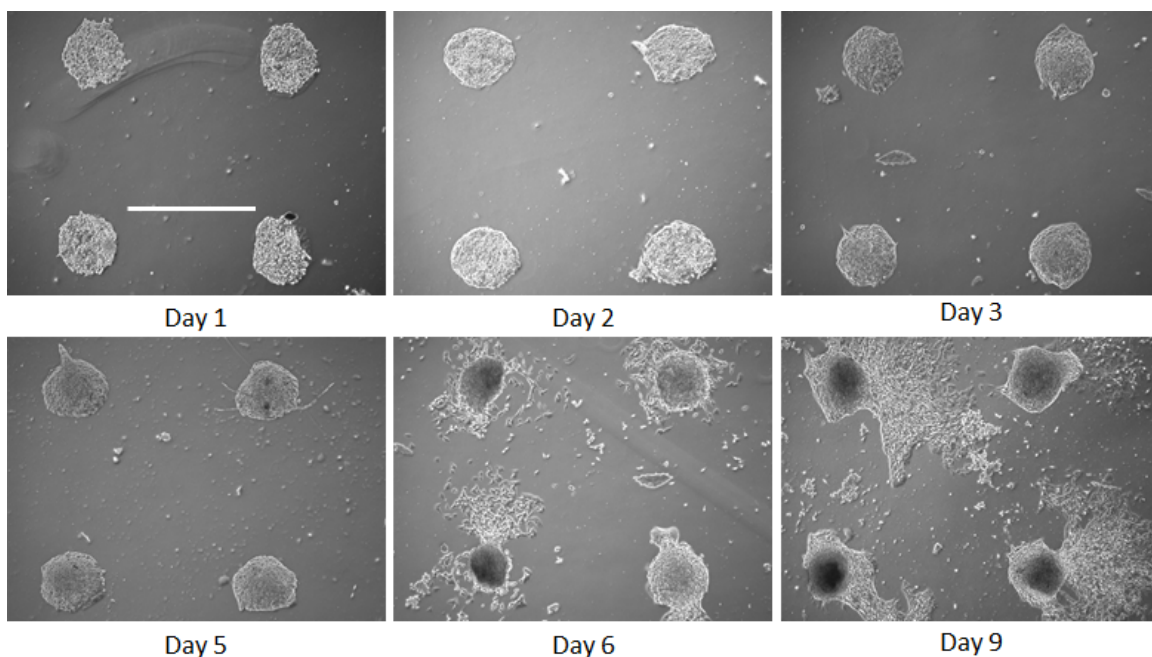


Figure 3.9: Pattern integrity of cells adhered via patterned RGD-functionalization of nanogel coatings. Pattern integrity of 3T3 fibroblasts was examined for up to 9 days on a VS:BSA nanogel coating patterned via Scheme II, after being capped under stamping with 12 x 5 min incubations (1 h total) of 200 mg/mL PEG-amine at 37 °C and then incubated with 50 nmol RGD overnight at 37 °C. Scale bar represents 1 mm.

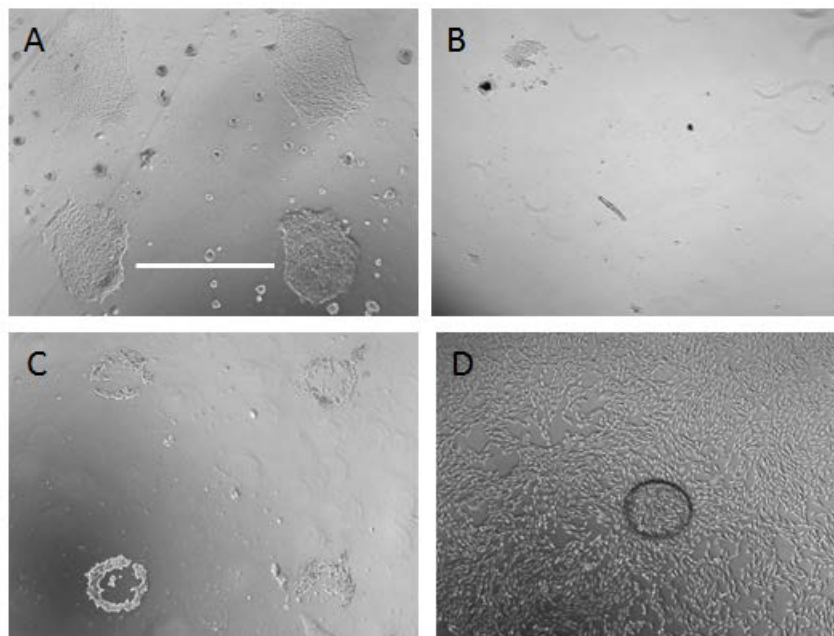


Figure 3.10: Cell adhesion on nanogel coatings after sham stamping. Cell adhesion of 3T3 fibroblasts was examined on VS:BSA nanogel coatings that underwent sham stamping under PBS (A) overnight, (B) for 3 h, or (C) for 1 h before the entire surface was capped overnight at 37 °C with 200 mg/mL PEG-amine. The VS:BSA nanogel coating in (D) was dried overnight, rehydrated in PBS for 3 h, and then capped overnight with 50 mg/mL BSA, all at 37 °C. Scale bar represents 1 mm.

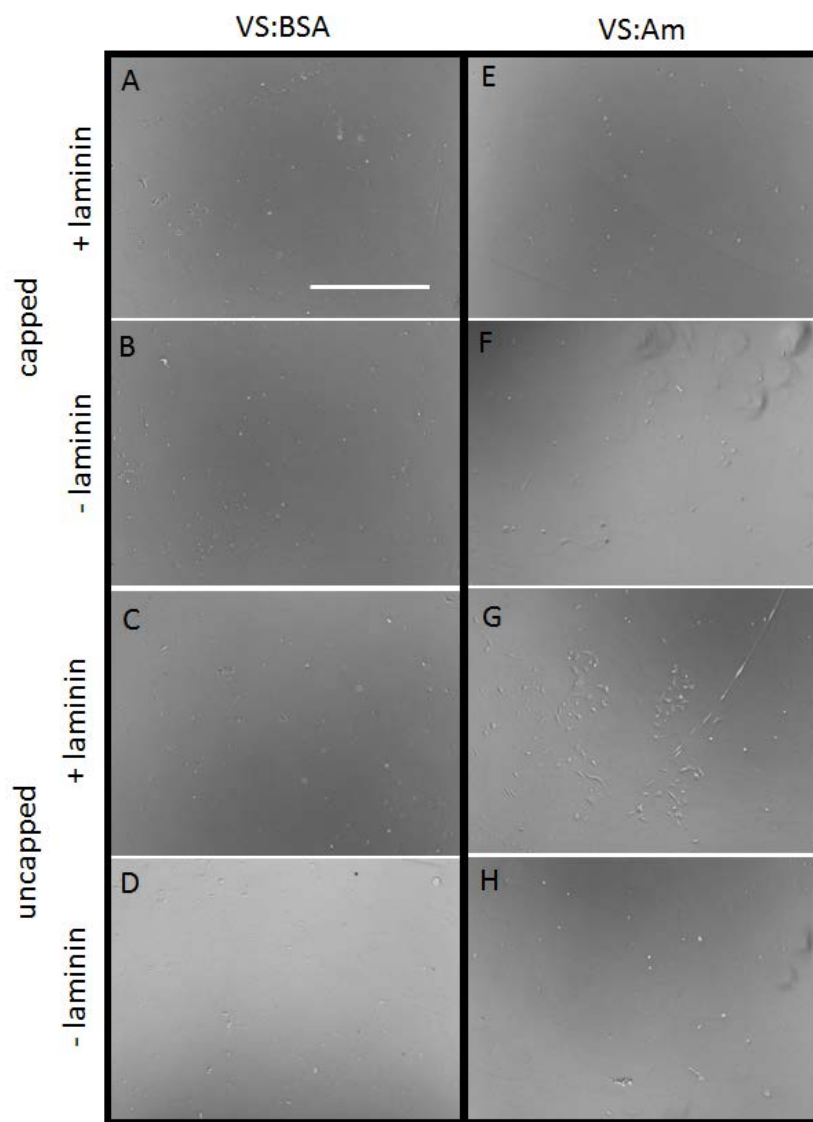


Figure 3.11: Cell adhesion to laminin-functionalized nanogel coatings. Cell adhesion of MEFs was examined on (A-D) VS:BSA and (E-H) VS:Am PEG nanogel coatings that were first incubated with (A, C, E G) 25 μ g laminin or (B, D, F, H) PBS and then incubated with (A, B) 200 mg/mL BSA, (E, F) 200 mg/mL PEG-amine or (C, D, G, H) PBS overnight at 37 °C. Scale bar represents 1 mm.

Because laminin was not capable of supporting fibroblast adhesion, we supplemented laminin in our direct reprogramming protocol with RGD, which has been used to provide robust adhesion for several cell types, including fibroblasts and cardiomyocytes.⁽¹⁹⁸⁾ A serial dilution of RGD incubated on VS:BSA nanogel coatings for 1 h at 37 °C showed a clear concentration dependent adhesion response of 3T3 fibroblasts in both cell density and cell spreading (Figure 3.12A). Maximal cell adhesion and spreading seems to be maintained with as little as 50 nmol RGD, with noticeable reductions beginning to appear between 25 and 12.5 nmol RGD. Using dry mass measurement previously obtained with OWLS on the VS:BSA nanogel coatings,⁽¹⁾ we calculated a theoretical vinyl sulfone content of 118 pmol per coverslip, although a large percentage of those will be reacted. This mass would correspond to a 2.66% (w/v) PEG hydrogel coating of 100 nm thickness, which is near the lower threshold of the PEG content that is reasonably required to form a bulk hydrogel. Clearly the RGD content required to achieve maximal cell adhesion (25 nmol) is much higher than what would be theoretically expected, considering these values are orders of magnitude above what should saturate the remaining vinyl sulfones. Because all free RGD molecules should have ample time to covalently react to the surface within the 1 h incubation period, we assume that disulfide bonding within the RGD solution drastically lowers the concentration of available thiols for surface reaction. We also tested the adhesion response of MEFs to a dilution of RGD and found a similar response with a drop-off in adhesion between 25 and 12.5 nmol RGD (Figure 3.12B). To assure adequate adhesion for our reprogramming experiments we incubated nanogel coatings with 50 nmol RGD for 1h at 37 °C after laminin conjugation.

3.3.2 Non-Patterned and Patterned Surfaces for Direct Reprogramming

We used the stamping schemes described above to create patterned surfaces with three different adhesive substrates: laminin adsorbed to mercaptosilanated glass (laminin), Matrigel adsorbed to mercaptosilanated glass (Matrigel), and PEG-functionalized with laminin and RGD in the form of our VS:BSA nanogel coating (PEG-laminin/RGD). The laminin and Matrigel patterned surfaces were created using Scheme I, while the PEG-laminin/RGD patterned surface was created using Scheme II. Surfaces were seeded with MEFs for reprogramming to cardiomyocytes and photographed every 3 days. Representative images of each sample are shown in Figures 3.13 (days 3, 6, 9) and 3.14 (days 12, 15). Because cells were seeded according to established protocols at a

much lower density than the preliminary experiments (3,600 vs. 40,000 cells/cm²), signs of patterning did not emerge until imaging on day 3 when cells became more confluent.

Surprisingly, the laminin and especially the Matrigel patterns were not as well-defined as those seen in preliminary experiments seeded with 3T3 fibroblasts (Figures 3.5 and 3.6). Although the stamped regions are detectable on most samples, the edges are loosely defined and a number of cells are adhered within the interstitial spaces. The patterned PEG-laminin/RGD surfaces, on the other hand, exhibit well defined and confined circular cell patches. While any semblance of a pattern is lost on the patterned laminin and patterned Matrigel samples by day 9, the patterned PEG-laminin/RGD surfaces maintain good integrity until day 9 and show gradual but incomplete degradation afterwards through day 18. However, while defined stamping boundaries were present across the patterned PEG-laminin/RGD surfaces, many of the patches never filled to confluency via cell proliferation. Additionally, beginning at day 9 we continually observed decreasing numbers of cell aggregates on the patterned PEG-laminin/RGD surfaces, indicating that the aggregates can become detached if they outgrow their adhesion areas. While the patterned PEG-laminin/RGD surfaces and parts of the patterned laminin and Matrigel surfaces began showing 3-dimensional cell growth evidenced by the phase-dark aggregates at day 9, the non-patterned surfaces mostly did not begin showing spontaneous cell aggregation until day 12.

Low objective micrographs of the whole surfaces on day 15 (Figure 3.15) depict areas of high cell density (phase bright) across the various samples and confirm that pattern integrity was best maintained on the patterned PEG-laminin/RGD surfaces relative to the patterned laminin and Matrigel surfaces. They also show, however, that only several of identifiable patterned spots on the patterned PEG-laminin/RGD surfaces have grown into larger more dense aggregates, confirming that most of the patterned spots either did not fill in or peeled off. These micrographs furthermore reveal that the non-patterned laminin surfaces promoted substantially more robust cell proliferation compared to other conditions, as seen by the expansive coverage of the surfaces by dense and large cell aggregates.

3.3.3 Quantification of Functional Contraction in Differentiated Cardiomyocytes

The first sign of cardiomyocyte contraction was detected at day 13. The number of synchronized beating patches was quantified by visual examination on days 14, 16 and 18 (Figure 3.16A). The number of contracting patches continually increased on virtually all samples until day 18 when the cells were fixed. Counts on all non-patterned surfaces more than doubled between days 16 and 18 suggesting significant maturation of cardiomyocytes during this time frame. All substrates presented more contracting patches on their non-patterned surfaces compared to their patterned counterparts and on none of the surfaces did the patterned substrates display earlier signs of functional contraction. Because the patterned samples did not maintain pattern integrity throughout the entire 18 days, it is not appropriate to normalize this data to the original adhesion area of the patterned surfaces. The non-patterned laminin and PEG-laminin/RGD surfaces displayed significantly higher numbers of contracting patches relative to the other surfaces examined. These results were mimicked by quantifications of the cumulative surface areas of the contracting patches (Figure 3.16B), except that the non-patterned PEG-laminin/RGD surfaces exhibited a higher proportion of contracting surface area than the non-patterned laminin surfaces, despite having a lower count of contracting patches.

When we examine the average surface area of all the individual contracting patches for each condition (Figure 3.17A), we see that the contracting patches displayed on non-patterned PEG are on average larger than those on all other surfaces, although not significantly so given the large size distribution evidenced by the standard deviation. A box plot of this data reveals that several extremely large contracting patches on the non-patterned PEG-laminin/RGD, the size of which is not seen on any other conditions, skewed its average towards larger dimensions (Figure 3.17B). The non-patterned laminin also displayed some contracting patches that were larger than other conditions, but is probably skewed downward by many tiny patches seen contracting within the cell monolayers (Figure 3.18). Unlike large 3-dimensional aggregates, smaller patches of cardiomyocytes are known to be less contractile^(187, 199) and mature cardiomyocytes outside of large 3-dimensional aggregates may be less likely to form large synchronized contractions because of strong cellular adhesions to the laminin functionalized surface. One relatively large contracting patch was also found on the patterned PEG-laminin/RGD surface, which seemed to skew the average size given the relatively low counts on these samples.

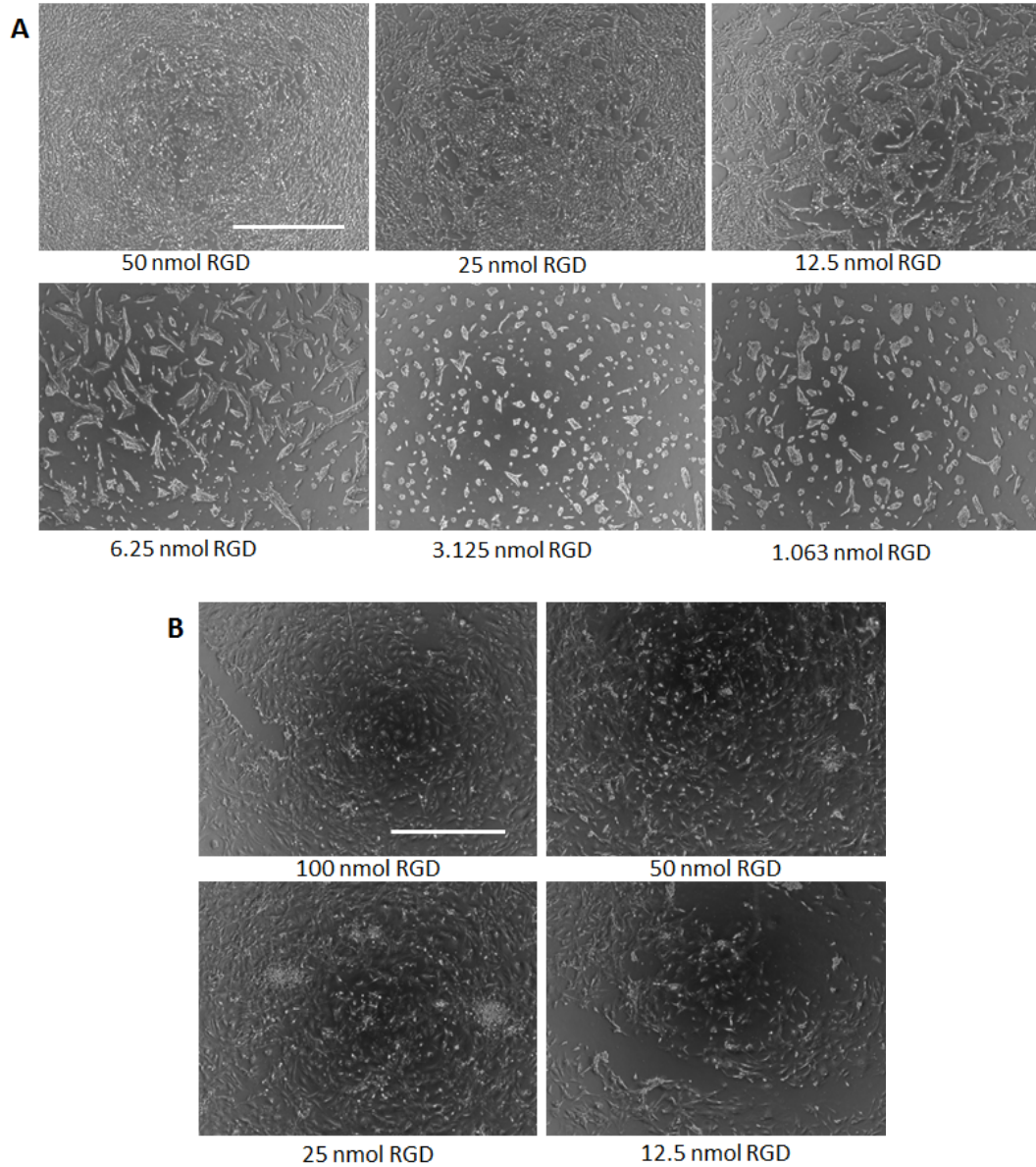


Figure 3.12: Cell adhesion to RGD-functionalized nanogel coatings. The extent of cell adhesion of (A) 3T3 fibroblasts and (B) MEFs on RGD-functionalized VS:BSA nanogels was examined across serial dilutions of RGD ranging from (A) 1.063-50 nmol/coverlip or (B) 12.5-100 nmol/coverlip. Samples were capped after RGD conjugation with overnight incubations of 200 mg/mL BSA at 37 °C. Scale bars represents 1 mm.

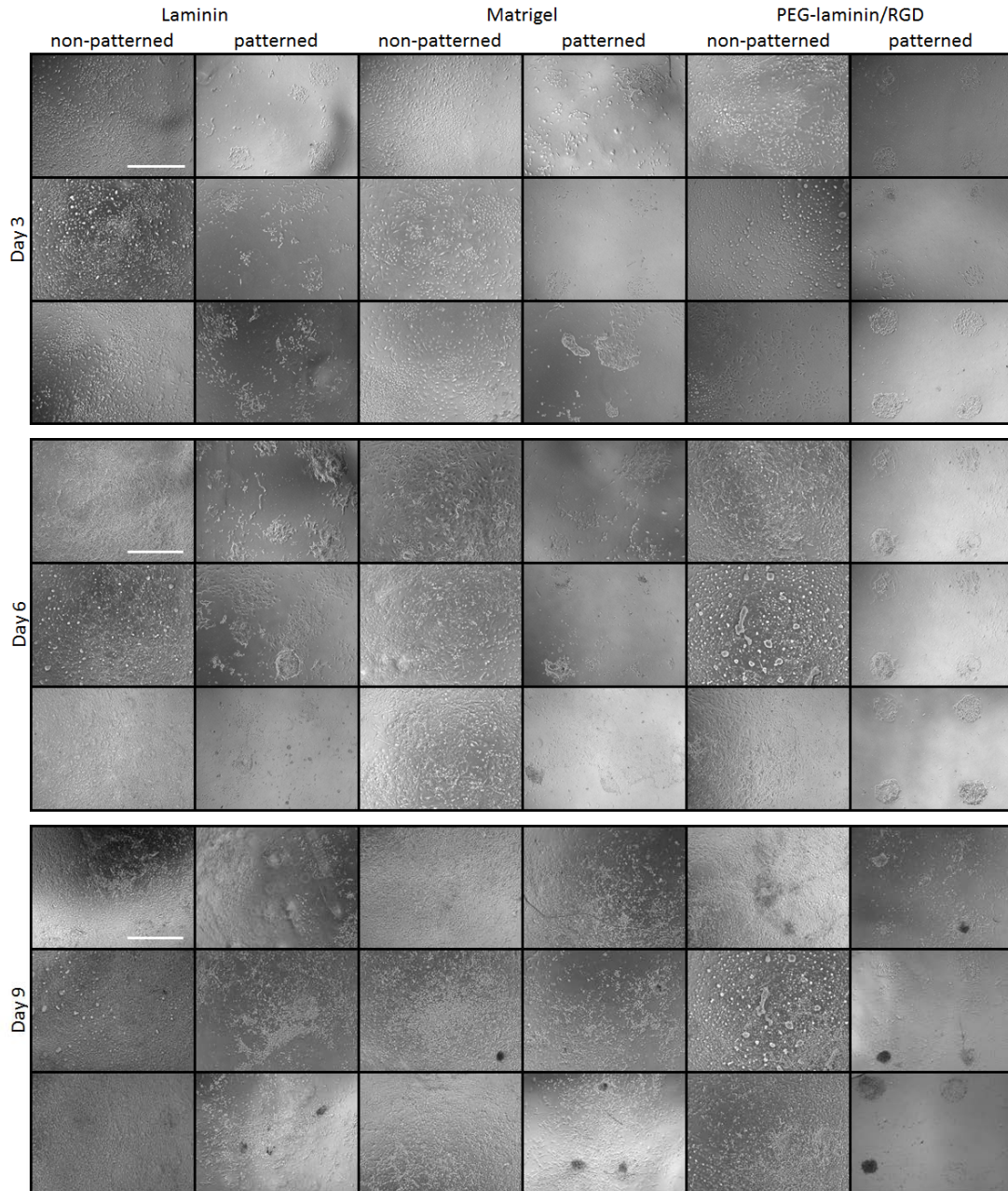


Figure 3.13: Cell adhesion at days 6, 9, and 12 of reprogramming. Representative micrographs from each of 3 samples for non-patterned and patterned laminin, Matrigel, and PEG-laminin/RGD surfaces show cell density and pattern integrity at days 3, 6, and 9 of the 18-day reprogramming protocol. Scale bars represent 1 mm.

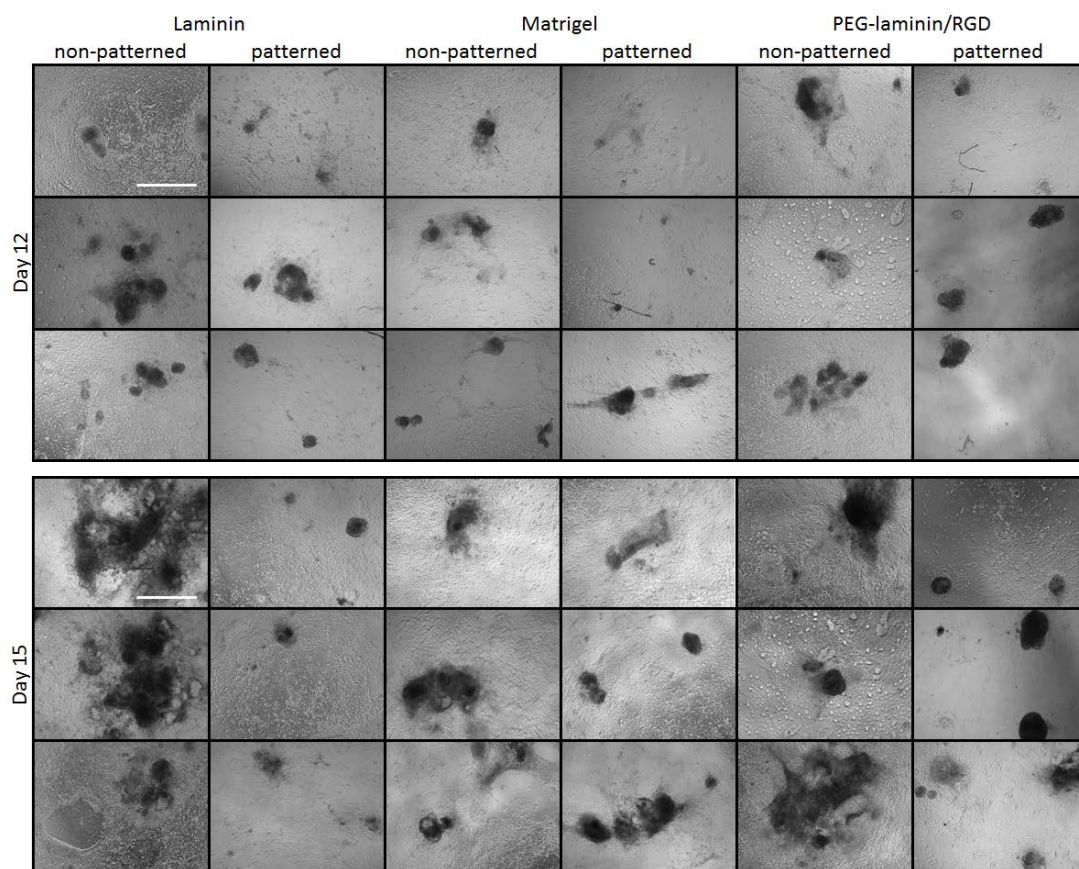


Figure 3.14: Cell adhesion at days 12 and 15 of reprogramming. Representative micrographs from each of 3 samples for non-patterned and patterned laminin, Matrigel, and PEG-laminin/RGD surfaces show cell density and pattern integrity at days 12 and 15 of the 18-day reprogramming protocol. Scale bars represent 1 mm.

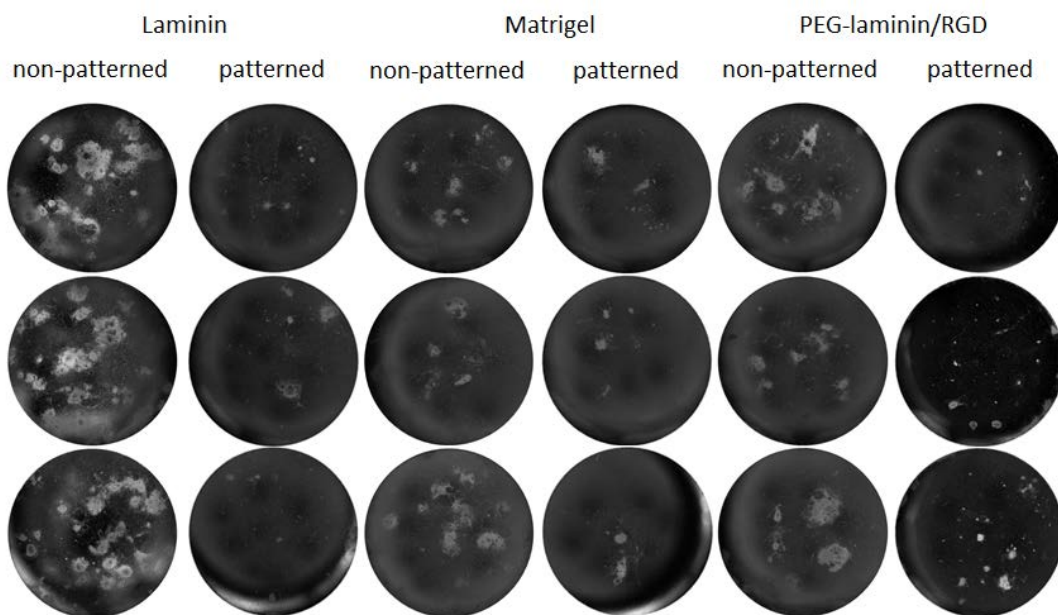


Figure 3.15: Low objective micrographs of cell adhesion at day 15 of reprogramming. Low objective micrographs of all 3 samples for non-patterned and patterned laminin, Matrigel, and PEG-laminin/RGD surfaces show cell density and pattern integrity across the entire 12 mm coverslips at day 15 of the 18-day reprogramming protocol.

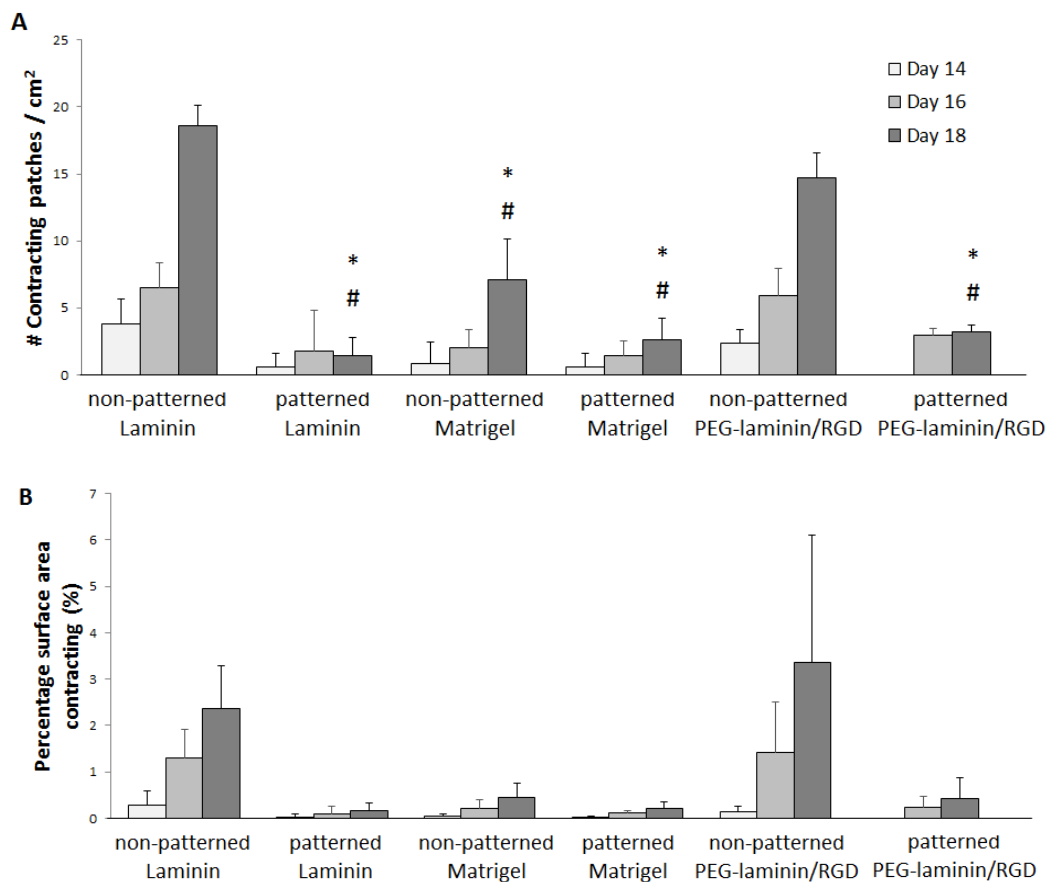


Figure 3.16: Quantified cardiomyocyte contraction during reprogramming. The (A) number of contracting patches and (B) cumulative surface area of contracting patches on each coverslip was quantified at days 14, 16, and 18 of reprogramming under the microscope. Statistical significance ($p < 0.05$) was determined for day 18 relative to non-patterned laminin (*) and non-patterned PEG-laminin/RGD (#). Data are presented as mean \pm standard deviation ($n = 3$).

3.3.4 Sarcomeric α -Actinin Expression in Differentiated Cardiomyocytes

On day 18, after final counts of beating clusters, the cell laden surfaces were fixed and stained for the cardiac marker sarcomeric α -actinin to visualize trends and relative extents of cardiac differentiation. Cell nuclei were also stained with DAPI so that α -actinin staining could be normalized to the total cell density (Figure 3.19). Notably, the non-patterned surfaces all exhibited relatively less variation between samples than the patterned surfaces, of which variation could result from sampling areas of intrinsically more heterogeneous surfaces or from genuine differences between the samples that arise due to the random and spontaneous breakdowns in pattern integrity. Images were taken at both 4x and 10x objectives and separately analyzed but revealed the same trends between the conditions. The non-patterned laminin showed the highest expression profile for α -actinin, corroborating the results seen in counts of contracting patches. Large cell aggregates on non-patterned laminin, like in other conditions, exhibited sporadic expression of α -actinin (Figure 3.20). However, large proportions of the cell monolayers surrounding these aggregates seemed to express a basal level of α -actinin as well, not seen in other conditions (Figure 3.21). The widespread expression across these cells on the non-patterned laminin surfaces accounts for the significantly increased α -actinin:DAPI expression found in this condition. This monolayer expression may relate to the large number of small contracting patches mentioned earlier to be found in the monolayer cells of this condition (Figure 3.18). Interestingly, the same extent of α -actinin expression was not found in the patterned laminin samples, even though the pattern integrity was not well maintained allowing monolayer expansion between the cell aggregates. Additionally we noted very strong α -actinin expression occasionally found along the edges of monolayers where circular holes were present (Figure 3.22). They are found across all conditions but appear most abundant on the non-patterned laminin surfaces. High α -actinin expression was also found across all conditions in cellular structures that appeared somewhat fibrillar, or appeared to form structures with large aspect ratios (Figure 3.23).

Patterned PEG-laminin/RGD surfaces were the only condition to show higher staining ratios than their non-patterned counterparts, although they did not demonstrate higher counts or surface areas of contracting patches. By visual assessment, the aggregates formed from patterning do not appear to express α -actinin more profusely than aggregates formed spontaneously on non-patterned PEG surfaces or on any other surface for that matter (Figure 3.20). Indeed, the

quantitative staining ratios for large cell aggregates are among the lowest of the sampled images for this condition. Rather, a number of tiny cellular aggregates surrounded by a diffuse field of single cells seem to comprise the best staining ratios for structures found on this condition (Figure 3.24). These aggregates show relatively well structured α -actinin throughout the cluster or at least expanding the entire dimensions of the cluster and were observed prominently on the patterned PEG-laminin/RGD surfaces. Intriguingly, these aggregates do also appear on the patterned laminin surfaces, which show almost identical staining ratios to the patterned PEG-laminin/RGD surfaces (Figure 3.19).

Finally, we looked at the α -actinin staining in images that were matched with relatively large contracting aggregates, as the latter would presumably indicate a sure sign of cardiomyocyte differentiation (and because these images were the easiest to pair). To our surprise these contracting areas did not appear to exhibit profuse or relatively strong (bright) α -actinin expression, although positive cells were detected within or near the edges of each (Figure 3.25). These comparisons indicate a subtle discrepancy in the two assays used to determine cardiomyocyte differentiation.

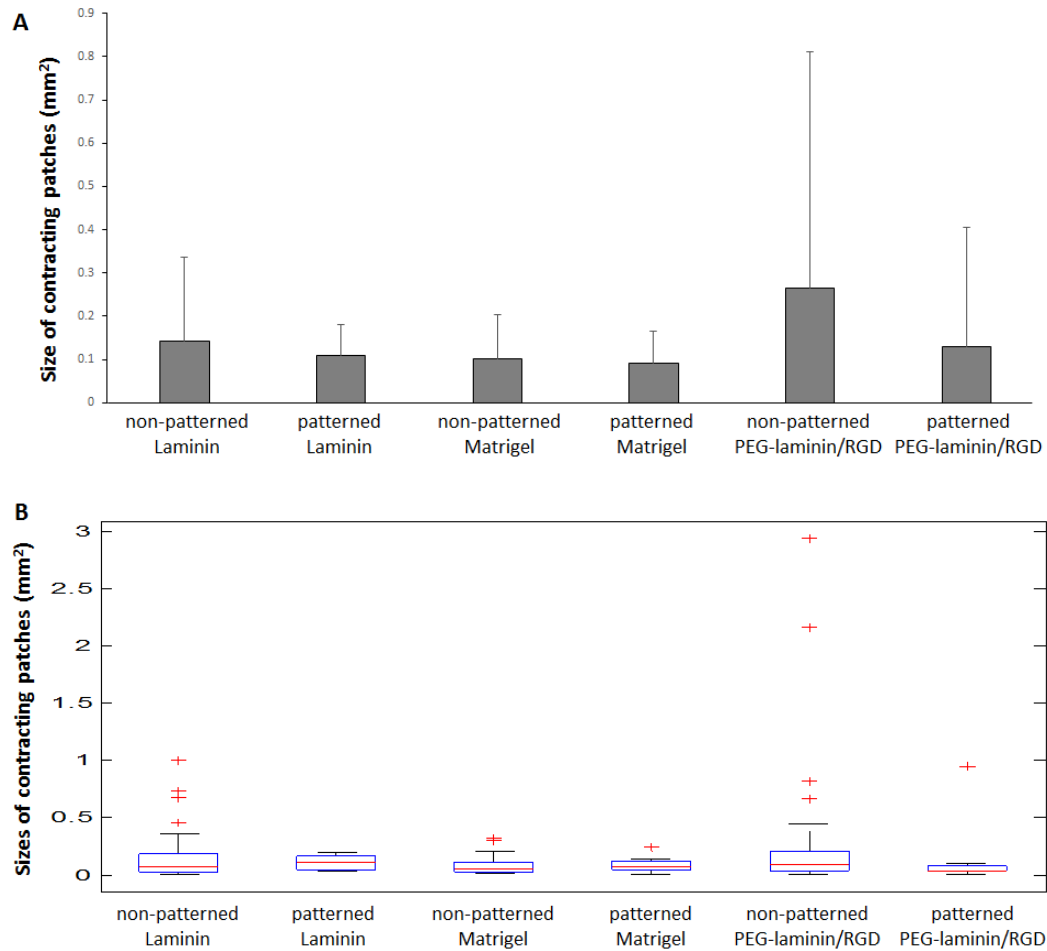


Figure 3.17: Size distributions of contracting cell patches. (A) The sizes of contracting patches from day 18 were pooled across samples from each condition and averaged. (B) A box plot of the data reveals similar median sizes of contracting patches but several outliers that skew the averages for certain conditions. Data are presented as mean \pm standard deviation.

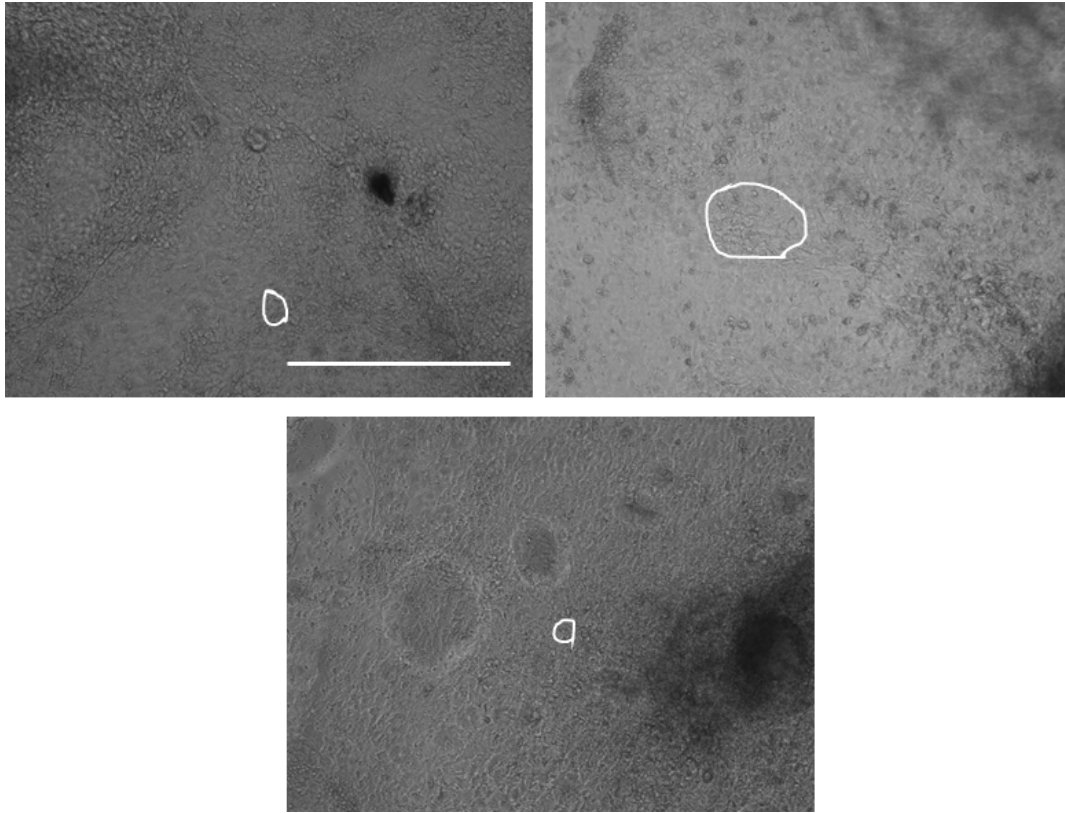


Figure 3.18: Images of small contracting patches on non-patterned laminin monolayers. Outlines of contracting cell patches (white) on micrographs of the non-patterned laminin surfaces show relatively small contracting patches that seem to uniquely appear within the 2-dimensional cell monolayers away from the larger 3-dimensional aggregates, which are more prone to show contraction. Scale bar represents 500 μm .

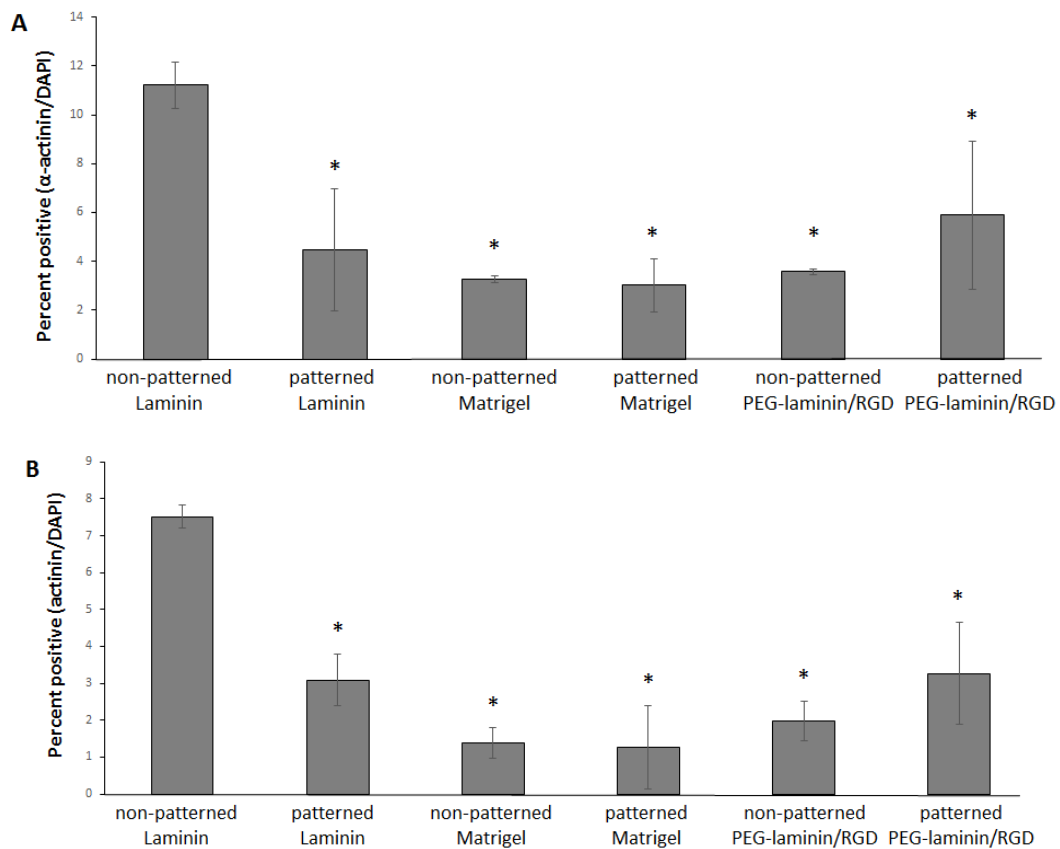


Figure 3.19: Quantification of α -actinin expression. Immunocytochemistry analysis performed at (A) 10x and (B) 4x objectives quantifies the staining for the cardiomyocyte protein sarcomeric α -actinin as a percentage of areas staining positive for DAPI. Statistical significance ($p < 0.05$) was determined relative to non-patterned laminin (*). Data are presented as mean \pm standard deviation ($n = 3$).

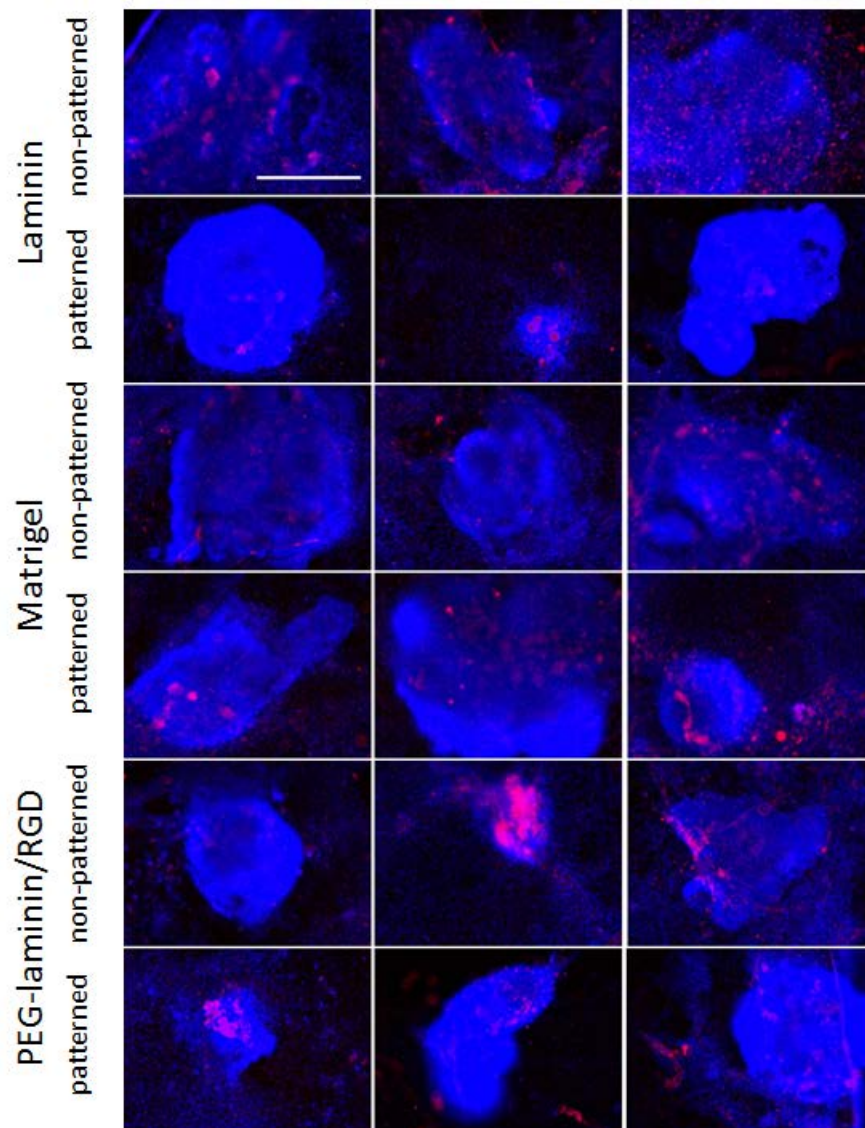


Figure 3.20: Images of α -actinin expression in cell aggregates. Representative merged fluorescent images show examples of sporadic α -actinin expression (red) within the 3-dimensional cell aggregates found across surfaces of all conditions. No obvious differences were found between the α -actinin staining within aggregates formed on different surfaces, including patterned vs. non-patterned. Cell nuclei were stained with DAPI (blue). Scale bar represents 500 μ m.

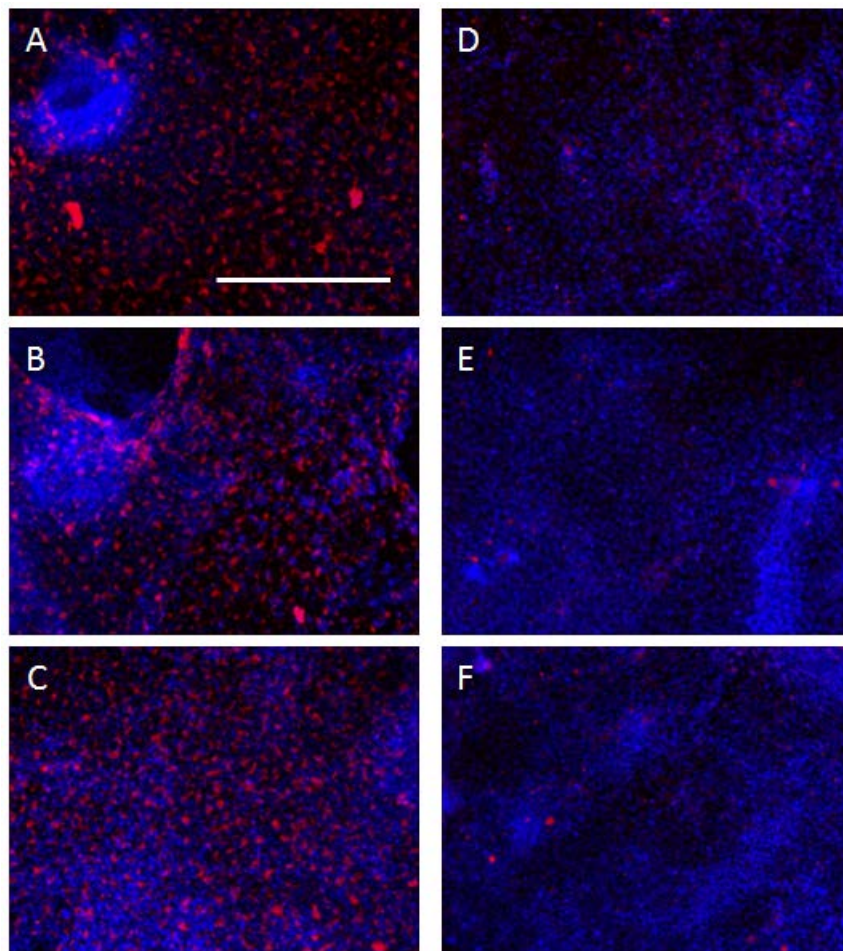


Figure 3.21: Images of α -actinin expression in cell monolayers. Representative merged fluorescent images comparing α -actinin expression (red) on (A, B, C) non-patterned laminin relative to other conditions, including (D) patterned laminin, (E) non-patterned Matrigel, and (F) non-patterned PEG-laminin/RGD, shows higher levels of expression within cell monolayers of non-patterned laminin surfaces. Cell nuclei were stained with DAPI (blue). Scale bar represents 500 μm .

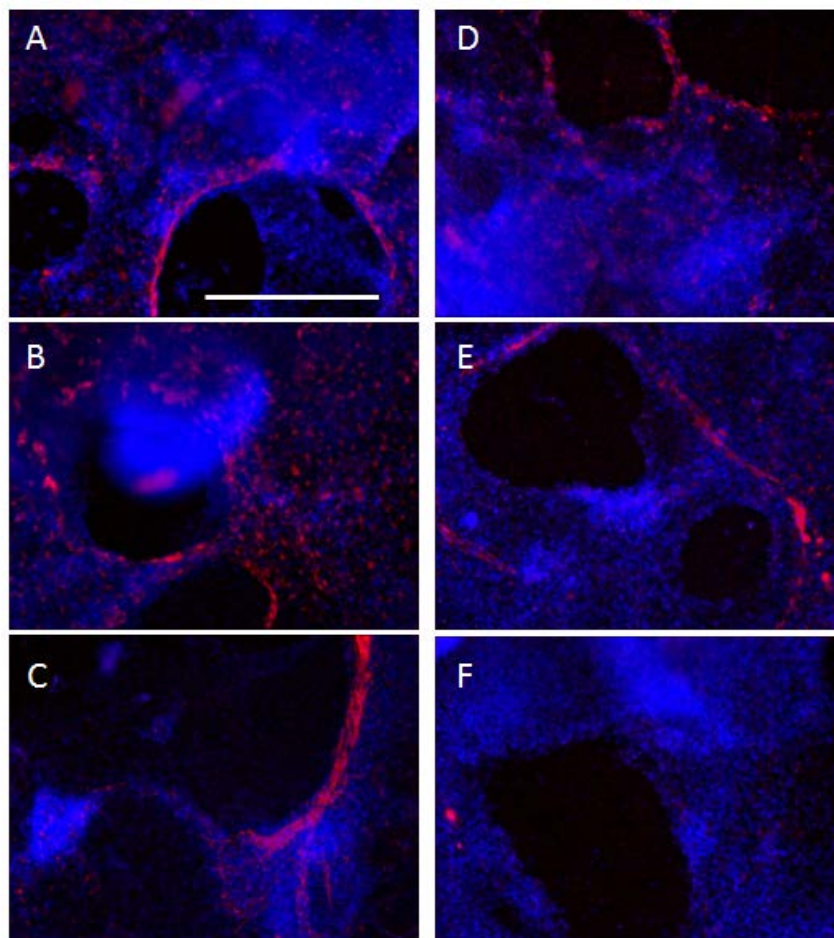


Figure 3.22: Images of α -actinin expression along monolayer edges. Representative merged fluorescent images show examples of strong α -actinin expression (red) that frequently occurs around the edges of holes in cell monolayers. Representative images are taken from (A, B, C) non-patterned laminin surfaces, (D, E) non-patterned Matrigel surfaces, and (F) a patterned PEG-laminin/RGD surface. The image in (F) provides an example where trend is not observed. Cell nuclei were stained with DAPI (blue). Scale bar represents 500 μm .

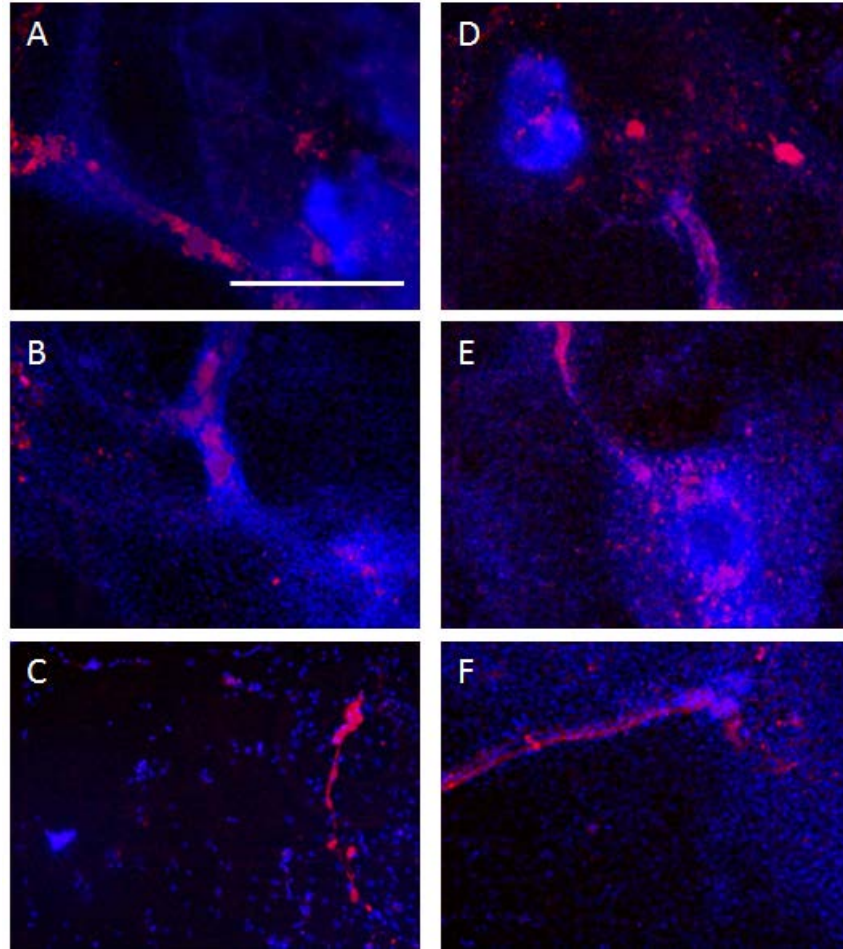


Figure 3.23: Images of α -actinin expression in elongated structures. Representative merged fluorescent images show examples of strong α -actinin expression (red) that is often found in elongated fibril-like cellular aggregates or of emerging elongated α -actinin structures that form among cells with no noticeable macro-organization. Representative images are taken from (A) a non-patterned laminin surface, (B, C) patterned laminin surfaces, (D, E) non-patterned PEG-laminin/RGD surfaces and (F) a patterned Matrigel surface. Cell nuclei were stained with DAPI (blue). Scale bar represents 500 μm .

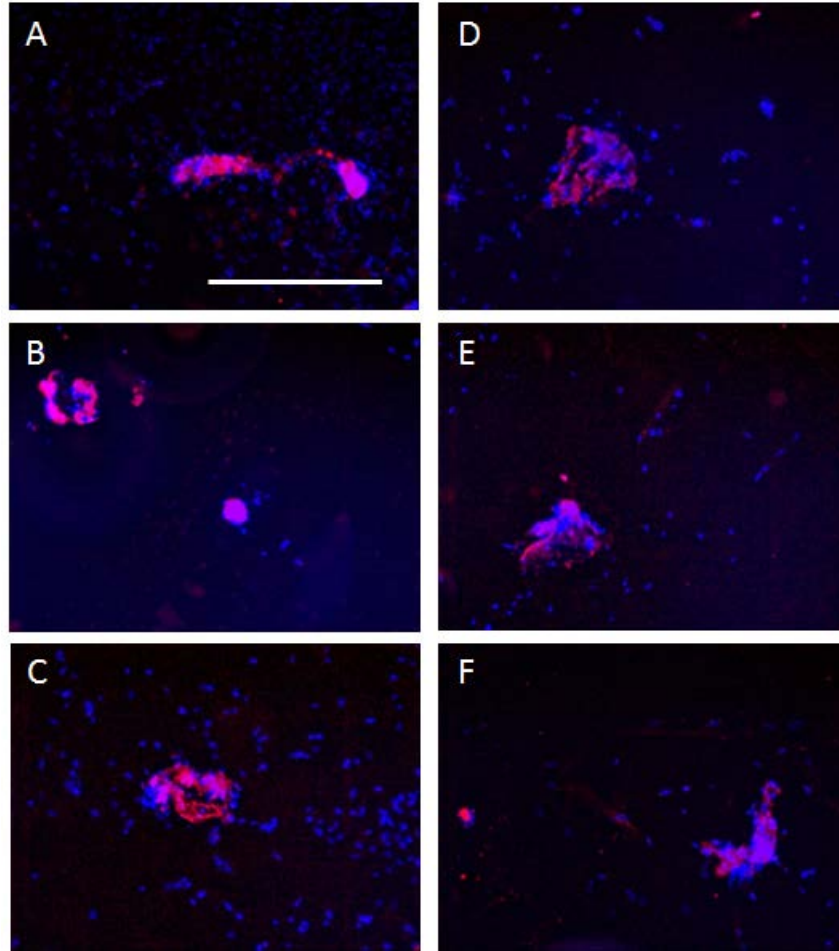


Figure 3.24: Images of α -actinin expression in small cellular aggregates. Representative merged fluorescent images show examples of strong α -actinin expression (red) that is often found in isolated cellular aggregates that are smaller than the 500 μm patterned aggregates. Representative images are taken from (A-C) patterned laminin surfaces and (D-F) patterned PEG-laminin/RGD surfaces. Cell nuclei were stained with DAPI (blue). Scale bar represents 500 μm .

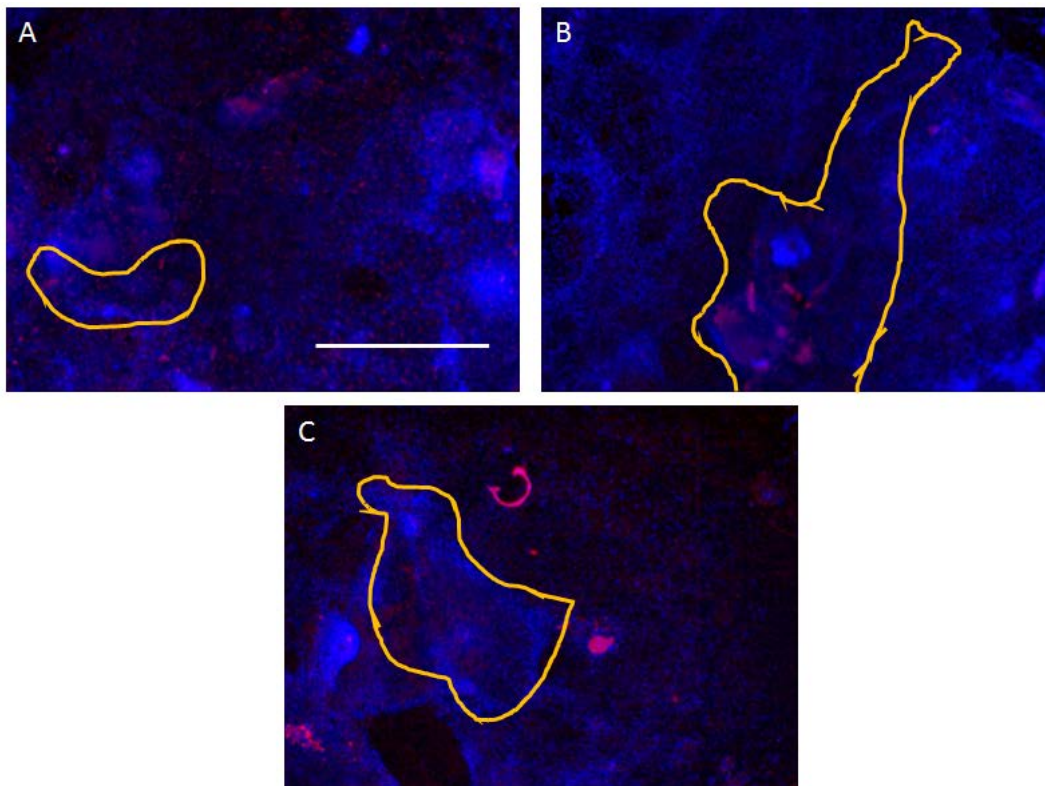


Figure 3.25: Images of α -actinin expression within boundaries of large contracting patches. Representative merged fluorescent images (at 4x objective) show α -actinin (red) expression profiles relative to approximate boundaries (yellow) of observed functional contraction. Examples are of relatively large contracting patches taken from (A) a non-patterned laminin surface, (B) a non-patterned PEG-laminin/RGD surface, and (C) a patterned PEG-laminin/RGD surface. Cell nuclei were stained with DAPI (blue). Scale bar represents 1 mm.

3.4 Discussion

As discussed in Chapter 2, patterning cells has been widely adopted to study the efficacy of various surface passivation strategies. We observed varying degrees of success with the same PEG nanogel substrate acting as the passivating background. For instance, when utilizing Scheme I we observed superb pattern integrity past 50 days for a sample backfilled with fibrinogen, but the same pattern began to collapse between 6 and 9 days when backfilled with either laminin or Matrigel. As our previous studies with TIRF using both fibrinogen and IgG(89) have hinted, different proteins may present different adsorption profiles to the same surface. We have also speculated this could contribute to discrepancies seen between TIRF and cell adhesion studies. So it is possible that laminin and the proteins found in Matrigel, including laminin and collagen IV, may adsorb more readily to the PEG nanogel surface or simply that they more readily promote fibroblast adhesion than fibrinogen. However, these two sets of experiments also used different capping molecules – cysteine with the fibrinogen and PEG-amine with the laminin and Matrigel – which might also explain the different responses. Interestingly, the surface created with Scheme II, which promoted specific fibroblast adhesion via RGD alone, also showed pattern collapse beginning between 6 and 9 days. The passivating background of this surface was also capped with PEG-amine just as the laminin and Matrigel surfaces which showed pattern collapse around the same time, bolstering support for the idea that the capping molecules may play a major factor in pattern integrity. It is difficult to compare pattern integrity of these experiments to those of MEFs seeded for the reprogramming experiment, as the cell seeding density was drastically different and took several days to reach confluency in the latter. However, the inferior patterning that emerged for the laminin and Matrigel surfaces was surprising when compared to the preliminary surfaces also incubated with laminin and Matrigel, because they were all prepared by the same methods, including capping with PEG-amine. It is unlikely that the lower seeding density would lead to an earlier collapse, but possible that the MEFs act more aggressively than the 3T3 fibroblasts. However, inter-experimental variability, especially in the stamping technique, cannot be negated as a possible reason for the inconsistent performances.

While the PEG-laminin/RGD surfaces patterned via Scheme II retained better pattern integrity than the patterned laminin and Matrigel surfaces during the reprogramming experiment, there remained several flaws with this strategy. For one, the non-negligible number of patterned spots that did not achieve cell confluency during the 18 day experiment, suggest that the nanogel

coating may be damaged from the stamping under these particular patches. We saw evidence of this in the preliminary experiments as well, especially under prolonged stamping. Yet, it is unclear why the damaged nanogels in our preliminary experiments invoked nonspecific cell adhesion, while those in our reprogramming experiment prevented any significant adhesion. Secondly, many of the cell aggregates that did form successfully under patterning, did not endure 18 days of proliferation without peeling off the substrate surface, suggesting a potential limitation in the patterning strategy in general. Previous studies from our group showed higher rates of proliferation over the first three days as well as over the first 15 days for samples that included RGD than those that did not.⁽¹⁹⁶⁾ The authors also noted confluent cells peeling off the edge of non-patterned PEG substrates with high concentrations of RGD by day 12 and by day 18 for PEG substrates with laminin. Interestingly, though, this problem was circumvented by the inclusion of both RGD and laminin, which we show here to be ineffective for patterned substrates, in which the surface area is much more limited. Also, we saw evidence of higher proliferation of cells on laminin surfaces than on PEG-laminin/RGD surfaces by day 15.

We had hypothesized that by controlling aggregate size we could replicate the spatial and paracrine cues found to be optimal for differentiation of PSCs. Whether or not the patterning increased the efficiency of differentiation within the patterned cellular aggregates relative to spontaneously formed clusters, we also supposed that the patterning might lead to earlier cardiac maturation given the early impetus to form 3-dimensional aggregates and thus more cell-to-cell contacts. Efe et al. observed cell contraction as early as 11 days, although this is not always standard.⁽¹⁵⁶⁾ Indeed our results showed earlier signs of dense cell aggregation on the patterned surfaces (day 9) than the non-patterned surfaces (day 12). Yet, even though cell aggregates seemed well formed on the patterned surfaces by the time we began implementing a regime of cardiogenic media (day 9), the data showed more contracting patches on all the non-patterned substrates for every time point examined. The onset of contraction at day 13 and drastic increase in the number of contracting patches on all our non-patterned surfaces between days 16 and 18 generally aligns well with a period of cardiac maturation indicated by a decrease in progenitor markers (*Mesp1* and *Isl1*) from day 14 onward in Efe et al.'s study.⁽¹⁵⁶⁾

The non-patterned laminin surfaces displayed the most proliferation, the highest number of contracting patches, and the highest staining ratios for α -actinin of all the conditions examined. Additionally, the non-pattern laminin adsorbed to mercaptosilanated glass contained almost double

the counts of contracting patches than the same amount of laminin adsorbed to TCPS in Smith et al.'s, study.(196) In that study she found that increasing the laminin concentration 5-fold (to the level used in this study) improved differentiation on PEG substrates but not on TCPS, suggesting that perhaps the adsorption of laminin had saturated. Indeed, laminin has been found to saturate at 850 ng/cm² on TCPS,(166) which is lower than both the PEG concentrations examined in Smith's study (11.4 and 64 µg/cm²). This leads us to believe that perhaps the mercaptosilanated glass is capable of adsorbing more laminin than TCPS due to either strong hydrophobic interactions or possibly even disulfide bonding to the thiol-functionalized surface. Given the higher counts of contracting patches and higher staining ratios, the mercaptosilane most likely adsorbs more laminin than can be conjugated to PEG nanogel coatings as well, especially considering that laminin adsorbed to TCPS or untreated glass has been shown capable of supporting cell adhesion while laminin conjugated to the nanogel coatings has not.

However, possible conformational changes in adsorbed laminin as opposed to the overall content, cannot be excluded as possible stimulants either. In fact, Healy et al. found by SEM Matrigel to form globular proteins (vs. the normal fibrillar) on untreated (hydrophobic) polystyrene that could not support ESC growth.(200) It was also shown that Matrigel adsorbed to glass formed denser protein layers and promoted ESC differentiation relative to Matrigel adsorbed to TCPS which preserved ESC pluripotency. However, adsorption to hydrophobic mercaptosilanated glass is unlikely to resemble adsorption to hydrophilic untreated glass. Regardless, the evidence presented here corroborates existing reports that laminin is vital to promoting cardiomyocyte differentiation. Furthermore, a noticeable difference exists between the non-patterned and patterned laminin surfaces as well in the lack of monolayer staining for α -actinin on the patterned laminin samples. Patterned laminin monolayers formed from a breakdown of pattern integrity and migration outward from the patterned aggregates. Monolayer cells found on the patterned surfaces are not necessarily adhered to laminin directly adsorbed to mercaptosilanated glass, though, and may still reside over PEG nanogels as well as serum proteins adsorbed to the glass or PEG. This could further imply that the laminin adsorption directly to mercaptosilane is responsible for the unique and pervasive staining found on all the non-patterned laminin surfaces.

The important role of laminin may also explain why the Matrigel surfaces performed notably worse than the other substrates, given the lower concentration of laminin found within Matrigel, which is lower than what was applied to the laminin or PEG-laminin/RGD surfaces and which

must compete against other proteins in the solution for adsorption to the surface. Because Matrigel solution will form a 3-dimensional gel at given concentrations and elevated temperatures it is, in general, not an ideal candidate for modulating laminin concentration. However, it is important to note that batch-to-batch variability has been reported to affect experimental results of cells grown on Matrigel as well.(201) Both the current study and the Smith et al. study(196) found lower day 18 counts of contracting patches on Matrigel (both around 7 patches/cm²) compared to the same condition in the original Efe et al. study(156) (approximated as 26 patches/cm²) suggesting a discrepancy in the efficiency of the reprogramming protocol between the groups. Additionally, Smith et al. noted a significantly lower efficiency of cardiomyocyte differentiation as determined by flow cytometry (4% vs. 40%).(196)

The non-patterned PEG surfaces were second only to the non-patterned laminin surfaces for the number of contracting patches and was superior to all surfaces in terms of total contracting area. Thus, it was slightly surprising to find that the percentage of cells staining positive for α -actinin was significantly less than non-patterned laminin and similar to non-patterned Matrigel, which displayed lower functional contraction. Smith et al. was the first to study the direct reprogramming protocol on PEG substrates and found that conjugating higher concentrations of laminin and/or RGD to bulk PEG hydrogels was able to both increase the number of contracting patches over Matrigel and increase the staining ratio over PEG substrates with lesser amounts of laminin and/or RGD. Thus, we would expect to see an improvement as well in the staining ratio on our PEG nanogel coatings over Matrigel adsorbed to mercaptosilane, given the higher concentration of laminin. It is unclear whether subtle chemical or structural differences between our PEG substrates and those in Smith et al.'s study, including the choice of cross-linking agent (BSA vs. PEG-amine) or the thickness of the substrate, may have influenced the results. Given that the previous study was able to perform a reprogramming experiment on bulk PEG gels functionalized with laminin and no RGD while we demonstrated no cell attachment to VS:BSA nanogel coatings and only moderate attachment to VS:Am nanogel coatings, it would seem that bulk PEG hydrogels, particularly VS:Am hydrogels, may afford a higher surface density of free PEG chains for protein conjugation or provide less steric resistance to protein attachment.

Additionally, substrate stiffness has been known to affect differentiation. Engler et al. has shown the ability to tune differentiation of stem cells via modulation of substrate stiffness (between 0.1 – 40 kPa)(202) and has also computed that cells mechanically sense their environment on the

length scale of adhesions.(203) It is perhaps possible that even if the PEG nanogel substrate is not promoting increased differentiation over Matrigel that it provides a relatively mechanically pliant substrate more appropriate for allowing large cell patch contractions. A substrate modulus of 10 kPa has been found to be ideal for promoting contractility,(182, 204) while we have previously measured moduli of our bulk PEG hydrogels to be around 7 kPa.(53) Glass on the other hand presents elastic moduli generally greater than 50 GPa, and the elastic modulus of serum proteins adsorbed to TCPS has been measured at 4 GPa.(205) It is uncertain the exact stiffness cells sense on thin nanogel coatings on glass, but an effectively higher stiffness than the bulk hydrogels examined previously may inhibit contractility and/or differentiation.

We noticed small cellular aggregates forming on the patterned laminin and patterned PEG-laminin/RGD surfaces that stained extremely well for α -actinin, seemingly increasing the surfaces' overall staining ratios (patterned laminin stained higher than non-patterned Matrigel and non-patterned PEG, but not non-patterned laminin due to reasons discussed above). It is uncertain whether these aggregates spontaneously formed from cells that migrated out of the larger patterned aggregates, they are remnants of the larger aggregates that over-proliferated and peeled off the surface, or if they are pieces of larger aggregates that were shed during proliferation and reattached to the surface. However these results resemble published trends that show larger proportions of cardiomyocytes in smaller embryoid bodies, which were additionally found unlikely to contract.(187) The lower amount of total cells found on these patterned surfaces altogether probably leads to lower cumulative DAPI values without a large loss in cumulative α -actinin values, since α -actinin-positive cells are generally found within or surrounding the cell clusters. The patterned laminin surfaces of course serve as an important exemption to this observation. Because the Matrigel patterned the least effectively, it is perhaps not surprising we did not see an improved staining ratio with this substrate. Given the relatively low efficiency of differentiation seen across the experiment, there may be an excess of cells, i.e. cell differentiation cannot keep pace with proliferation, especially on non-confined surfaces. This would suggest an innate advantage to patterning, except when considering the non-patterned laminin surface. It is also important to consider that the immunocytochemistry provides a 2-dimensional assessment of the surface, and so the actual differentiation efficiency may be skewed relative to the staining by larger numbers of cells found in aggregates than in monolayers.

Soares et al. studied the phenotypic differences between primary chick embryo cardiac cells cocultured as 3-dimensional aggregates and as single cells on 2-dimensional surfaces.(199) The 2-dimensional cells possessed flat and well-spread morphologies and tended to be isolated while the aggregate cells were smaller and formed many cell-to-cell junctions. They found evidence of more differentiated cardiomyocytes in the 3-dimensional aggregates, including increased α -actinin expression and more frequent contraction, while the 2-dimensional cells displayed evidence of higher proliferation rates, possibly indicating a less differentiated state. The authors speculate that the spatial organization influences the phenotype which may change upon movement between the two environments. This study corroborates what we observed on most conditions with the α -actinin-positive cells found within or near the edges of the 3-dimensional aggregates and could provide further motivation to maximize the proportion of cells associated with clusters, such as through a patterning method.

Other cellular structures that showed notably efficient actinin staining include cells with elongated shapes. Given known relationships between cell strain and cell shape,(175) it is reasonable to question whether the cellular remodeling and α -actinin upregulation observed here is a result of cardiogenic differentiation or a cause of it. Cyclic strain has been shown to upregulate cardiac gene expression in ESC derived cardiomyocytes(206, 207) and promote differentiation of ESCs (downregulation of *Oct3/4*),(208) especially at higher frequencies, but the results are not suggestive that cells experiencing static strain (perhaps such as those forming elongated shapes) would see the same benefits. However, sets of mouse cardiac progenitor cells (*Isl1*⁺/*Nkx2.5*) from both embryos (day 9.5) and ESC-derived embryoid bodies (day 6) were sorted in another study and grown on non-patterned or patterned (20 μ m stripes) fibronectin coated slides for 5 days. Interestingly, α -actinin staining revealed significantly higher numbers of cardiomyocytes on the elongated patterned surfaces.(209) Yet, the proportion of cardiomyocytes was still lower than cells grown from mature cardiac populations (*Nkx2.5*+) on either patterned or non-patterned surfaces. This data could suggest that cellular organization in both aggregate structures and longitudinal alignments may regulate cardiac differentiation but the temporal stages at which they would be most beneficial remains unknown.

The best examples of α -actinin staining observed were not found within the borders of several of the largest contracting patches. Figures 3.25A and 3.25B show relatively common trends of contraction, in which the cells found immediately surrounding 3-dimensional aggregates tend to

show synchronized contraction, which may or may not include the bulk of the aggregate itself (Figures 3.25B vs. 3.25A). Both these examples show some α -actinin within the corresponding aggregate but less (bright or profuse) or no staining in the contracting cells surrounding it. It is possible that differentiated cardiomyocytes are found mostly within the aggregates, but the pull of the contraction is felt most by the cells extending from the aggregates. In some instances, staining seems to reveal a layer of faintly stained cardiomyocytes that appear near the bottom of a 3-dimensional aggregate, possibly adhered directly to the substrate, but not within the dense aggregate above (Figures 3.25A and 3.25C vs. 3.25B). These trends might indicate that the combination of direct integrin signaling from the surface with paracrine signaling from the cellular aggregate above act synergistically in promoting differentiation. A dense mass of undifferentiated cells above might also muffle the ability these cardiomyocytes to functionally contract. Still it cannot be discounted that strong α -actinin expression might be lagging in functional cardiomyocytes that have not completely matured by day 18 and in fact, many more of the cells within the contracting regions than indicated by staining could be differentiated. It is also noted that many of the brightly stained regions found in these images are not contracting, which could imply that even differentiated cardiomyocytes require a certain degree of cellular organization to functionally contract. While it would be difficult to quantify many of the specific trends discussed here, these observations all provide insight into the effects of cellular organization on cardiomyocyte differentiation that might prove useful in designing future studies.

3.5 Conclusion

As direct reprogramming is a very new development, it is difficult to know what knowledge learned from differentiation of PSCs is appropriate to apply to the techniques used here. Comparisons would depend on the similarity of the “unstable intermediates” that Efe et al. describes in this protocol to PSCs more commonly studied, especially with regards to cellular organization (i.e. embryoid bodies). “Pre-iPSCs” have been isolated after partial completion of iPSC reprogramming protocols and found to exhibit the proliferative and biosynthetic characteristics of iPSCs with the silencing of many somatic genes, but not the exogenous expression of vital pluripotency genes such as *Oct4* and *Nanog*.⁽²¹⁰⁾ Similar biosynthetic output should promote similar responses to cellular organization. Yet, we found no evidence of improved cardiac differentiation within the patterned cell aggregates, although our assays may not be sensitive enough to detect subtle increases in

efficiency. We did, however, observe increased α -actinin staining efficiencies in patterned samples believed to result from reduced cell densities between aggregates. Furthermore, we observed efficient α -actinin staining of particular types of cellular organization including elongated cells, fibrillar structures, and small cell aggregates, providing possible motivation for alternative patterns that might prove beneficial. Most importantly though, we unexpectedly found that laminin adsorbed to mercaptosilanated glass appears to significantly enhance cardiac differentiation and uniquely so in cells unassociated with cellular aggregates. These results further advance the importance of laminin in cardiac differentiation. Finally, both the laminin and PEG-laminin/RGD surfaces proved to be superior alternatives to Matrigel for cardiac differentiation, providing more chemically defined and presumably consistent substrates that should prove useful for stem cell research. Given the highly temporal regulation known to occur in developing cardiomyocytes, especially when originating from somatic fibroblasts, it is unlikely that one immutable substrate is ideal for directing all the various stages of differentiation. The laminin surfaces are likely most beneficial near later stages of cardiomyocyte differentiation. Future methods of dynamically regulating substrate signaling and cellular organization, including proliferation, may prove useful in the overall efficiency of cardiac differentiation.

Chapter 4

Conclusions

4.1 Summary of Dissertation

In Chapter 2 we determined that the packing density of nanogel coatings can greatly influence the surface's protein resistance. Click chemistry allowed surface attachment under phase separation conditions which resulted in a much higher packing density and lower protein adsorption. These coatings were easily fabricated with monolayer precision, required no capping, and could be further functionalized with subsequent click reactions. However, we also confirmed that PEG nanogel coatings containing albumin outperformed all 100% PEG nanogel coatings, establishing a unique and unexplained synergy between the albumin and PEG. We further found discrepancies between single molecule detection and cell adhesion assays in terms of surface cross-linking, suggesting a difference in the protein adsorption profiles examined by these methodologies. In Chapter 3, we showed that the nanogel coatings functionalized with laminin and RGD outperformed Matrigel coatings in both the number and area of contracting patches. However, we discovered that laminin adsorbed to mercaptosilanated glass demonstrated the highest number of contracting patches and highest expression of α -actinin by significant margins. Patterning seemed to slightly increase the efficiency of α -actinin staining on the functionalized nanogel coatings (PEG-laminin/RGD) by limiting cells expansion outside of cardiac clusters. We also observed strong α -actinin staining in fibrillar structures and small cellular aggregates, the latter found solely within the patterned surfaces due to the passivating background that prevented significant cell expansion on the surfaces.

4.2 Future Directions

While the aim of this research, Chapter 2 in particular, was to apply existing knowledge about PEG and protein adsorption to the design of a better biomaterial, our studies of protein

adsorption on PEG nanogel coatings have actually uncovered intriguing and unexplained structure-property relationships. Despite some speculation, we have yet to fully understand how PEG and albumin work synergistically in resisting protein adsorption, how internal cross-linking density affects protein adsorption and cell adhesion, and why PEG-VS:Am nanogel coatings outperformed clickable PEG nanogel coatings (attached without salt). The most straight-forward experiments to pursue would include protein adsorption studies on coatings fabricated from nanogels of modulated architectures (e.g. four-arm vs. eight-arm, MW 10,000 vs. MW 5,000, etc.), which should immediately help to answer whether the discrepancies we saw with TIRF between the 100% PEG nanogel coatings stem from physical parameters or chemical differences between the functional groups. Our nanogel coatings are distinct from most research in protein adsorption in that the dense ~100 nm coatings comprise legitimate hydrogels relative to the more common grafting of PEG monomers to surfaces. Thus, our protein adsorption studies could reflect protein adsorption to PEG itself more so than to the underlying surface, protected by a PEG barrier. As such, protein adsorption to our thin hydrogels has larger implications for the design of large hydrogel constructs for tissue engineering. Future studies would greatly benefit from the development of analytical detection methods which can distinguish between protein adsorption to the surface and PEG chains or which could be applied to thick hydrogel constructs. Additionally, as the clickable nanogel coatings are distinct in allowing attachment of defined monolayers, it could be beneficial to study the effect that multiple nanogel layers have on protein adsorption, such as by using a PEG-cyclooctyne interface between the individual layers. Experiments using other proteins or even synthetic peptides for the cross-linking of PEG nanogel solutions could also help determine if albumin is unique in its ability to enhance resistance to protein adsorption and whether this resistance derives from physical or chemical origins.

As discussed at several points in this dissertation, mechanical properties can influence adhesion and behavior of cells. While mechanical properties have been characterized for bulk PEG hydrogels of similar makeup by rheometry, we have not characterized our thin nanogel coatings. The stiffness felt by cells on nanogel coatings could likely be modulated by the much stiffer substrates beneath. It would be helpful to characterize this stiffness through AFM or force indentation studies. Additionally, the mechanical durability of the nanogel coatings comprises an important consideration for long-term, *in vivo* use. We have previously found evidence that the nanogel coatings are easily scratched, most likely removing PEG from the glass surface. More

extensive characterization needs to be undertaken, and importantly, possible steps to curtail any damage such as surface cross-linking or new attachment schemes need to be studied before any possible implantation, which could easily damage a fragile coating. It would also be prudent to conduct *in vitro* studies under flowing plasma or serum, to test for adsorption of plasma proteins or blood coagulation, which would offer insight into how the coatings would perform in use with a blood contacting vascular implant.

We have demonstrated that PEG nanogel coatings possess great potential in an array of applications requiring protein resistant interfaces, including biomaterials, biological diagnostics, and cell culture. In this dissertation, we examined the nanogel coatings' resistance to protein adsorption and cell adhesion, as well as their ability to provide a platform for designed cell growth and maintenance. All of the experiments presented here were performed on nanogel coatings covalently attached to glass surfaces. Glass provides a standard platform in the field, which is easy to functionalize with a diverse range of silanes, conveniently is optically clear, and can be employed in many *in vitro* applications. However, the ability to functionalize a large assortment of substrate materials, including metals, hard plastics, and softer rubbers, would greatly expand the utility of the coatings, and is especially necessary for implantable biomaterials. Previously, our group demonstrated the ability to attach PEG nanogels to polyethylene terephthalate (PET) using plasma glow discharge – which provides a powerful tool for achieving these goals.⁽¹⁾ We have also had limited success in applying plasma glow discharge to functionalize polystyrene plastics (data not shown), which provides great potential for use with standard cell culture materials. Additionally, the ability to functionalize surfaces with a cyclooctyne molecule, as demonstrated by Popik et al., ⁽¹⁴⁶⁾ will allow more versatile attachment of clickable nanogel coatings without the requirement for UV irradiation. We anticipate that our findings regarding nanogel packing density and residual cross-linking of nanogel surfaces would apply to any substrate if the attachment chemistry can be optimized to provide robust conjugation.

The results discussed in Chapter 3 provide an immediate impetus for further studies. In order to determine, whether the laminin adsorbed to mercaptosilane glass actually improved cardiomyocyte differentiation to the significant extent we detected, direct reprogramming should be repeated on surfaces of laminin adsorbed to mercaptosilanated glass, untreated glass, and TCPS, perhaps at multiple concentrations, and analyzed by flow cytometry for a more quantitative analysis of differentiation efficiency. Furthermore, by some means such as oxidizing the mercaptosilane

surface or replacing it with a sulfonate surface, we should be able to determine whether laminin is attaching via disulfide formations or simply adsorbing at much higher surface densities. Applying advanced analytical methods to these surfaces, perhaps X-ray photoelectron spectroscopy (XPS) or MALDI mass spectrometry, might also aid in quantifying the attachment of laminin to these surfaces or even the surface density of functional PEG groups available for reaction on nanogel coatings, which could present a limiting factor. Patterning laminin adsorbed to mercaptosilane could also be improved, perhaps with multiple applications of the passivating PEG nanogel coating under stamping, such as was found to improve capping efficiency under stamping. However, given the widespread α -actinin expression observed for this condition, it is unlikely that patterning would improve efficiency here.

With regards to the patterning of functionalized ligands on nanogel coatings, it appears that the stamping technique described in Chapter 3 is not ideal for use with nanogel coatings. While stamping is a cheap and quick way to create patterns, the mechanical pressure necessary seems to damage the fragile nanogel coatings. Also, this technique would be difficult to scale-up for patterning on a large number of surfaces and without more sophisticated fabrication techniques has limited spatial resolution. Photonic patterning has been well used with PEG hydrogels, particularly with clickable moieties, either in the form of laser writing or photo-mask polymerization. These techniques could allow fabrication of precise and intricate patterns without compromising the protein-resistant structure of the hydrogel, however, they would also face challenges with scalability. As some observational trends discussed in Chapter 3 indicate, more intricate patterns which include aligning cells in longitudinal arrangements or grouping cells within much smaller aggregates could greatly enhance differentiation. It would further be interesting to attempt patterning the cells at a later stage in the reprogramming process to circumvent the problems associated with maintaining pattern integrity over long periods of high proliferation. However, passaging of cells at various developmental stages can prove challenging for reforming surface attachments if cell-cell contacts are preferred, and a large loss in yield might occur if cells are lost during this process. As was discussed, PEG substrates have previously been used for both defined differentiations and expansion of PSCs. Given the low protein adsorption of the PEG nanogel surfaces, it would be worthwhile to pursue their application for long term culture of PSCs since they should not inadvertently stimulate differentiation pathways given their inert nature. Additionally, because we have fabricated nanogel solutions from various polymerization chemistries, great potential exists for

creating modular nanogel assemblies presenting an array of functionalities. Using this strategy, surfaces could also be patterned via different surface chemistries prior to nanogel attachment, which might provide a more convenient method of patterning the nanogel coatings. Finally, it was demonstrated by Kamp et al. that cardiac differentiation could be improved by replicating the 3-dimensional nature of the extracellular matrix with an overlay of Matrigel, sandwiching the cells.⁽²¹¹⁾ Our nanogel coatings might allow an effective way of recapitulating the dimensionality of the extracellular matrix, as well, within a thin sandwich of nanogel coatings, which would still allow optimal diffusion for waste-nutrient exchange.

The work described in this dissertation provides the foundations for an array of research. The PEG nanogel coatings possess unique properties that allow for studying the effects of hydrogel architecture, cross-linking chemistry, and surface attachment chemistry on protein adsorption. These coatings have demonstrated potential for uses with *in vitro* diagnostics and as substrates for stem cell culture, and may someday be applied as biomaterials for *in vivo* applications such as implantable device coatings.

References

1. E. A. Scott *et al.*, Protein adsorption and cell adhesion on nanoscale bioactive coatings formed from poly(ethylene glycol) and albumin microgels. *Biomaterials* **29**, 4481 (Dec, 2008).
2. E. Ostuni, R. G. Chapman, E. Holmlin, S. Takayama, G. M. Whitesides, A survey of structure-property relationships of surfaces that resist adsorption of protein. *Langmuir* **17**, 5605 (2001).
3. D. A. Herold, K. Keil, D. E. Bruns, Oxidation of polyethylene glycols by alcohol dehydrogenase. *Biochem Pharmacol* **38**, 73 (Jan 1, 1989).
4. S. Sharma, R. W. Johnson, T. A. Desai, Evaluation of the stability of nonfouling ultrathin poly(ethylene glycol) films for silicon-based microdevices. *Langmuir : the ACS journal of surfaces and colloids* **20**, 348 (Jan 20, 2004).
5. J. H. Lee, J. Kopecek, J. D. Andrade, Protein-resistant surfaces prepared by PEO-containing block copolymer surfactants. *J Biomed Mater Res* **23**, 351 (Mar, 1989).
6. D. H. Atha, K. C. Ingham, Mechanism of precipitation of proteins by polyethylene glycols. *The Journal of Biological Chemistry* **256**, 12108 (1981).
7. Y. Mori *et al.*, A new antithrombogenic material with long polyethyleneoxide chains. *Transactions - American Society for Artificial Internal Organs* **28**, 459 (1982).
8. M. A. Carignano, I. Szleifer, Prevention of protein adsorption by flexible and rigid chain molecules. *Colloids and Surfaces B: Biointerfaces* **18**, 169 (2000).
9. T. McPherson, A. Kidane, I. Szleifer, K. Park, Prevention of protein adsorption by tethered poly(ethylene oxide) layers: Experiments and single-chain mean-field analysis. *Langmuir* **14**, 176 (1998).
10. D. J. Irvine *et al.*, Comparison of tethered star and linear poly(ethylene oxide) for control of biomaterials surface properties. *J Biomed Mater Res* **40**, 498 (Jun 5, 1998).
11. P. Hamilton-Brown, T. Gengenbach, H. J. Griesser, L. Meagher, End terminal, poly(ethylene oxide) graft layers: Surface forces and protein adsorption. *Langmuir* **25**, 9149 (2009).
12. P. Kingshott, H. Thissen, H. J. Griesser, Effects of cloud-point grafting, chain length, and density of PEG layers on competitive adsorption of ocular proteins. *Biomaterials* **23**, 2043 (2002).
13. A. Halperin, M. Kroger, Ternary protein adsorption onto brushes: Strong versus weak. *Langmuir* **25**, 11621 (2009).

14. L. Li, S. Chen, S. Jiang, Protein interactions with oligo(ethylene glycol) (OEG) self-assembled monolayers: OEG stability, surface packing density and protein adsorption. *Journal of biomaterials science. Polymer edition* **18**, 1415 (2007).
15. G. Altankov *et al.*, Modulating the biocompatibility of polymer surfaces with poly(ethylene glycol): Effect of fibronectin. *Journal of Biomedical Materials Research* **52**, 219 (2000).
16. B. Zhu, T. Eurell, R. Gunawan, D. Leckband, Chain-length dependence of the protein and cell resistance of oligo(ethylene glycol)-terminated self-assembled monolayers on gold. *Journal of Biomedical Materials Research* **56**, 406 (Sep 5, 2001).
17. X. Fan, L. Lin, P. B. Messersmith, Cell fouling resistance of polymer brushes grafted from ti substrates by surface-initiated polymerization: effect of ethylene glycol side chain length. *Biomacromolecules* **7**, 2443 (Aug, 2006).
18. B. W. Muir *et al.*, Characterization of low-fouling ethylene glycol containing plasma polymer films. *Langmuir : the ACS journal of surfaces and colloids* **24**, 3828 (Apr 15, 2008).
19. J. M. Harris *et al.*, Reduction of fibrinogen adsorption on PEG-coated polystyrene surfaces. *Journal of Biomedical Materials Research* **26**, 779 (1992).
20. T. Satomi, Y. Nagasaki, H. Kobayashi, H. Otsuka, K. Kataoka, Density control of poly(ethylene glycol) layer to regulate cellular attachment. *Langmuir* **23**, 6698 (2007).
21. T. Satomi, Y. Nagasaki, H. Kobayashi, H. Otsuka, K. Kataoka, Density control of poly(ethylene glycol) layer to regulate cellular attachment. *Langmuir : the ACS journal of surfaces and colloids* **23**, 6698 (Jun 5, 2007).
22. J. Groll, Z. Ademovic, T. Ameringer, D. Klee, M. Moeller, Comparison of coatings from reactive star shaped PEG-stat-PPG prepolymers and grafted linear PEG for biological and medical applications. *Biomacromolecules* **6**, 956 (Mar-Apr, 2005).
23. J. Groll *et al.*, A novel star PEG-derived surface coating for specific cell adhesion. *Journal of Biomedical Materials Research. Part A.* **74**, 607 (2005).
24. E. Vogler, Water and the acute biological response to surfaces. *J Biomater Sci Polym Ed* **10**, 1015 (1998).
25. T. Tsuruta, On the role of water molecules in the interface between biological systems and polymers. *Journal of biomaterials science. Polymer edition* **21**, 1831 (2010).
26. M. Heuberger, T. Drobek, J. Voros, About the role of water in surface-grafted poly(ethylene glycol) layers. *Langmuir : the ACS journal of surfaces and colloids* **20**, 9445 (Oct 26, 2004).
27. M. Heuberger, T. Drobek, N. D. Spencer, Interaction forces and morphology of a protein-resistant poly(ethylene glycol) layer. *Biophys J* **88**, 495 (Jan, 2005).

28. Z. Zhang, H. Ma, D. B. Hausner, A. Chilkoti, T. P. Beebe, Jr., Pretreatment of amphiphilic comb polymer surfaces dramatically affects protein adsorption. *Biomacromolecules* **6**, 3388 (Nov-Dec, 2005).
29. M. Bjorling, G. Karlstrom, P. Linse, Conformational adaptation of poly(ethylene oxide). A ¹³C NMR study. *Physical Chemistry I* **95**, 6706 (1991).
30. C. Ma, Y. Hou, S. Liu, G. Zhang, Effect of microphase separation on the protein resistance of a polymeric surface. *Langmuir* **25**, 9467 (2009).
31. N. Ngadi, J. Abrahamson, C. Fee, K. Morison, Are PEG Molecules a Universal Protein Repellent? *World Academy of Science, Engineering and Technology* **49**, 144 (2009).
32. N. V. Efrenova, S. R. Sheth, D. E. Leckband, Protein-induced changes in poly(ethylene glycol) brushes: Molecular weight and temperature dependence. *Langmuir* **17**, 7628 (2001).
33. P. A. George, B. C. Donose, J. J. Cooper-White, Self-assembling polystyrene-block-poly(ethylene oxide) copolymer surface coatings: resistance to protein and cell adhesion. *Biomaterials* **30**, 2449 (May, 2009).
34. H.-W. Jun, J. L. West, Endothelialization of microporous YIGSR/PEG-modified polyurethaneurea. *Tissue Engineering* **11**, 1133 (2005).
35. R. Michel, S. Pasche, M. Textor, D. G. Castner, Influence of PEG architecture on protein adsorption and conformation. *Langmuir : the ACS journal of surfaces and colloids* **21**, 12327 (Dec 20, 2005).
36. A. Z. Piao *et al.*, Synthesis and characterization of poly(dimethylsiloxane)-poly(ethylene oxide)-heparin CBABC type block copolymers. *Journal of Biomaterials Science. Polymer edition.* **1**, 299 (1990).
37. D. L. Elbert, J. A. Hubbell, Self-assembly and steric stabilization at heterogeneous, biological surfaces using adsorbing block copolymers. *Chem Biol* **5**, 177 (Mar, 1998).
38. G. L. Kenausis *et al.*, Poly(L-lysine)-g-Poly(ethylene glycol) Layers on Metal Oxide Surfaces: Attachment Mechanism and Effects of Polymer Architecture on Resistance to Protein Adsorption. *The Journal of Physical Chemistry. A* **104**, 3298 (2000, 2000).
39. S. Tosatti *et al.*, Peptide functionalized poly(L-lysine)-g-poly(ethylene glycol) on titanium: resistance to protein adsorption in full heparinized human blood plasma. *Biomaterials* **24**, 4949 (Dec, 2003).
40. N. P. Desai, J. A. Hubbell, Solution technique to incorporate polyethylene oxide and other water-soluble polymers into surfaces of polymeric biomaterials. *Biomaterials* **12**, 144 (1991).
41. K. Park, H. S. Shim, M. K. Dewanjee, N. L. Eigler, In vitro and in vivo studies of PEO-grafted blood-contacting cardiovascular prostheses. *Journal of Biomaterials Science. Polymer edition.* **11**, 1121 (2000).

42. J. Ji, L. Feng, M. A. Barbosa, Stearyl poly(ethylene oxide) grafted surfaces for preferential adsorption of albumin. *Biomaterials* **22**, 3015 (2001).
43. N. Singh, A. W. Bridges, A. J. Garcia, L. A. Lyon, Covalent tethering of functional microgel films onto poly(ethylene terephthalate) surfaces. *Biomacromolecules* **8**, 3271 (2007).
44. Z. Ademovic *et al.*, The method of surface PEGylation influences leukocyte adhesion and activation. *J Mater Sci Mater Med* **17**, 203 (Mar, 2006).
45. D. S. Kumar *et al.*, Surface modification of poly(ethylene terephthalate) by plasma polymerization of poly(ethylene glycol). *Journal of Material Science: Material Medicine* **18**, (2007).
46. J. L. Hill-West, S. M. Chowdhury, M. J. Slepian, J. A. Hubbell, Inhibition of thrombosis and intimal thickening by in situ photopolymerization of thin hydrogel barriers. *Proc Natl Acad Sci U S A* **91**, 5967 (Jun 21, 1994).
47. M. D. Lyman, D. Melanson, A. S. Sawhney, Characterization of the formation of interfacially photopolymerized thin hydrogels in contact with arterial tissue. *Biomaterials* **17**, 359 (1996).
48. W. K. Cho *et al.*, Long-term stability of cell micropatterns on poly((3-(methacryloylamino)propyl)-dimethyl(3-sulfopropyl)ammonium hydroxide)-patterned silicon oxide surfaces. *Biomaterials* **31**, 9565 (Dec, 2010).
49. S. A. Ahmad, G. J. Leggett, A. Hucknall, A. Chilkoti, Micro- and nanostructured poly[oligo(ethylene glycol)methacrylate] brushes grown from photopatterned halogen initiators by atom transfer radical polymerization. *Biointerphases* **6**, 8 (Mar, 2011).
50. C. M. Nolan, C. D. Reyes, J. D. Debord, A. J. Garcia, L. A. Lyon, Phase transition behavior, protein adsorption, and cell adhesion resistance of poly(ethylene glycol) cross-linked microgel particles. *Biomacromolecules* **6**, 2032 (Jul-Aug, 2005).
51. Y. Murakami *et al.*, A novel synthetic tissue-adhesive hydrogel using a crosslinkable polymeric micelle. *Journal of Biomedical Materials Research. Part A*. **80**, 421 (2007).
52. M. D. Nichols, E. A. Scott, D. L. Elbert, Factors affecting size and swelling of poly(ethylene glycol) microspheres formed in aqueous sodium sulfate solutions without surfactants. *Biomaterials* **30**, 5283 (Oct, 2009).
53. E. A. Scott, M. D. Nichols, R. Kuntz-Willits, D. L. Elbert, Modular scaffolds assembled around living cells using poly(ethylene glycol) microspheres with macroporation via a non-cytotoxic porogen. *Acta biomaterialia* **6**, 29 (Jan, 2010).
54. J. N. George, Direct assessment of platelet adhesion to glass: A study of the forces of interaction and the effects of plasma and serum factors, platelet function, and the modification of the glass surface. *Blood* **40**, 862 (1972).
55. S. L. Verdon *et al.*, Scanning electron microscopy analysis of polyethylene oxide hydrogels for blood contact. *Scanning Microscopy* **4**, 341 (1990).

56. J. Hoffmann *et al.*, Blood cell and plasma protein repellent properties of star-PEG-modified surfaces. *Journal of Biomaterials Science. Polymer edition.* **17**, 985 (2006).
57. J. Yu *et al.*, Blood interactions with novel polyurethaneurea hydrogels. *Biomaterials* **12**, (1991).
58. D. W. Grainger, C. Nojiri, T. Okano, S. W. Kim, In vitro and ex vivo platelet interactions with hydrophilic-hydrophobic poly(ethylene glycol)-polystyrene multiblock copolymers. *Journal of Biomedical Materials Research* **23**, 979 (1989).
59. D. K. Han, K. Park, K. D. Park, K. D. Ahn, Y. H. Kim, In vivo biocompatibility of sulfonated PEO-grafted polyurethanes for polymer heart valve and vascular graft. *Artificial Organs* **30**, 955 (Dec, 2006).
60. K. Takahashi, S. Yamanaka, Induction of pluripotent stem cells from mouse embryonic and adult fibroblast cultures by defined factors. *Cell* **126**, 663 (Aug 25, 2006).
61. X. Bao *et al.*, MicroRNAs in somatic cell reprogramming. *Curr Opin Cell Biol* **25**, 208 (Apr, 2013).
62. D. Dey, G. R. Evans, Generation of Induced Pluripotent Stem (iPS) Cells by Nuclear Reprogramming. *Stem Cells Int* **2011**, 619583 (2011).
63. Y. Zhang *et al.*, A poor imitation of a natural process: a call to reconsider the iPSC engineering technique. *Cell Cycle* **11**, 4536 (Dec 15, 2012).
64. U. Tiemann *et al.*, Optimal reprogramming factor stoichiometry increases colony numbers and affects molecular characteristics of murine induced pluripotent stem cells. *Cytometry A* **79**, 426 (Jun, 2011).
65. M. H. Chin *et al.*, Induced pluripotent stem cells and embryonic stem cells are distinguished by gene expression signatures. *Cell Stem Cell* **5**, 111 (Jul 2, 2009).
66. M. K. Gupta *et al.*, Global transcriptional profiles of beating clusters derived from human induced pluripotent stem cells and embryonic stem cells are highly similar. *BMC Dev Biol* **10**, 98 (2010).
67. K. H. Narsinh *et al.*, Single cell transcriptional profiling reveals heterogeneity of human induced pluripotent stem cells. *J Clin Invest* **121**, 1217 (Mar, 2011).
68. K. Kim *et al.*, Epigenetic memory in induced pluripotent stem cells. *Nature* **467**, 285 (Sep 16, 2010).
69. T. Zhao, Z. N. Zhang, Z. Rong, Y. Xu, Immunogenicity of induced pluripotent stem cells. *Nature* **474**, 212 (Jun 9, 2011).
70. S. Martino, F. D'Angelo, I. Armentano, J. M. Kenny, A. Orlacchio, Stem cell-biomaterial interactions for regenerative medicine. *Biotechnol Adv* **30**, 338 (Jan-Feb, 2012).

71. Y. J. Li, E. H. Chung, R. T. Rodriguez, M. T. Firpo, K. E. Healy, Hydrogels as artificial matrices for human embryonic stem cell self-renewal. *Journal of biomedical materials research. Part A* **79**, 1 (Oct, 2006).
72. T. P. Krachenbuehl *et al.*, Three-dimensional extracellular matrix-directed cardioprogenitor differentiation: systematic modulation of a synthetic cell-responsive PEG-hydrogel. *Biomaterials* **29**, 2757 (Jun, 2008).
73. G. G. Giobbe *et al.*, Confined 3D microenvironment regulates early differentiation in human pluripotent stem cells. *Biotechnol Bioeng* **109**, 3119 (Dec, 2012).
74. C. C. Lin, K. S. Anseth, PEG hydrogels for the controlled release of biomolecules in regenerative medicine. *Pharm Res* **26**, 631 (Mar, 2009).
75. S. T. Lee *et al.*, Engineering integrin signaling for promoting embryonic stem cell self-renewal in a precisely defined niche. *Biomaterials* **31**, 1219 (Feb, 2010).
76. B. G. Keselowsky, D. M. Collard, A. J. Garcia, Integrin binding specificity regulates biomaterial surface chemistry effects on cell differentiation. *Proceedings of the National Academy of Sciences of the United States of America* **102**, 5953 (Apr 26, 2005).
77. J. Mauney, V. Volloch, Collagen I matrix contributes to determination of adult human stem cell lineage via differential, structural conformation-specific elicitation of cellular stress response. *Matrix Biol* **28**, 251 (Jun, 2009).
78. E. F. Irwin, R. Gupta, D. C. Dashti, K. E. Healy, Engineered polymer-media interfaces for the long-term self-renewal of human embryonic stem cells. *Biomaterials* **32**, 6912 (Oct, 2011).
79. R. Konradi, C. Acikgoz, M. Textor, Polyoxazolines for nonfouling surface coatings - a direct comparison to the gold standard PEG. *Macromol Rapid Commun* **33**, 1663 (Oct 15, 2012).
80. G. Mahmud *et al.*, Carboxybetaine Methacrylate Polymers Offer Robust, Long-Term Protection against Cell Adhesion. *Langmuir* **27**, 10800 (2011).
81. S. Abraham, M. S. Bahniuk, L. D. Unsworth, Plasma Protein Adsorption to Zwitterionic Poly(Carboxybetaine Methacrylate) Modified Surfaces: Chain Chemistry and End-Group Effects on Protein Adsorption, Kinetics, Adsorbed Amounts and Immunoblots. *Biointerphases* **7**, (2012).
82. Y. Inoue, K. Ishihara, Reduction of protein adsorption on well-characterized polymer brush layers with varying chemical structures. *Colloids Surf B Biointerphases* **81**, 350 (2010).
83. S. Jo, K. Park, Surface modification using silanated poly(ethylene glycol)s. *Biomaterials* **21**, 605 (Mar, 2000).
84. S. Kizilel, E. Sawardecker, F. Teymour, V. H. Perez-Luna, Sequential formation of covalently bonded hydrogel multilayers through surface initiated photopolymerization. *Biomaterials* **27**, 1209 (Mar, 2006).

85. J. P. Bearinger, D. G. Castner, K. E. Healy, Biomolecular modification of p(AAm-co-EG/AA) IPNs supports osteoblast adhesion and phenotypic expression. *J Biomater Sci Polym Ed* **9**, 629 (1998).
86. I. Saaem, V. Papasotiropoulos, T. Wang, P. Soteropoulos, M. Libera, Hydrogel-based protein nanoarrays. *J Nanosci Nanotechnol* **7**, 2623 (Aug, 2007).
87. A. B. South, R. E. Whitmire, A. J. Garcia, L. A. Lyon, Centrifugal deposition of microgels for the rapid assembly of nonfouling thin films. *ACS Appl Mater Interfaces* **1**, 2747 (Dec, 2009).
88. Q. Wang, E. Uzunoglu, Y. Wu, M. Libera, Self-assembled poly(ethylene glycol)-co-acrylic acid microgels to inhibit bacterial colonization of synthetic surfaces. *ACS Appl Mater Interfaces* **4**, 2498 (May, 2012).
89. L. A. Tessler *et al.*, Nanogel surface coatings for improved single-molecule imaging substrates. *J R Soc Interface* **8**, 1400 (Oct 7, 2011).
90. E. A. Vogler, Protein adsorption in three dimensions. *Biomaterials* **33**, 1201 (Feb, 2012).
91. A. G. Shard, P. E. Tomlins, Biocompatibility and the efficacy of medical implants. *Regen Med* **1**, 789 (Nov, 2006).
92. B. D. Ratner, S. J. Bryant, Biomaterials: where we have been and where we are going. *Annu Rev Biomed Eng* **6**, 41 (2004).
93. A. Shimoda *et al.*, Dual crosslinked hydrogel nanoparticles by nanogel bottom-up method for sustained-release delivery. *Colloids Surf B Biointerfaces* **99**, 38 (Nov 1, 2012).
94. M. J. Kettel, H. Hildebrandt, K. Schaefer, M. Moeller, J. Groll, Tenside-free Preparation of Nanogels with High Functional beta-Cyclodextrin Content. *ACS Nano* **6**, 8087 (Sep 25, 2012).
95. C. Cheng, X. Zhu, A. Pich, M. Moller, Aqueous microgels modified by wedge-shaped amphiphilic molecules: hydrophilic microcontainers with hydrophobic nanodomains. *Langmuir* **26**, 4709 (Apr 6, 2010).
96. X. Wu, A. El Ghzaoui, S. Li, Aggregates and hydrogels prepared by self-assembly of amphiphilic copolymers with surfactants. *J Colloid Interface Sci* **374**, 127 (May 15, 2012).
97. A. W. Bridges *et al.*, Chronic inflammatory responses to microgel-based implant coatings. *J Biomed Mater Res A* **94**, 252 (Jul, 2010).
98. P. F. Holmes *et al.*, Surface-modified nanoparticles as a new, versatile, and mechanically robust nonadhesive coating: suppression of protein adsorption and bacterial adhesion. *J Biomed Mater Res A* **91**, 824 (Dec, 2009).
99. K. Albrecht, M. Moeller, J. Groll, Nano- and Microgels Through Addition Reactions of Functional Oligomer and Polymers. *Advances in Polymer Science* **234**, 65 (2011).

100. B. Mizrahi *et al.*, Microgels for efficient protein purification. *Adv Mater* **23**, H258 (Sep 22, 2011).
101. Y. Hong, P. Krsko, M. Libera, Protein surface patterning using nanoscale PEG hydrogels. *Langmuir* **20**, 11123 (Dec 7, 2004).
102. L. A. Tessler, J. G. Reifenger, R. D. Mitra, Protein quantification in complex mixtures by solid phase single-molecule counting. *Anal Chem* **81**, 7141 (Sep 1, 2009).
103. E. Balasse, J. Odot, G. Gatouillat, M. C. Andry, C. Madoulet, Enhanced immune response induced by BSA loaded in hydroxyethylstarch microparticles. *Int J Pharm* **353**, 131 (Apr 2, 2008).
104. H. C. Kolb, M. G. Finn, K. B. Sharpless, Click Chemistry: Diverse Chemical Function from a Few Good Reactions. *Angew Chem Int Ed* **40**, 2004 (2001).
105. K. Nwe, M. W. Brechbiel, Growing applications of "click chemistry" for bioconjugation in contemporary biomedical research. *Cancer Biother Radiopharm* **24**, 289 (Jun, 2009).
106. R. K. Lim, Q. Lin, Bioorthogonal chemistry: recent progress and future directions. *Chem Commun (Camb)* **46**, 1589 (Mar 14, 2010).
107. S. Hiki, K. Kataoka, Versatile and selective synthesis of "click chemistry" compatible heterobifunctional poly(ethylene glycol)s possessing azide and alkyne functionalities. *Bioconjug Chem* **21**, 248 (Feb 17, 2010).
108. N. J. Agard, J. A. Prescher, C. R. Bertozzi, A strain-promoted [3 + 2] azide-alkyne cycloaddition for covalent modification of biomolecules in living systems. *J Am Chem Soc* **126**, 15046 (Nov 24, 2004).
109. J. M. Baskin *et al.*, Copper-free click chemistry for dynamic in vivo imaging. *Proc Natl Acad Sci U S A* **104**, 16793 (Oct 23, 2007).
110. J. C. Jewett, E. M. Sletten, C. R. Bertozzi, Rapid Cu-free click chemistry with readily synthesized biarylazacyclooctynones. *J Am Chem Soc* **132**, 3688 (Mar 24, 2010).
111. R. Hoogenboom, Thiol-yne chemistry: a powerful tool for creating highly functional materials. *Angew Chem Int Ed Engl* **49**, 3415 (May 3, 2010).
112. C. E. Hoyle, A. B. Lowe, C. N. Bowman, Thiol-click chemistry: a multifaceted toolbox for small molecule and polymer synthesis. *Chem Soc Rev* **39**, 1355 (Apr, 2010).
113. M. Malkoch *et al.*, Synthesis of well-defined hydrogel networks using click chemistry. *Chem Commun (Camb)*, 2774 (Jul 14, 2006).
114. M. van Dijk, C. F. van Nostrum, W. E. Hennink, D. T. Rijkers, R. M. Liskamp, Synthesis and characterization of enzymatically biodegradable PEG and peptide-based hydrogels prepared by click chemistry. *Biomacromolecules* **11**, 1608 (Jun 14, 2010).

115. P. Lundberg *et al.*, Poly(ethylene glycol)-based thiol-ene hydrogel coatings-curing chemistry, aqueous stability, and potential marine antifouling applications. *ACS Appl Mater Interfaces* **2**, 903 (Mar, 2010).
116. S. Q. Liu, P. L. Ee, C. Y. Ke, J. L. Hedrick, Y. Y. Yang, Biodegradable poly(ethylene glycol)-peptide hydrogels with well-defined structure and properties for cell delivery. *Biomaterials* **30**, 1453 (Mar, 2009).
117. B. J. Adzima *et al.*, Spatial and temporal control of the alkyne-azide cycloaddition by photoinitiated Cu(II) reduction. *Nat Chem* **3**, 256 (Mar, 2011).
118. A. A. Aimetti, A. J. Machen, K. S. Anseth, Poly(ethylene glycol) hydrogels formed by thiol-ene photopolymerization for enzyme-responsive protein delivery. *Biomaterials* **30**, 6048 (Oct, 2009).
119. B. D. Polizzotti, B. D. Fairbanks, K. S. Anseth, Three-dimensional biochemical patterning of click-based composite hydrogels via thiolene photopolymerization. *Biomacromolecules* **9**, 1084 (Apr, 2008).
120. C. A. DeForest, B. D. Polizzotti, K. S. Anseth, Sequential click reactions for synthesizing and patterning three-dimensional cell microenvironments. *Nat Mater* **8**, 659 (Aug, 2009).
121. B. D. Fairbanks *et al.*, A Versatile Synthetic Extracellular Matrix Mimic via Thiol-Norbornene Photopolymerization. *Advanced Materials* **21**, 5005 (2009).
122. D. A. Ossipov, J. Hilborn, Poly(vinyl alcohol)-Based Hydrogels Formed by "Click Chemistry". *Macromolecules* **39**, 1709 (2006).
123. X. Hu, D. Li, F. Zhou, C. Gao, Biological hydrogel synthesized from hyaluronic acid, gelatin and chondroitin sulfate by click chemistry. *Acta Biomater* **7**, 1618 (Apr, 2011).
124. V. Crescenzi, L. Cornelio, C. Di Meo, S. Nardecchia, R. Lamanna, Novel hydrogels via click chemistry: synthesis and potential biomedical applications. *Biomacromolecules* **8**, 1844 (Jun, 2007).
125. R. T. Chen *et al.*, Photoinitiated alkyne-azide click and radical cross-linking reactions for the patterning of PEG hydrogels. *Biomacromolecules* **13**, 889 (Mar 12, 2012).
126. A. Barras, S. Szunerits, L. Marcon, N. Monfiliette-Dupont, R. Boukherroub, Functionalization of diamond nanoparticles using "click" chemistry. *Langmuir* **26**, 13168 (Aug 17, 2010).
127. M. J. Joralemon, R. K. O'Reilly, C. J. Hawker, K. L. Wooley, Shell click-crosslinked (SCC) nanoparticles: a new methodology for synthesis and orthogonal functionalization. *J Am Chem Soc* **127**, 16892 (Dec 7, 2005).
128. M. T. Gokmen, J. Brassinne, R. A. Prasath, F. E. Du Prez, Revealing the nature of thio-click reactions on the solid phase. *Chem Commun (Camb)* **47**, 4652 (Apr 28, 2011).

129. X. Wang, L. Liu, Y. Luo, H. Zhao, Bioconjugation of Biotin to the Interfaces of Polymeric Micelles via In Situ Click Chemistry. *Langmuir* **25**, 744 (2009).
130. J. A. Johnson *et al.*, Core-Clickable PEG-Branch-Azide Bivalent-Bottle-Brush Polymers by ROMP: Grafting-Through and Clicking-To. *J Am Chem Soc*, (Dec 13, 2010).
131. J. Guo *et al.*, Surface modification of polymeric micelles by strain-promoted alkyne-azide cycloadditions. *Chemistry* **16**, 13360 (Dec 3, 2010).
132. Z. Meng, G. R. Hendrickson, L. A. Lyon, Simultaneous Orthogonal Chemoligations on Multiresponsive Microgels. *Macromolecules* **42**, 7664 (2009).
133. C. Tissandier *et al.*, One-pot synthesis of hybrid multifunctional silica nanoparticles with tunable coating by click chemistry in reverse w/o microemulsion. *Langmuir* **28**, 209 (Jan 10, 2012).
134. H. P. Yap, A. P. R. Johnston, G. K. Such, Y. Yan, F. Caruso, Click-Engineered, Bioresponsive Drug Loaded PEG Spheres. *Advanced Materials* **21**, 4384 (2009).
135. X. Liu, H.-N. Zheng, Y.-Z. Ma, Q. Yan, S.-J. Xiao, Microwave irradiated click reactions on silicon surfaces via derivatization of covalently grafted poly(PEGMA) brushes. *J Colloid Interface Sci* **358**, 116 (2011).
136. R. M. Hensarling, V. A. Doughty, J. W. Chan, D. L. Patton, "Clicking" polymer brushes with thiol-yne chemistry: indoors and out. *J Am Chem Soc* **131**, 14673 (Oct 21, 2009).
137. C. Wendeln, S. Rinnen, C. Schulz, H. F. Arlinghaus, B. J. Ravoo, Photochemical microcontact printing by thiol-ene and thiol-yne click chemistry. *Langmuir* **26**, 15966 (Oct 19, 2010).
138. X. L. Sun, C. L. Stabler, C. S. Cazalis, E. L. Chaikof, Carbohydrate and protein immobilization onto solid surfaces by sequential Diels-Alder and azide-alkyne cycloadditions. *Bioconjug Chem* **17**, 52 (Jan-Feb, 2006).
139. V. R. Krishnamurthy *et al.*, Chemoselective immobilization of peptides on abiotic and cell surfaces at controlled densities. *Langmuir* **26**, 7675 (Jun 1, 2010).
140. G. A. Hudalla, W. L. Murphy, Using "click" chemistry to prepare SAM substrates to study stem cell adhesion. *Langmuir* **25**, 5737 (May 19, 2009).
141. G. A. Hudalla, W. L. Murphy, Immobilization of peptides with distinct biological activities onto stem cell culture substrates using orthogonal chemistries. *Langmuir* **26**, 6449 (May 4, 2010).
142. G. K. Such, J. F. Quinn, A. Quinn, E. Tjijto, F. Caruso, Assembly of ultrathin polymer multilayer films by click chemistry. *J Am Chem Soc* **128**, 9318 (Jul 26, 2006).
143. R. V. Ostaci *et al.*, Polymer brushes grafted to "passivated" silicon substrates using click chemistry. *Langmuir* **24**, 2732 (Mar 18, 2008).

144. R. V. Ostaci, D. Damiron, Y. Grohens, L. Leger, E. Drockenmuller, Click chemistry grafting of poly(ethylene glycol) brushes to alkyne-functionalized pseudobrushes. *Langmuir* **26**, 1304 (Jan 19, 2010).
145. Y. Y. Durmaz, M. Sangermano, Y. Yagci, Surface Modification of UV-Cured Epoxy Resins by Click Chemistry. *J Polym Sci Pol Chem* **48**, 2862 (2010).
146. A. Kuzmin, A. Poloukhine, M. A. Wolfert, V. V. Popik, Surface functionalization using catalyst-free azide-alkyne cycloaddition. *Bioconjug Chem* **21**, 2076 (Nov 17, 2010).
147. R. Ogaki *et al.*, Temperature-Induced Ultradense PEG Polyelectrolyte Surface Grafting Provides Effective Long-Term Bioresistance against Mammalian Cells, Serum, and Whole Blood. *Biomacromolecules* **13**, 3668 (Nov 12, 2012).
148. P. K. Nguyen, C. G. Snyder, J. D. Shields, A. W. Smith, D. L. Elbert, Clickable poly(ethylene glycol)-microsphere-based cell scaffolds. *Macromolecular Chemistry and Physics*, 10.1002/macp.201300023 (2013).
149. J. A. Johnson *et al.*, Core-Clickable PEG-Branch-Azide Bivalent-Bottle-Brush Polymers by ROMP: Grafting-Through and Clicking-To. *J Am Chem Soc* **133**, 559 (Jan 26, 2011).
150. V. O. Rodionov, V. V. Fokin, M. G. Finn, Mechanism of the ligand-free CuI-catalyzed azide-alkyne cycloaddition reaction. *Angew Chem Int Ed Engl* **44**, 2210 (Apr 8, 2005).
151. M. V. Turturro, S. Sokic, J. C. Larson, G. Papavasiliou, Effective tuning of ligand incorporation and mechanical properties in visible light photopolymerized poly(ethylene glycol) diacrylate hydrogels dictates cell adhesion and proliferation. *Biomed Mater* **8**, 025001 (Jan 23, 2013).
152. Y.-Y. Luk, M. Kato, M. Mrksich, Self-assembled monolayers of alkanethiolates presenting mannitol groups are inert to protein adsorption and cell adhesion. *Langmuir* **16**, 9604 (2000).
153. K. Malliaras, E. Marban, Cardiac cell therapy: where we've been, where we are, and where we should be headed. *Br Med Bull* **98**, 161 (2011).
154. K. H. So *et al.*, Generation of functional cardiomyocytes from mouse induced pluripotent stem cells. *Int J Cardiol* **153**, 277 (Dec 15, 2011).
155. M. Ieda *et al.*, Direct reprogramming of fibroblasts into functional cardiomyocytes by defined factors. *Cell* **142**, 375 (Aug 6, 2010).
156. J. A. Efe *et al.*, Conversion of mouse fibroblasts into cardiomyocytes using a direct reprogramming strategy. *Nat Cell Biol* **13**, 215 (Mar, 2011).
157. S. Protze *et al.*, A new approach to transcription factor screening for reprogramming of fibroblasts to cardiomyocyte-like cells. *J Mol Cell Cardiol* **53**, 323 (Sep, 2012).
158. T. M. Jayawardena *et al.*, MicroRNA-mediated in vitro and in vivo direct reprogramming of cardiac fibroblasts to cardiomyocytes. *Circ Res* **110**, 1465 (May 25, 2012).

159. A. Behfar *et al.*, Stem cell differentiation requires a paracrine pathway in the heart. *Faseb J* **16**, 1558 (Oct, 2002).
160. R. P. Koche *et al.*, Reprogramming factor expression initiates widespread targeted chromatin remodeling. *Cell Stem Cell* **8**, 96 (Jan 7, 2011).
161. M. T. Lam, M. T. Longaker, Comparison of several attachment methods for human iPS, embryonic and adipose-derived stem cells for tissue engineering. *J Tissue Eng Regen Med* **6 Suppl 3**, s80 (Dec, 2012).
162. H. K. Kleinman, G. R. Martin, Matrigel: basement membrane matrix with biological activity. *Semin Cancer Biol* **15**, 378 (Oct, 2005).
163. L. E. Dickinson, S. Kusuma, S. Gerecht, Reconstructing the differentiation niche of embryonic stem cells using biomaterials. *Macromol Biosci* **11**, 36 (Jan 10, 2011).
164. S. Battista *et al.*, The effect of matrix composition of 3D constructs on embryonic stem cell differentiation. *Biomaterials* **26**, 6194 (Nov, 2005).
165. A. van Dijk, H. W. Niessen, B. Zandieh Doulabi, F. C. Visser, F. J. van Milligen, Differentiation of human adipose-derived stem cells towards cardiomyocytes is facilitated by laminin. *Cell Tissue Res* **334**, 457 (Dec, 2008).
166. B. C. Heng *et al.*, Translating human embryonic stem cells from 2-dimensional to 3-dimensional cultures in a defined medium on laminin- and vitronectin-coated surfaces. *Stem cells and development* **21**, 1701 (Jul 1, 2012).
167. A. Domogatskaya, S. Rodin, A. Boutaud, K. Tryggvason, Laminin-511 but not -332, -111, or -411 enables mouse embryonic stem cell self-renewal in vitro. *Stem Cells* **26**, 2800 (Nov, 2008).
168. K. Schenke-Layland *et al.*, Recapitulation of the embryonic cardiovascular progenitor cell niche. *Biomaterials* **32**, 2748 (Apr, 2011).
169. J. D. Humphries, A. Byron, M. J. Humphries, Integrin ligands at a glance. *J Cell Sci* **119**, 3901 (Oct 1, 2006).
170. K. Saha *et al.*, Surface-engineered substrates for improved human pluripotent stem cell culture under fully defined conditions. *Proc Natl Acad Sci U S A* **108**, 18714 (Nov 15, 2011).
171. G. Chen *et al.*, Chemically defined conditions for human iPSC derivation and culture. *Nat Methods* **8**, 424 (May, 2011).
172. T. J. Rowland *et al.*, Roles of integrins in human induced pluripotent stem cell growth on Matrigel and vitronectin. *Stem Cells Dev* **19**, 1231 (Aug, 2010).
173. S. R. Braam *et al.*, Recombinant vitronectin is a functionally defined substrate that supports human embryonic stem cell self-renewal via α 5 β 1 integrin. *Stem Cells* **26**, 2257 (Sep, 2008).

174. R. S. Ross, T. K. Borg, Integrins and the myocardium. *Circ Res* **88**, 1112 (Jun 8, 2001).
175. M. L. McCain, K. K. Parker, Mechanotransduction: the role of mechanical stress, myocyte shape, and cytoskeletal architecture on cardiac function. *Pflugers Arch* **462**, 89 (Jul, 2011).
176. H. Nandivada *et al.*, Fabrication of synthetic polymer coatings and their use in feeder-free culture of human embryonic stem cells. *Nat Protoc* **6**, 1037 (Jul, 2011).
177. Z. Melkounmian *et al.*, Synthetic peptide-acrylate surfaces for long-term self-renewal and cardiomyocyte differentiation of human embryonic stem cells. *Nat Biotechnol* **28**, 606 (Jun, 2010).
178. B. K. Wacker *et al.*, Endothelial cell migration on RGD-peptide-containing PEG hydrogels in the presence of sphingosine 1-phosphate. *Biophys J* **94**, 273 (Jan 1, 2008).
179. C. N. Salinas, K. S. Anseth, The enhancement of chondrogenic differentiation of human mesenchymal stem cells by enzymatically regulated RGD functionalities. *Biomaterials* **29**, 2370 (May, 2008).
180. L. Schukur, P. Zorlutuna, J. M. Cha, H. Bae, A. Khademhosseini, Directed Differentiation of Size-Controlled Embryoid Bodies Towards Endothelial and Cardiac Lineages in RGD-Modified Poly(Ethylene Glycol) Hydrogels. *Adv Healthc Mater* **2**, 195 (Jan, 2013).
181. Y. Liu, X. Wang, D. S. Kaufman, W. Shen, A synthetic substrate to support early mesodermal differentiation of human embryonic stem cells. *Biomaterials* **32**, 8058 (Nov, 2011).
182. H. C. Moeller, M. K. Mian, S. Shrivastava, B. G. Chung, A. Khademhosseini, A microwell array system for stem cell culture. *Biomaterials* **29**, 752 (Feb, 2008).
183. C. L. Bauwens *et al.*, Geometric control of cardiomyogenic induction in human pluripotent stem cells. *Tissue Eng Part A* **17**, 1901 (Aug, 2011).
184. Y. S. Hwang *et al.*, Microwell-mediated control of embryoid body size regulates embryonic stem cell fate via differential expression of WNT5a and WNT11. *Proc Natl Acad Sci U S A* **106**, 16978 (Oct 6, 2009).
185. C. L. Bauwens *et al.*, Control of human embryonic stem cell colony and aggregate size heterogeneity influences differentiation trajectories. *Stem Cells* **26**, 2300 (Sep, 2008).
186. P. W. Burrridge *et al.*, Improved human embryonic stem cell embryoid body homogeneity and cardiomyocyte differentiation from a novel V-96 plate aggregation system highlights interline variability. *Stem Cells* **25**, 929 (Apr, 2007).
187. J. C. Mohr *et al.*, The microwell control of embryoid body size in order to regulate cardiac differentiation of human embryonic stem cells. *Biomaterials* **31**, 1885 (Mar, 2010).
188. D. Falconnet, G. Csucs, H. M. Grandin, M. Textor, Surface engineering approaches to micropattern surfaces for cell-based assays. *Biomaterials* **27**, 3044 (Jun, 2006).

189. M. Thery, M. Piel, Adhesive micropatterns for cells: a microcontact printing protocol. *Cold Spring Harb Protoc* **2009**, pdb prot5255 (Jul, 2009).
190. A. Ruiz *et al.*, Micro-stamped surfaces for the patterned growth of neural stem cells. *Biomaterials* **29**, 4766 (Dec, 2008).
191. J. W. Lussi, D. Falconnet, J. A. Hubbell, M. Textor, G. Csucs, Pattern stability under cell culture conditions--a comparative study of patterning methods based on PLL-g-PEG background passivation. *Biomaterials* **27**, 2534 (Apr, 2006).
192. R. Peerani, C. Bauwens, E. Kumacheva, P. W. Zandstra, Patterning mouse and human embryonic stem cells using micro-contact printing. *Methods Mol Biol* **482**, 21 (2009).
193. Y. Sakai, Y. Yoshiura, K. Nakazawa, Embryoid body culture of mouse embryonic stem cells using microwell and micropatterned chips. *J Biosci Bioeng* **111**, 85 (Jan, 2011).
194. R. Peng, X. Yao, J. Ding, Effect of cell anisotropy on differentiation of stem cells on micropatterned surfaces through the controlled single cell adhesion. *Biomaterials* **32**, 8048 (Nov, 2011).
195. J. Tang, R. Peng, J. Ding, The regulation of stem cell differentiation by cell-cell contact on micropatterned material surfaces. *Biomaterials* **31**, 2470 (Mar, 2010).
196. A. W. Smith *et al.*, Direct reprogramming of mouse embryonic fibroblasts to cardiomyocyte-like cells using Yamanaka factors on engineered poly(ethylene glycol) (PEG) hydrogels. *Biomaterials* **34**, 6559 (2013).
197. M. R. Hynd, J. P. Frampton, N. Dowell-Mesfin, J. N. Turner, W. Shain, Directed cell growth on protein-functionalized hydrogel surfaces. *J Neurosci Methods* **162**, 255 (2007).
198. A. W. Smith *et al.*, Long-term culture of HL-1 cardiomyocytes in modular poly(ethylene glycol) microsphere-based scaffolds crosslinked in the phase-separated state. *Acta biomaterialia* **8**, 31 (Jan, 2012).
199. C. P. Soares *et al.*, 2D and 3D-Organized cardiac cells shows differences in cellular morphology, adhesion junctions, presence of myofibrils and protein expression. *PLoS One* **7**, (2012).
200. N. T. Kohen, L. E. Little, K. E. Healy, Characterization of Matrigel interfaces during defined human embryonic stem cell culture. *Biointerphases* **4**, 69 (Dec, 2009).
201. M. Baker, Stem cells in culture: defining the substrate. *Nature Methods* **8**, 293 (2011).
202. A. J. Engler, S. Sen, H. L. Sweeney, D. E. Discher, Matrix elasticity directs stem cell lineage specification. *Cell* **126**, 677 (Aug 25, 2006).
203. S. Sen, A. J. Engler, D. E. Discher, Matrix strains induced by cells: Computing how far cells can feel. *Cell Mol Bioeng* **2**, 39 (Mar 1, 2009).

204. L. B. Hazeltine *et al.*, Effects of substrate mechanics on contractility of cardiomyocytes generated from human pluripotent stem cells. *Int J Cell Biol* **2012**, 508294 (2012).
205. R. Khanna, K. S. Katti, D. R. Katti, Experiments in Nanomechanical Properties of Live Osteoblast Cells and Cell-Biomaterial Interface. *J Nanotechnol Eng Med* **2**, (2012).
206. S. J. Gwak *et al.*, The effect of cyclic strain on embryonic stem cell-derived cardiomyocytes. *Biomaterials* **29**, 844 (Mar, 2008).
207. V. F. Shimko, W. C. Claycomb, Effect of mechanical loading on three-dimensional cultures of embryonic stem cell-derived cardiomyocytes. *Tissue engineering. Part A* **14**, 49 (Jan, 2008).
208. F. Chowdhury *et al.*, Material properties of the cell dictate stress-induced spreading and differentiation in embryonic stem cells. *Nature materials* **9**, 82 (Jan, 2010).
209. I. J. Domian *et al.*, Generation of functional ventricular heart muscle from mouse ventricular progenitor cells. *Science* **326**, 426 (Oct 16, 2009).
210. K. Plath, W. E. Lowry, Progress in understanding reprogramming to the induced pluripotent state. *Nat Rev Genet* **12**, 253 (Apr, 2011).
211. J. Zhang *et al.*, Extracellular matrix promotes highly efficient cardiac differentiation of human pluripotent stem cells: the matrix sandwich method. *Circ Res* **111**, 1125 (Oct 12, 2012).